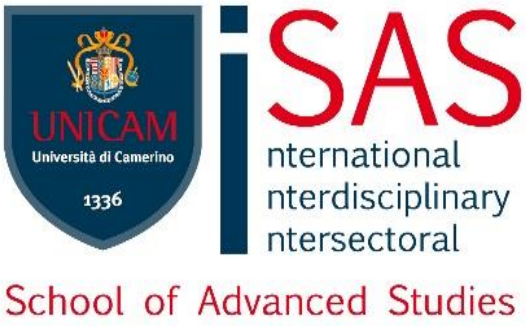

UNIVERSITY OF CAMERINO

School of Advanced Studies

Ph.D. Course in Life and Health Sciences

Curriculum in Molecular Biology and Cellular Biotechnology

XXXV cycle

Immunogenicity of two recombinant DNA COVID-19 vaccines in young and aged mice

Ph.D. candidate

Dr. Lishan Cui

Supervisors

Prof. Cristina Marchini

Prof. Augusto Amici

Academic year 2019/2022

INDEX

ABSTRACT **1**

INTRODUCTION **3**

1. SARS-CoV-2 3

1.1 Epidemiology *3*

1.2 Phylogenetics and taxonomy *4*

1.3 Genome and structure of SARS-CoV-2 *5*

2. SARS-CoV-2 VARIANTS OF CONCERN (VOCs) 8

2.1 Alpha (lineage B.1.1.7) *9*

2.2 Beta (lineage B.1.351) *10*

2.3 Gamma (lineage P.1) *10*

2.4 Delta (lineage B.1.617.2) *11*

2.5 Omicron (lineage B.1.1.529) *11*

3. COVID-19 VACCINES 12

3.1 Live attenuated and inactivated COVID-19 vaccines *13*

3.2 Protein subunit COVID-19 vaccines *14*

3.3 Adenovirus vector COVID-19 vaccines *15*

3.4 Messenger RNA (mRNA) COVID-19 vaccines *16*

3.5 DNA COVID-19 vaccine *19*

4. DELIVERY SYSTEMS FOR DNA VACCINES 25

4.1 Intramuscular injection *26*

4.2 Intramuscular electroporation *27*

4.3 Gene gun *28*

4.4 Jet injection *29*

4.5 From liposomes to lipid nanoparticles (LNPs) mediated delivery *30*

5. AGE-RELATED IMMUNE RESPONSES TO VACCINES 34

AIM OF THE THESIS **37**

MATERIALS AND METHODS **40**

1. CONSTRUCTION OF pVAX-S1 DNA VACCINE AGAINST SARS-CoV-2 40

2. CONSTRUCTION OF pVAX-S1-TM DNA VACCINE AGAINST SARS-CoV-2 43

2.1 Selection of S1 anchored to TM gene region based on in silico analysis *44*

3. CONSTRUCTION OF DNA VACCINES AGAINST SARS-CoV-2 VARIANTS 45

3.1 DNA vaccines specifically conceived against the United Kingdom (UK) (B.1.1.7): Insertion of key mutations into pVAX-S1-TM of SARS-CoV-2 *48*

3.1.1. Insertion of A570D mutation into pVAX-S1-TM (D614G) 48

3.1.2 Insertion of N501Y mutation into pVAX-S1-TM (including D614G and A570D) 48

3.1.3 Verification of pVAX-S1-TM-UK by sequencing 49

3.2 DNA vaccines specifically conceived against Indian (IND) lineage (B.1.617) *49*

3.2.1 Insertion of E484Q and L452R mutations by single-site mutagenesis into pVAX-S1-TM including D614G mutation 49
3.2.3 Verification of pVAX-S1-TM-Indian by sequencing 49
3.3 A chimeric DNA vaccine designed against both the United Kingdom (UK) (B.1.1.7) and Indian (IND) lineage (B.1.617) *50*
3.3.1 Insertion of E484Q and L452R mutations into pVAX-S1-TM-UK 50
3.3.3 Verification of pVAX-S1-TM-INDUK by sequencing 50
3.4 In vitro validation of SARS-CoV-2 DNA vaccines *51*
3.4.1 Cell culture 51
3.4.2 Immunofluorescence analysis for in vitro validation of candidate DNA vaccines 51
3.4.3 Confocal microscopy analysis 52
3.5 In vivo validation of SARS-CoV-2 DNA vaccines *52*
3.5.1 Mice 52
3.5.2 SARS-CoV-2 DNA vaccines preparation 53
3.5.3 Mice immunization with SARS-CoV-2 DNA vaccines 53
3.5.4 Immunofluorescence analysis of antibody response 53
3.5.5 Analysis of antibody response by flow cytometry 54
4. NANOPARTICLES AS POSSIBLE DELIVERY SYSTEM FOR DNA VACCINES 54
4.1 Microfluidic preparation of LNP-pDNA complexes *54*
4.2 Transfection efficiency experiments for evaluate LNPs *57*
4.3 Cell viability assay *57*
4.4 LNPs encapsulated pVAX-hECTM DNA vaccine preparation *58*
4.5 Immunofluorescence analysis of LNPs encapsulated pVAX-hECTM *58*
4.6 Immunization of mice with LNP15 encapsulated pVAX- hECTM DNA vaccine *59*
4.7 Analysis of antibody response elicited by LNP15 encapsulated pVAX-hECTM vaccinated mice *59*
4.8 Statistical analysis *60*
RESULTS **61**
1. GENERATION AND IN VITRO VALIDATION OF PVAX-S1 DNA VACCINE 61
1.1 pVAX-S1 DNA vaccine *61*
1.2 In vitro validation of pVAX-S1: antigen is expressed in transfected HEK-293 cells *62*
2. GENERATION AND IN VITRO VALIDATION OF PVAX-S1-TM DNA VACCINE 63
2.1 pVAX-S1-TM DNA vaccine *63*
2.2 In silico analysis of the antigen encoded by pVAX-S1-TM *65*
2.3 In vitro validation of pVAX-S1-TM: Spike S1-TM antigen is successfully expressed in HEK-293 cells *66*
3. GENERATION AND IN VITRO VALIDATION OF PVAX-S1-TM-D614G DNA VACCINE 67
3.1 pVAX-S1-TM-D614G elicited a better anti-SARS-CoV-2 immune reaction in mice with respect to pVAX-S1 *69*
4. DNA VACCINES AGAINST THE SARS-COV-2 VARIANTS 71
4.1 pVAX-S1-TM-UK: the DNA vaccine against the United Kingdom (UK) (B.1.1.7) variant *71*

4.2 pVAX-S1-TM-Indian: the DNA vaccine against the Indian (IND) variant (B.1.617) *73*
4.3 pVAX-S1-TM-INDUK: the chimeric DNA vaccine *75*
4.4. In vitro validation of DNA vaccines against the SARS-CoV-2 variants *77*
4.4.1 Strong expression of antigenic sequences on mammalian cells 77
4.5 Immunogenicity of pVAX-S1-TM-D614G and pVAX-S1-TM-INDUK DNA vaccines in C57BL/6 young and aged mice *77*
5. GENERATION AND VALIDATION OF MULTICOMPONENT LNPS FOR DNA VACCINATION 82
5.1 Transfection efficiency and cell toxicity of LNPs: LNP15 displays optimal characteristics *83*
5.2 In vitro and in vivo validation of LNP15 as DNA delivery system *84*
DISCUSSION **87**
CONCLUSIONS **92**
BIBLIOGRAPHY **93**
PATENT **101**
PUBLICATIONS **102**
ACKNOWLEDGMENTS **109**

ABSTRACT

Background: SARS-CoV-2 emerged in December 2019 and spread rapidly around the world. Vaccination is the most effective way to control the pandemic morbidity and mortality. While most of the currently available vaccines against COVID-19 have shown high efficacy against the original strain of SARS-CoV-2, their effectiveness has declined due to the emergence of new variants and diminished immunity remains a major threat, especially in older individuals. Therefore, the development of safe and effective vaccines that can be rapidly adapted to new SARS-CoV-2 variants represents an urgent health priority. We assessed the immunogenicity of two DNA vaccines against SARS-CoV-2 variants: pVAX-S1-TM-D614G and pVAX-S1-TM-INDUK.

Methods: pVAX-S1-TM-D614G, encoding the S1 spike subunit in fusion with the transmembrane region, that allows protein trimerization as predicted by *in silico* analysis, was constructed by recombinant DNA technologies; the dominant D614G substitution was introduced by a PCR-based mutagenesis protocol. pVAX-S1-TM-INDUK was obtained by the insertion of additional key mutations from Delta (E484Q and L452R) and Alpha (N501Y and A570D) variants. Antigen expression was verified *in vitro* by immunofluorescence assay. To test the immunogenicity of pVAX-S1-TM-D614G and pVAX-S1-TM-INDUK, they were administered, via intramuscular injection followed by electroporation, in young and aged mice. The elicited immune responses were monitored for 6 months.

Results: pVAX-S1-TM-D614G and pVAX-S1-TM-INDUK were first validated *in vitro*: a robust expression and membrane localization of antigenic proteins was demonstrated on transiently transfected HEK-293 cells. Our candidates DNA vaccines were then tested *in vivo* in both young (11 weeks of age) and aged (20 months of age) C57BL/6 mice. When delivered by electroporation, they were able to trigger a significant anti-SARS-CoV-2 antibody production in immunized mice, although antibody titer declined 6 months after the second dose, especially in aged animals. Of

note, a third booster dose, given at 6 months from the last vaccination, significantly increased the magnitude of humoral immunity, suggesting that immune recall can improve antibody durability. Moreover, we optimized a lipid nanoparticle formulation, we called LNP15, to encapsulate DNA plasmids by microfluidic technology. Preliminary *in vitro* and *in vivo* results obtained with a prototype DNA vaccine, indicate that LNP15 can successfully encapsulate DNA vaccines for their easier administration.

Conclusions: We developed two recombinant DNA vaccines (pVAX-S1-TM-D614G and pVAX-S1-TM-INDUK) against SARS-CoV-2 variants, able to elicit a significant anti-Spike antibody response in both young and aged mice. Although the humoral response declined within 6 months, a booster dose can efficiently recall immune memory and reverse anti-SARS-CoV-2 antibody waning even in aged population. Moreover, LNP15 formulation might permit to successfully deliver candidate DNA vaccines by intramuscular injection without electroporation. Given that DNA vaccines can be easily adapted in response to new variants, are cheaper and more stable than currently approved vaccines, they represent a promising strategy to achieve global immunization.

Key words: SARS-CoV-2; DNA vaccines; Lipid nanoparticles (LNPs); Antibody response

INTRODUCTION

1. SARS-CoV-2

1.1 Epidemiology

In December 2019, Severe Acute Respiratory Syndrome Coronavirus 2 (SARS-CoV-2) has been identified in Wuhan, the capital of the province of Hubei in China and caused a large global outbreak [1]. On 30 January 2020, the WHO declared a novel coronavirus (COVID-19) outbreak as the sixth public health emergency of international concern [2], following the 2009 H1N1 influenza pandemic, the 2013-2014 polio outbreak, West African Ebola virus epidemic in 2014, the 2016 Zika virus outbreak, the 2018-2020 Kivu Ebola epidemic in Democratic Republic of Congo [3]. Up to now, the cumulative number of confirmed cases of SARS-CoV-2 has reached 630 million, and the global death toll has exceeded 6 million, this unprecedented event caused a devastating impact on the world population (Figure 1). Available online: https://www.worldometers.info/coronavirus/ (Accessed on 17 October 2022).

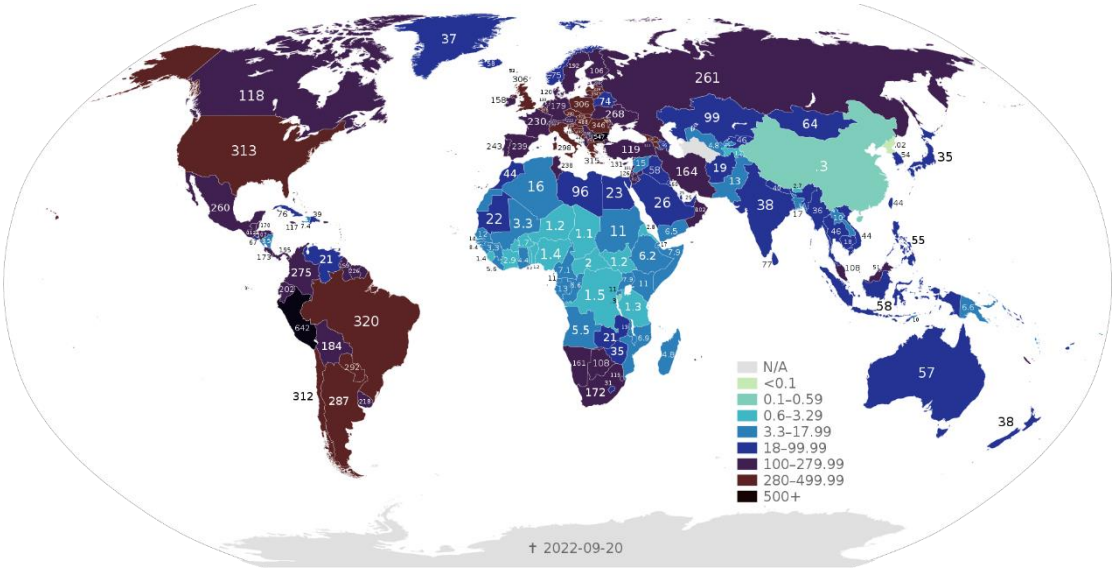

Figure 1. COVID-19 Outbreak World Map Total Deaths per Capita [https://en.wikipedia.org/wiki/COVID-19_pandemic_by_country_and_territory#/media/File:COVID-19_Outbreak_World_Map_Total_Deaths_per_Capita.svg]

Data were converted from deaths per million to deaths per 100,000 people.

555+ deaths per 100,000 inhabitants

100–554.99 deaths per 100,000 inhabitants

18–99.99 deaths per 100,000 inhabitants

3.3–17.99 deaths per 100,000 inhabitants

0.6–3.29 deaths per 100,000 inhabitants

0.1–0.59 deaths per 100,000 inhabitants

No deaths or no data

1.2 Phylogenetics and taxonomy

SARS-CoV-2, a member of the large family of coronaviruses (CoV), categorized into four important genera including Alphacoronavirus, Betacoronavirus, Gammacoronavirus and Deltacoronavirus [4]. Three zoonotic coronaviruses: 1) SARS-CoV or SARS, the beta coronavirus that causes the severe acute respiratory syndrome outbreak in 2002; 2) MERS-CoV or MERS, the beta coronavirus that causes Middle East Respiratory Syndrome in 2012; 3) SARS-CoV-2 or COVID-19, the novel coronavirus that causes coronavirus disease 2019, shares close genetic similarities with bat coronaviruses, suggesting that it was produced by a bat-borne virus (Figure 2) [5-7]. Bats for Alphacoronavirus and Betacoronavirus, and birds for Gammacoronavirus and Deltacoronavirus, warm-blooded flying vertebrates, can be considered ideal hosts for coronaviruses, able to fuel their evolution and dissemination [4]. Since these viruses share~~s~~ several common characteristics, they have caused relatively high numbers of cases and deaths in humans.

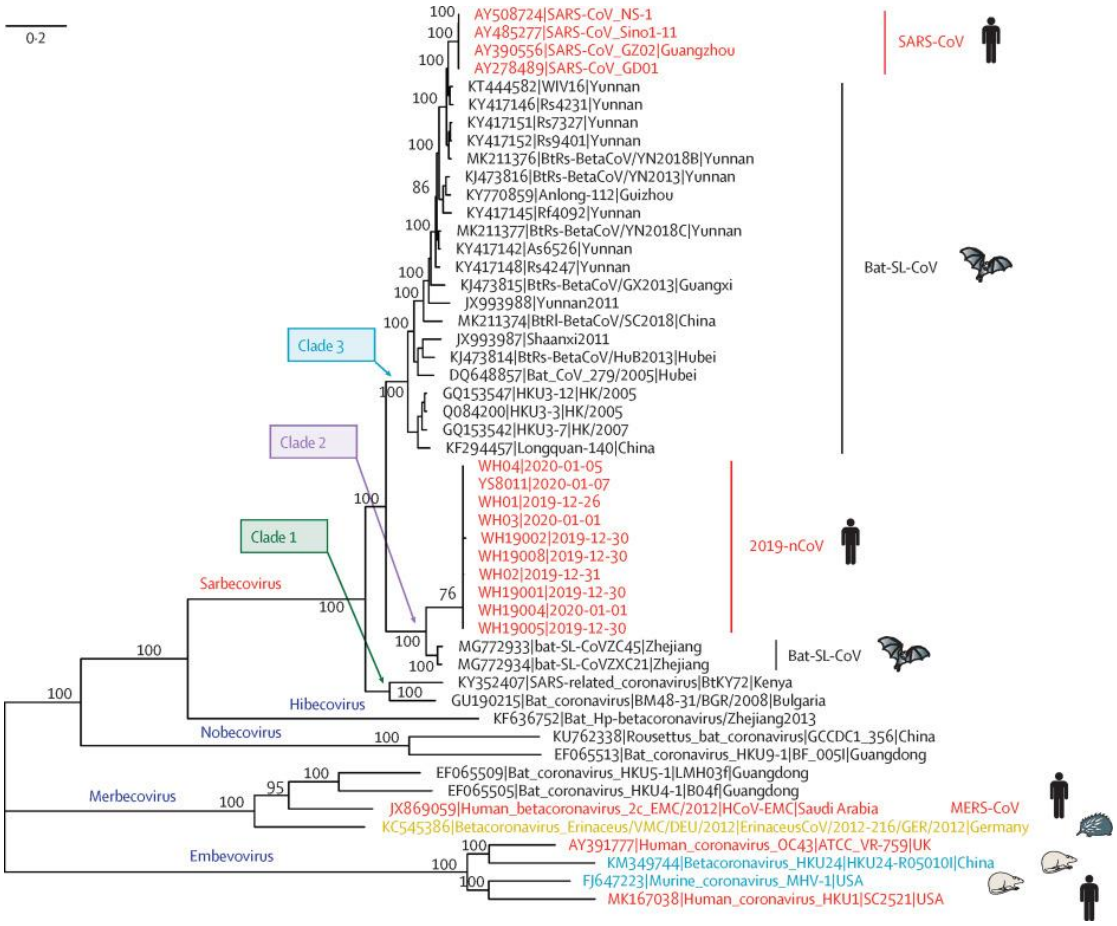

Figure 2. Phylogenetic analysis of full-length genomes of 2019-nCoV and representative viruses of the genus Betacoronavirus. 2019-nCoV=2019 novel coronavirus. MERS-CoV=Middle East respiratory syndrome coronavirus. SARS-CoV=severe acute respiratory syndrome coronavirus [8].

1.3 Genome and structure of SARS-CoV-2

The SARS-CoV-2 are spherical, enveloped, around 80–120 nm in diameter, with multiple outwardly projected club-like homotrimeric, glycosylated Spike proteins. The genome of SARS-CoV-2 is a positive-sense single-stranded RNA (+ssRNA) containing a 5' methyl-guanosine cap, poly (A)-tail, ranging from 26.0 kb to 32.0 kb [9]. It retains four major structural proteins: the spike (S) protein, the envelope (E) protein, the membrane (M) protein, and the nucleocapsid (N) protein, all of which are essential for building its spherical, spike-covered shape (Figure 3) [10].

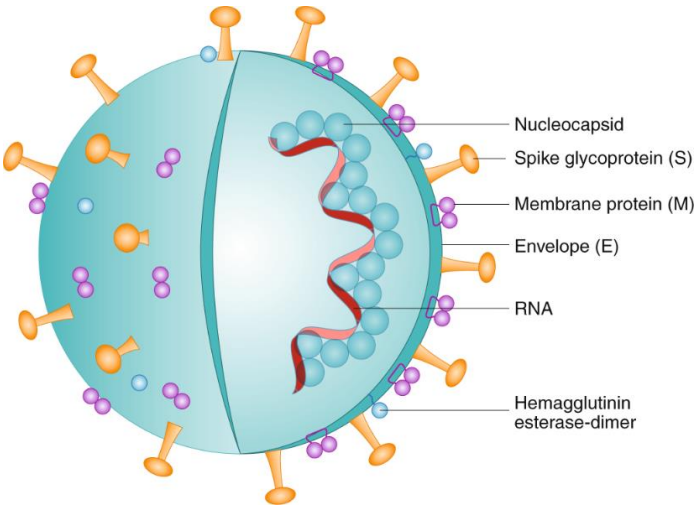

Figure 3. Schematic representation of SARS-CoV-2 structure. This is an enveloped, positive-sense RNA virus with four main structural proteins, including spike (S) and membrane (M) glycoproteins, as well as envelope (E) and nucleocapsid (N) proteins [10].

The SARS-CoV-2 S glycoprotein is 1273 amino acids (aa) in length and 180-200 kDa in size. The S protein is divided into two functional parts, the S1 subunit (14-685 residues) and the S2 subunit (686-1273 residues), responsible for receptor binding and membrane fusion, respectively. In the S1 subunit, there is an extracellular N-terminal domain (14-305 residues) and a receptor-binding domain (RBD, 319-541 residues), whereas the fusion peptide (FP) (788-806 residues), the heptapeptide repeat sequence 1 (HR1) (912-984 residues), the HR2 (1163-1213 residues), the transmembrane (TM) domain (1213-1237 residues) anchored in the viral membrane, and the cytoplasm domain (1237-1273 residues) are comprised in the S2 subunit [11]. The S protein, being exposed on the surface of the virus, plays a crucial role in viral infection. It can bind to angiotensin-converting enzyme 2 (ACE2), a protein on the surface of human cells that mediates trimeric attachment of the virus to host cells through the receptor-binding domain (RBD) of the S1 subunit (Figure 4) [12]. The properties of the S-glycoprotein exposed on the surface of the virus make it an excellent target for developing vaccines against SARS-CoV-2.

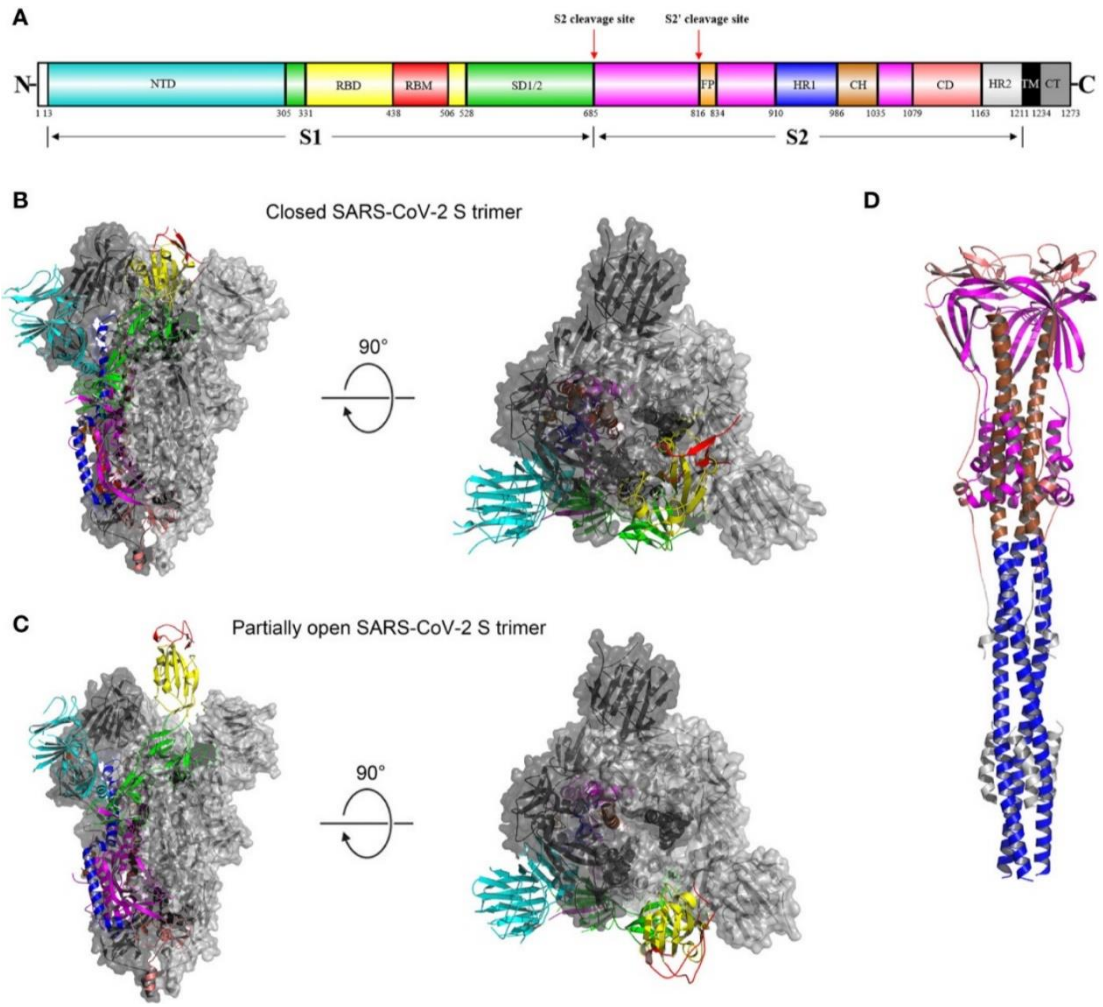

Figure 4. Overall structures of the SARS-CoV-2 S glycoprotein trimer in different conformations. (A) Schematic representation of the domain arrangement of the SARS-CoV-2 S protein precursor. SS, signal peptide; NTD: N-terminal domain; RBD: receptor-binding domain; RBM: receptor-binding motif; SD1/2: subdomain 1 and 2; FP, fusion peptide; HR1, heptad repeat 1; CH, central helix; CD, connector domain; HR2, heptad repeat 2; TM, transmembrane domain; CT, cytoplasmic tail. Arrows denote protease cleavage sites. (B) Side and top views of the prefusion structure of the SARS-CoV-2 S ectodomain trimer with all three RBDs in the down conformation (PDB ID: 6VXX). One protomer is shown in ribbon representation colored corresponding to the schematic in (A), a second protomer in light gray surface representation, and the third protomer in dark gray surface representation. (C) is identical to (B) except that a single RBD assumes the up conformation and is shown in ribbon representation (PDB ID: 6VYB). (D) Overall structure of the SARS-CoV-2 S2 trimer in the postfusion conformation is shown in ribbon representation colored corresponding to the schematic in (A) (PDB ID: 6XRA). The glycans were omitted for clarity [13].

Interestingly, both SARS-CoV and SARS-CoV-2 use the host cell ACE2 receptor to enter human cells [14]. The major antibody-neutralizing epitope of the S protein is within the RBD with over 90% of all neutralizing activity [15]. In fact, anti-MERS

antibodies targeting the RBD of the S protein tend to have greater neutralizing potency than those directed to other epitopes [16]. Moreover, the SARS-CoV-2 genome shares approximately 82% sequence identity with SARS-CoV and MERS-CoV, while essential enzymes and structural proteins share over 90% sequence identity [17]. This sequence similarity provides insights for designing improved therapeutics approaches, further accelerating the development of vaccines against SARS-CoV-2.

2. SARS-CoV-2 variants of concern (VOCs)

As the virus continues to circulate in the world, several SARS-CoV-2 variants have emerged, and some of them are concerning for their characteristics of transmissibility, severity of caused disease and/or immunity. In July 2020, Korber, B. *et al*. reported that the D614G mutation, in which glycine (G) replaces aspartic acid (D) at position 614 in the S glycoprotein, became the predominant form in global epidemics and posing a serious threat [18]. While D614G mutation is not located in the RBD, this mutation could shift conformation toward an ACE2 binding-competent state via an allosteric effect and thus promotes the fusion of the virion membrane with target cells, thereby increasing the infectivity of the virion [19-21]. To date, WHO has declared the following five variants of concern (VOCs) with names taken from the Greek alphabet, Alpha (lineage B.1.1.7), Beta (lineage B.1.351), Gamma (lineage P.1), Delta (lineage B.1.617.2) and Omicron (Lineage B.1.1.529) (Tabel 1).

Table 1. WHO proposed labels for global SARS-CoV-2 variants of concern (VOCs)+:

WHO label	Pango lineage•	GISAID clade	Nextstrain c lade	Additional amino acid changes monitored°	Earliest documented samples	Date of designation
Alpha	B.1.1.7	GRY	20I (V1)	+S:484K +S:452R	United Kingdom, Sep-2020	18-Dec-2020
Beta	B.1.351	GH/501Y.V2	20H (V2)	+S:L18F	South Africa, May-2020	18-Dec-2020
Gamma	P.1	GR/501Y.V3	20J (V3)	+S:681H	Brazil, Nov-2020	11-Jan-2021
Delta	B.1.617.2	GK	21A, 21I, 21J	+S:417N +S:484K	India, Oct-2020	VOI: 4-Apr-2021 VOC: 11-May-2021
Omicron*	B.1.1.529	GRA	21K, 21L 21M	+S:R346K	Multiple countries, Nov-2021	VUM: 24-Nov-2021 VOC: 26-Nov-2021

• Includes all descendent lineages.

* Omicron includes Pango lineage B.1.1.529 and descendent Pango lineages BA.1, BA.1.1, BA.2 and BA.3. Omicron-defining constellation of mutations fully overlaps with Pango lineage BA.1, as this accounts for the vast majority of Omicron sequences up. Most evidence we have to date about VOC Omicron is therefore based on Pango lineage BA.1. As of 24.01.2022, the BA.2 descendent lineage, which differs from BA.1 in some of the mutations, including in the spike protein, is increasing in many countries. Investigations into the characteristics of BA.2, including immune escape properties and virulence, should be prioritized independently (and comparatively) to BA.1.

° Only found in a subset of sequences

2.1 Alpha (lineage B.1.1.7)

The Alpha variant (B.1.1.7) was the first variant of concern detected in September 2020, initially discovered in the United Kingdom and spread rapidly around the world [22]. The B.1.1.7 variant carries eight substitutions or deletions (Δ69-70, Δ145, N501Y, A570D, P681H, T716I, S982A and D1118H) in the spike protein among 17 mutations in the viral genome [23]. In particular, N501Y, one of the key mutations of the Alpha lineage, changed from asparagine to tyrosine the amino

acid in position 501 in the RBD of the spike protein. It results in an increased binding affinity of the spike protein to the ACE2 receptor, enhancing viral attachment to the host cells [24]. Early in the outbreak, a significant increase in the transmission rate of the B.1.1.7 variant was detected compared to the initial emergence of SARS-CoV-2 [25]. Multiple mutations in the S protein give rise to important concerns about evading immune surveillance.

2.2 Beta (lineage B.1.351)

Beta variant (B.1.351 lineage) was first documented in Southern Africa in October 2020, with an increased number of mutations. The B.1.351 variant includes nine mutations (L18F, D80A, D215G, R246I, K417N, E484K, N501Y, D614G, and A701V) in the spike protein, of which three mutations (K417N, E484K, and N501Y) are located in the RBD and increase the binding affinity for the ACE receptors [26]. It is worth noting that B.1.351 is more resistant to neutralization than the original SARS-CoV-2 lineage, highlighting the exacerbating potential of immune escape [27, 28].

2.3 Gamma (lineage P.1)

The lineage Gamma (P.1 lineage), the third designated variant of concern, emerged in the northern state of Amazonas, Brazil. The P.1 variant harbors 17 mutations, including a trio of alarming mutations (N501Y, E484K and K417T) within the RBD of S protein [29]. In particular, the N501Y mutation, which is also present in the B.1.1.7 variant and B.1.351 variant, enhances the binding affinity to human cells, making it more infectious [30, 31]. Moreover, the E484K mutation, converting glutamic acid (E) to lysine (K) at amino acid position 484, may impede natural immunity, thus the effectiveness of vaccination as well as antibody-based therapies [32]. It has been reported that P.1 lineage is 1.7- to 2.4-fold more transmissible than the original Wuhan lineage [29].

2.4 Delta (lineage B.1.617.2)

The fourth and more contagious variant of concern is the Delta variant (lineage B.1.617.2). It was initially identified in India in December 2020 and has quickly become the dominant strain in the world until Omicron has replaced it. The most notable mutations in the S protein of the Delta variant are L452R and P681R, which allow the S protein to bind to the ACE2 receptor with higher affinity and enhance viral fusogenicity [33]. The E484Q substitution within the receptor binding domain (RBD) plays a similar role with antibody-escape mutation E484K, which is present in both Beta and Gamma variants (lineage B.1.351 and P.1) [34]. It has been reported that the two RBD mutations E484Q and L452R reduced binding properties to selected monoclonal antibodies (mAbs) and potentially affect their neutralization capacity [35]. The Delta lineage was more resistant to antibody neutralization, which is associated with the evasion of antibodies against non-RBD and RBD epitopes of the spike protein [34]. Up to 50% more transmissibility than the previous dominant alpha variant has been reported [7].

2.5 Omicron (lineage B.1.1.529)

On 26 November 2021, the WHO named the highly mutated Omicron (B.1.1.529) as the new variant of concern [36]. This newly emerged variant further replaced the Delta variant and spread worldwide at an alarming rate [37]. As the most heavily mutated among the variants of concern, such variant includes at least 32 amino acid mutations in the S protein [38]. A previous study found that Omicron is associated with an increased risk of reinfection and is better at evading vaccine-induced immunity [39]. Nevertheless, omicron appears to cause less severe disease compared with prior variants [40]. While the virulence of VOCs is diminishing, but still highly contagious, the emergence of new variants could be a potential risk for the continuation of the COVID-19 pandemic.

3. COVID-19 vaccines

The COVID-19 outbreak has driven an extraordinary speed in vaccine development to combat the pandemic. Several vaccine platforms are designed to train our immune system, including live-attenuated or inactivated viruses, protein subunits, virus-like particles, nucleic acid-based vaccines, non-replicating and replicating viral vector vaccines (Figure 5).

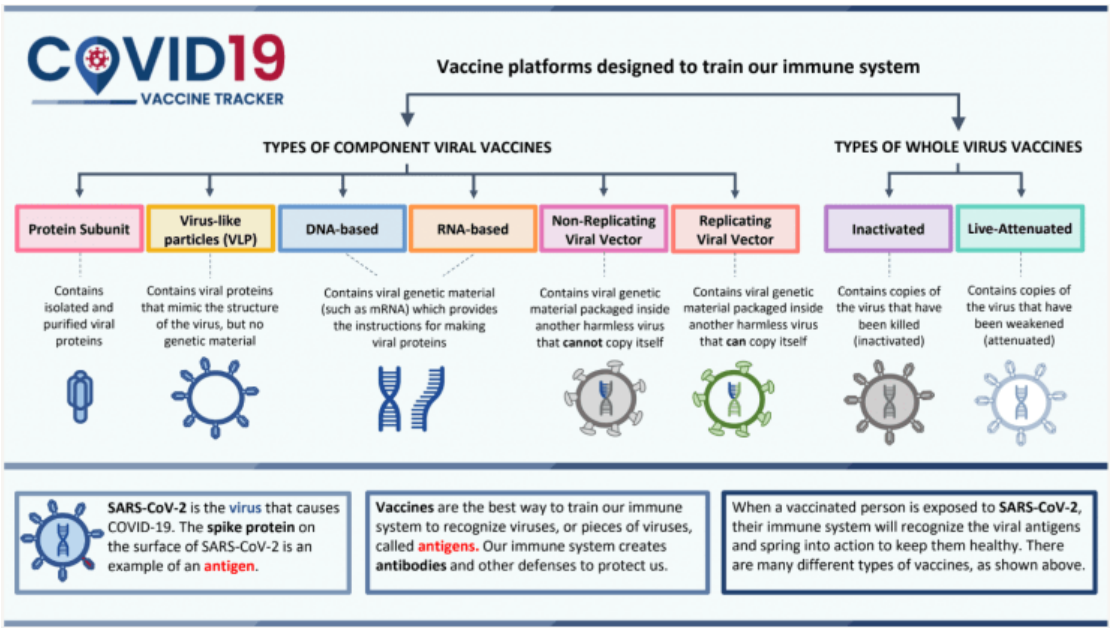

Figure 5. Types of vaccines against COVID-19, adapted from © 2022 VIPER Group COVID19 Vaccine Tracker Team.

Up to now, there are 172 vaccine candidates in the clinical development and 199 vaccines are in the pre-clinical studies (Accessed on 21 October 2022) (Table 2). Available online: https://www.who.int/publications/m/item/draft-landscape-of-covid-19-candidate-vaccines]. Of them, eleven vaccines were granted emergency use by WHO [https://covid19.trackvaccines.org/agency/who/]. European Medicines Agency (EMA) authorized six vaccines for European Union (EU) to prevent COVID-19, which are Comirnaty (developed by BioNTech and Pfizer), COVID-19 Vaccine (inactivated, adjuvanted) Valneva, Jcovden (previously COVID-19 Vaccine Janssen), Nuvaxovid, Spikevax (previously COVID-19 Vaccine Moderna) and Vaxzevria (previously COVID-19 Vaccine AstraZeneca).

Table 2. Vaccines currently in clinical phase for SARS-CoV-2 according to the World Health Organization (WHO) as of October 21, 2022.

Platform		Candidate vaccines (no. and %)	
PS	Protein subunit	55	32%
VVnr	Viral Vector (non-replicating)	23	13%
DNA	DNA	16	9%
IV	Inactivated Virus	22	13%
RNA	RNA	40	23%
VVr	Viral Vector (replicating)	4	2%
VLP	Virus Like Particle	6	4%
VVr + APC	VVr + Antigen Presenting Cell	2	1%
LAV	Live Attenuated Virus	2	1%
VVnr + APC	VVnr + Antigen Presenting Cell	1	1%
BacAg-SpV	Bacterial antigen-spore expression vector	1	1%
		172	

3.1 Live attenuated and inactivated COVID-19 vaccines

Live attenuated and inactivated vaccines are vaccines traditionally designed against viruses to generate immunity. Live attenuated vaccines are produced from live organisms (viruses or bacteria) that are modified to retain the ability to replicate and generate immunity but usually does not cause illness. Given its long history, live attenuated vaccines may be a good option for developing a vaccine against COVID-19. Measles, mumps, and rubella (MMR) vaccine, varicella (chickenpox) vaccine, zoster, yellow fever, rotavirus, and influenza vaccine (intranasal) are examples of live attenuated vaccinations currently available. What needs to be considered is the potential for such vaccines to replicate in an uncontrolled manner in immunocompromised individuals, in which case their use carries enormous risks. There is a trade-off between more adequate replication of vaccine pathogens to induce robust immune responses and the strength of pathogen attenuation to avoid symptomatic disease [41]. Codagenix Inc: COVI-VAC is a single-dose intranasal live attenuated vaccine against SARS-CoV-2 produced by Codagenix in the United Kingdom (UK) and the Serum Institute of India. In the Phase 1 clinical trial, COVI-VAC was well tolerated, with no significant adverse events reported in the 48 patients

enrolled [42]. The vaccine is currently in Phase 3 clinical trials. As the first live attenuated vaccine to enter clinical trials, it appears to have broad potential against SARS-CoV-2.

Inactivated COVID-19 vaccines contain inactivated (killed) whole virus SARS-CoV-2, which can be destroyed by heat, chemicals or radiation. This inactivated virus can be recognized by the immune system as foreign and triggers immune response without causing illness. In contrast to live vaccines, the immune response to inactivated vaccines is predominantly humoral with little or no cellular immunity. Inactivated pathogens simply cannot replicate, nor are they as virulent to cause disease as they were previously inactivated, so boosters are needed to create long-term immunity. Most inactivated vaccines are available as whole-cell inactivated vaccines against viruses such as polio, hepatitis A, and rabies. Due to the fast pace of the COVID-19 spreading, several inactivated COVID-19 vaccines have been developed and approved for emergency use, including COVID-19 vaccine (inactivated, adjuvanted) Valneva, Sinovac (CoronaVac), Sinopharm (BBIBP-CorV) and Bharat Biotech (Covaxin).

3.2 Protein subunit COVID-19 vaccines

Protein subunit COVID-19 vaccines contain harmless and purified pieces proteins from SARS-CoV-2 virus. This type of vaccine only contains small purified fragments of proteins instead of the whole virus, so lacks an active pathogen and is considered very safe because it doesn’t cause COVID-19. These characteristics provide benefits for immunocompromised individuals [43]. Other examples of protein-based vaccines are represented by Hepatitis B and acellular pertussis protein subunit vaccines, that have been widely used [44]. Meanwhile, most of protein subunit vaccines require adjuvants to help generate a stronger and longer-lasting immune response to the vaccine. As the fifth vaccine recommended by the EU to prevent COVID-19, the NVX-CoV2373 vaccine (Novavax) is composed by a protein

(made using moth cells) plus a Matrix-M™ adjuvant (made from tree bark) to boost the immune response, which has shown approximately 90% efficacy in preventing COVID-19, according to the WHO (13 June 2022). In particular, the Novavax active substance is the protein product of a recombinant SARS-CoV-2 S-gene encoding the 1260 amino acid spike protein (the full length 1273 amino acid protein minus the signal peptide). The S gene was codon optimized for expression in Spodoptera frugiperda (Sf9) insect cells from a full-length, prefusion, stabilized SARS-CoV-2 S genetic sequence. A total of five amino acid changes were introduced to stabilize the protein. The saponin-based Matrix-M adjuvant facilitates activation of the cells of the innate immune system, which enhances the magnitude of the S protein-specific immune response.

3.3 Adenovirus vector COVID-19 vaccines

Viral vector vaccines typically use an unrelated, harmless virus vector virus to deliver the gene sequence encoding the desired antigen into cells in the body. Both the European Medicines Agency (EMA) and the Italian Medicines Agency (AIFA) authorized two COVID-19 viral vector vaccines that employed replication-defective adenovirus as the gene delivery vehicle. Janssen (Ad26.COV2.S), a recombinant, replication-incompetent adenoviral vector based on human adenovirus type 26 (Ad26) encoding a full-length and stabilized SARS-CoV-2 Spike (S) protein [45], and Oxford/AstraZeneca (ChAdOx1), that consists of the replication-deficient adenoviral vector ChAdOx1 derived from chimpanzees, containing the full-length structural surface glycoprotein (spike protein) of SARS-CoV-2, with a tissue plasminogen activator leader sequence [46]. In particular, ChAdOx1 nCoV-19 expresses a codon-optimized coding sequence for the spike protein (GenBank accession number MN908947). Both vaccines are able to elicit a strong innate and adaptive immune response through Toll-like Receptor (TLR)-dependent and TLR-independent mechanisms [47]. The WHO announced that the viral vector vaccine

Oxford/AstraZeneca (ChAdOx1-S [recombinant] vaccine) COVID-19 vaccine is 76% effective against symptomatic SARS-CoV-2 infection, and Janssen Ad26.CoV2.S exhibits 66.9% efficacy against symptomatic moderate and severe SARS-CoV-2 infection. Regrettably, a rare side effect, unusual blood clots with low blood platelets, occurred in the people who received Vaxzevria (formerly COVID-19 Vaccine AstraZeneca). Along with safety concerns, a number of European countries are advising people to get the first dose of adenovirus-based ChAdOx1 (AstraZeneca) COVID-19 vaccine from Oxford, and a second dose of another vaccine. Surprisingly, several studies have shown that a mixed vaccine approach, in which people receive different COVID-19 vaccines in a first and second dose, induces a strong immune response to SARS-CoV-2 [48, 49].

3.4 Messenger RNA (mRNA) COVID-19 vaccines

Messenger RNA (mRNA) vaccines utilize the host's cellular machinery to synthesize harmless pieces of S protein, recognized by the immune system which produces specific antibodies and a cellular immune response (Figure 6) [50]. The mRNA vaccine does not use a live virus; therefore, it does not cause any infection after vaccination. The extremely unstable characteristics of negatively charged mRNA requires encapsulation in a delivery vehicle for entry into target cells. As an excellent delivery route for mRNA vaccines, lipid nanoparticles (LNPs) have demonstrated successful delivery of small molecules, such as mRNA [51]. Both the BNT162b2 (Pfizer-BioNTech) and mRNA-1273 (Moderna) mRNA COVID-19 vaccines consist of nucleoside-modified mRNAs encoding mutant forms of the full-length Spike protein, also employing a promising vector PEGylated LNP as delivery system. Specifically, Pfizer-BioNTech mRNA vaccine codes for membrane-anchored, full-length S protein with 2 proline substitutions within the central helix; while Moderna COVID-19 mRNA vaccine codes for full-length S protein modified with 2 proline substitutions within the heptad repeat 1 domain (S-2P) [52]. Both of these

modifications (K986P and V987P) lock S in an antigenically preferred prefusion conformation.

Moreover, the mRNA components of the vaccine need to have a 5′-UTR to load ribosomes efficiently onto the mRNA for translation initiation, optimized codon usage for efficient translation elongation, and optimal stop codon for efficient translation termination. Both mRNA vaccines have modulated 5′ and 3′ untranslated sequences to optimize mRNA stability and translation efficiency and all uridines are replaced by N1-methylpseudouridine (m1Ψ) to further increase RNA stability and to reduce innate immune responses.

The Moderna COVID-19 mRNA is encapsulated in an LNP composed of four lipids: Lipid SM-102 (heptadecan-9-yl 8-[52] octanoate), Cholesterol, 1,2-distearoyl-sn-glycero-3-phosphocholine (DSPC), and 1,2-Dimyristoyl-rac-glycero-3-methoxypolyethylene glycol-2000 (PEG2000 DMG). Similarly, Pfizer-BioNTech utilizes formulations of ((4-hydroxybutyl) azanediyl) bis (hexane-6,1-diyl) bis (2-hexyldecanoate) (ALC-0315),2- [(polyethylene glycol)-2000]-N, N-ditetradecylacetamide (ALC-0159), 1,2-Distearoyl-sn-glycero-3-phosphocholine (DSPC), and Cholesterol. The WHO announced that the Pfizer-BioNTech COVID-19 vaccine BNT162b2 is 95% effective against symptomatic SARS-CoV-2 infection and Moderna COVID-19 (mRNA-1273) was approximately 94.1% effective in preventing COVID-19.

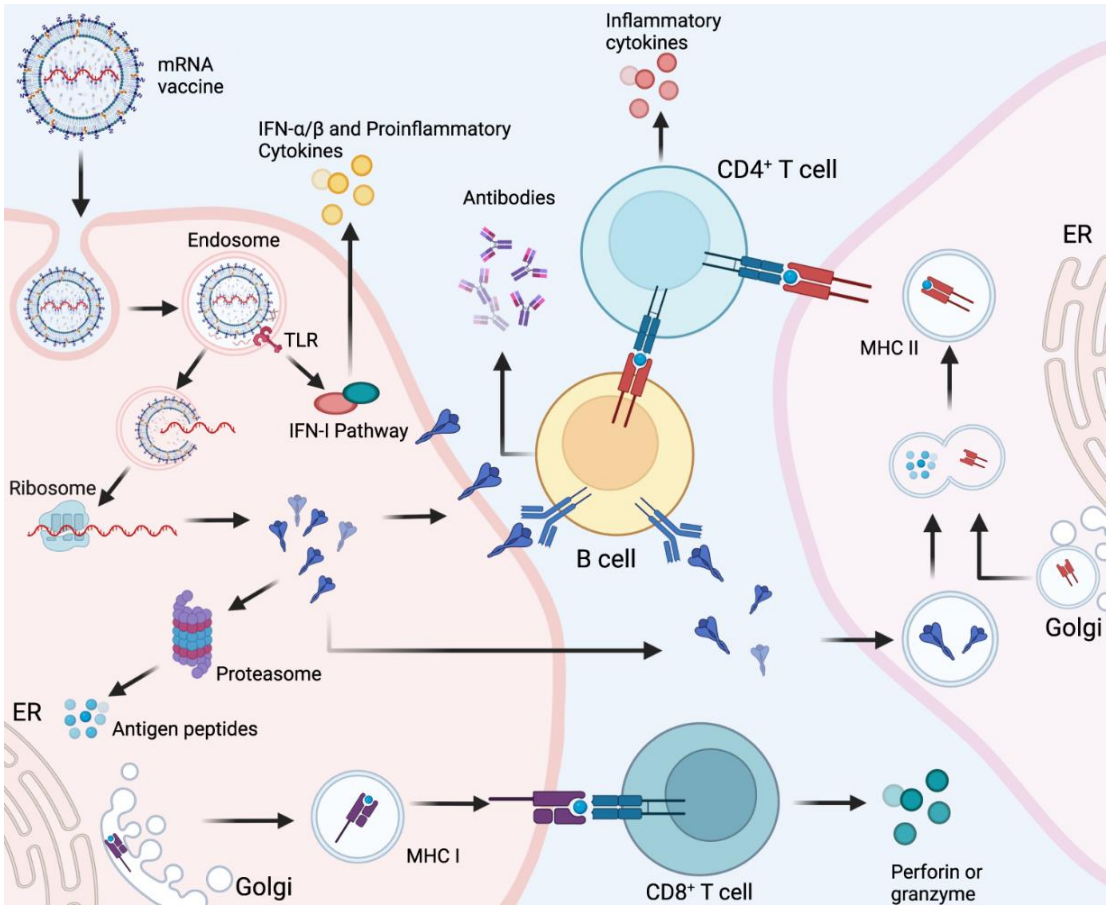

Figure 6: Cellular and humoral immune responses induced by messenger RNA (mRNA) vaccine. mRNA delivered in an mRNA vaccine enters cells by endocytosis and, after release from the endosome, is translated into protein by ribosomes. Translated proteins can then activate the immune system primarily in two ways: i) proteins are degraded by the proteasome into peptides subsequently presented as antigens on the cell surface by major histocompatibility complex (MHC) class I molecules which bind to the T cell receptor (TCR) to activate CD8+ T cells to kill infected cells through the secretion of perforin and granzyme; ii) proteins secreted extracellularly are engulfed by antigen-presenting cells (APCs) and degraded into peptides subsequently presented on the cell surface by MHC class II molecules for recognition by CD4+ T cells, which can activate both the cellular immune responses by secreting cytokines and the humoral immune responses by co-activating B cells. In addition, single-stranded RNA and double-stranded RNA delivered in mRNA vaccines bind to Toll-like receptor (TLR) in the endosome to activate the antiviral innate immune responses via the production of type-I interferon (IFN-I) which results in the induction of several IFN-1-stimulated genes involved in antiviral innate immunity, in a mechanism known as the self-adjuvant effect of a sequence-engineered mRNA [50].

3.5 DNA COVID-19 vaccine

DNA vaccines are referred to as the third-generation vaccines, which use plasmid DNA as a vector to deliver genes encoding target antigens into host cells. DNA vaccines present a range of advantages, they are stable in transportation and storage, inexpensive, easy to manufacture and safe. A major advantage of DNA vaccination is the ability to induce wider range of immune response types, not only humoral immune responses but also cellular immunity. In 1990, Wolff, J A *et al*. reported that the injection of naked plasmid DNA into murine skeletal muscle *in vivo* results in the transgene expression for up to two months [53]. This research permitted the rapid advances in DNA vaccine development. However, DNA vaccines have been shown to be effective in small animals, while the effect is less pronounced in primates [54]; such intrinsic low immunogenicity remains a hurdle to overcome. Efforts to improve DNA vaccine efficacy have focused on optimizing delivery methods using gene guns or electroporation (EP); targeting immune effector cells; and using potent adjuvants. Ballistic delivery (gene gun) to the skin is the most effective way for delivering DNA vaccines [55, 56]. Recombinant DNA technology allows the manipulation of DNA sequences to achieve genetically engineered DNA plasmids in which the cDNA encoding the antigen is under the transcriptional control of a strong mammalian promoter, that ensures the antigen expression *in vivo.* After a DNA vaccine enter mammalian cells, it needs to reach the nucleus for antigen transcription; translation will occur then in the cytoplasm to obtain the desired antigen (Figure 7).

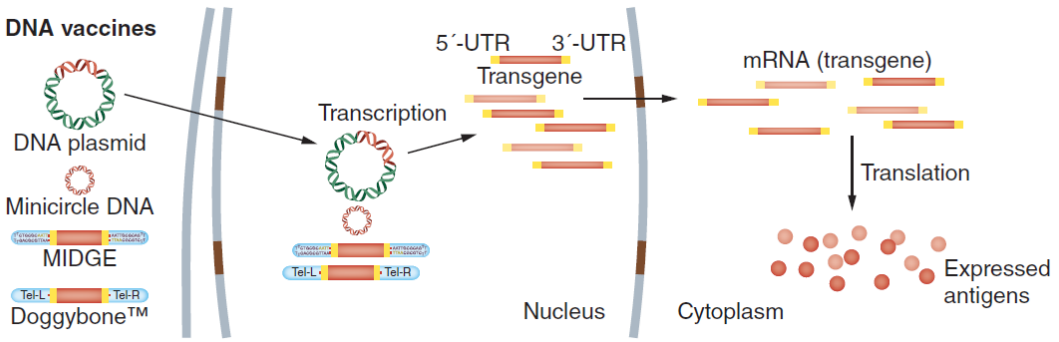

Figure 7. Antigen expression by DNA vaccines. The DNA construct encoding the transgene (vaccine antigen) translocates to the nucleus, where the transcription to mRNA takes place. Produced mRNAs are then delivered to the cytoplasm to ensure efficient translation of the vaccine antigen [57].
MIDGE: Minimalistic, immunologically defined gene expression.

Direct transfection of APC permits the host-synthesized antigens to activate the CD8+ cytolytic T lymphocytes (CTL). In case myocytes or epithelial cells are transfected, they produce and release the antigen. Dendritic cells take up these materials and present antigens preferentially via MHC II to CD4+ T helper cells in draining lymph nodes. The antigen-specific CD4+ T helper cells can induce humoral immune response when the B cells recognize directly the protein antigen (Figure 8) [57]. Thus, the antigen encoded by the DNA vaccine can be presented by both MHC class I and class II molecules, for the proper induction of the adaptive immunity [58, 59]. Furthermore, the bacterial DNA itself can stimulate the innate immune response thanks to the presence of a specific hypomethylated CpG motif which directly interacts with Toll-like receptors (TLRs) expressed on innate immune cells. Thus, DNA vaccines can be administered without adjuvants.

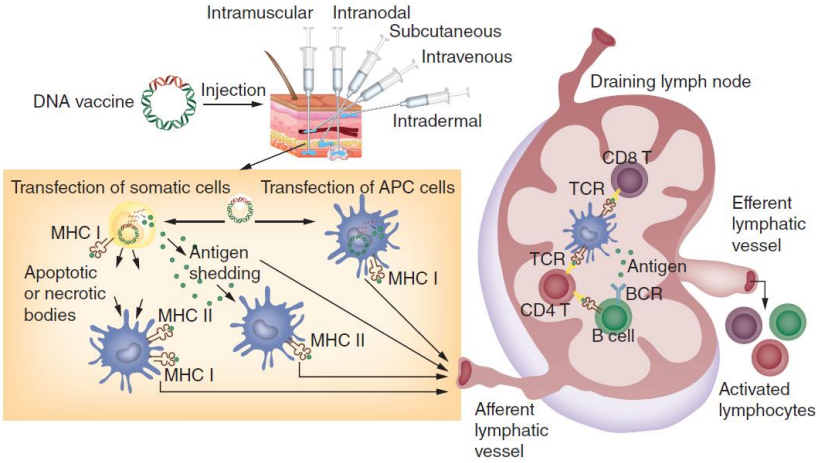

Figure 8. Induction of adaptive immune responses by DNA vaccines. DNA vaccines are administered by multiple routes. The injected DNA enters the somatic cells and/or APCs to produce target antigens, which are the subject of immune surveillance by both MHC class I and class II molecules of APCs. Following the presentation of antigens, activated APCs travel to the draining lymph nodes to present antigenic peptides to CD4 and CD8 T cells. This interaction allows activation and expansion of T cells, as well as antibody-producing B cells. Both humoral and cellular immune responses are induced to trigger a robust response against the target antigens [57].
APC: Antigen-presenting cell; BCR: B-cell receptor; MHC: Major histocompatibility complex; TCR: T-cell receptor.

Considering that DNA vaccines are more versatile and flexible than the other vaccine prototypes, they can be quickly and easily modified and adapted in response to new variants. Moreover, thanks also to their lower cost of production, they might be the most potential vaccine type in pandemic situation to achieve global immunization.

There are currently 16 candidate DNA vaccines in clinical trials for COVID-19, as shown in the table below (Table 3).

Table 3. Overview of clinical trials of DNA vaccines against COVID-19 based on WHO reports as of 21 October 2022. Available at: https://www.who.int/publications/m/item/draft-landscape-of-covid-19-candidate-vaccines

DNA vaccines	Developer	Status	Administration	Doses	Number of doses	Schedule
Zydus Cadila: ZyCoV-D	International Vaccine Institute; Coalition for Epidemic Preparedness Innovations; Inovio Pharmaceuticals	Approved	Needle-free ID (PharmaJet®)	2 mg	3	0+28+56
Inovio: INO-4800 (Clinical trial registration number, ISRCTN15779782)	International Vaccine Institute; Coalition for Epidemic Preparedness Innovations; Inovio Pharmaceuticals	Phase III	ID followed by EP using CELLECTRA® 2000 device	1 mg	2	0+28
AnGes AG0302-COVID19 (Clinical trial registration number, NCT04655625)	AnGes, Inc.; Japan Agency for Medical Research and Development	Phase II/III	IM	2 mg	2	0+14 or 0+28
Genexine: GX-19 (Clinical trial registration number, NCT05067946)	Genexine, Inc.; PT Kalbe Farma TBK	Phase II/III	IM administered via EP	3 mg	2	0+28
Nykode Therapeutics VB10.2210 (Clinical trial	Nykode Therapeutics ASA; Vaccibody AS	Phase I/II	IM	0.3, 1 or 3 mg	1-2	0+21

registration number, NCT05069623)						
Nykode Therapeutics: VB10.2129 (Clinical trial registration number, NCT05069623)	Nykode Therapeutics ASA; Vaccibody AS	Phase I/II	IM	0.3, 1 or 3 mg	1-2	0+21
Takis: COVID-eVax (Clinical trial registration number, EUCTR2020-003734-20, NCT04788459)	Takis S.r.l.; Rottapharm Biotech	Phase I/II	IM	0.5,1 and 2 mg	2	0+28
Entos Pharmaceuticals Inc: Covigenix VAX-001 (Clinical trial registration number, NCT04591184)	Entos Pharmaceuticals Inc.; Aegis Life, Inc.; Canadian Institutes of Health Research (CIHR); Clinical Pharma Solutions Inc; Centre national de recherche et de formation sur le paludisme (CNRFP)	Phase II	IM	/	2	0+14
AnGes: AG0301-COVID19 (Clinical trial registration number, NCT04463472)	AnGes, Inc.; Japan Agency for Medical Research and Development	Phase II	IM	1 and 2 mg	2	0+14
GeneOne Life Science, Inc.: GLS-5310 (Clinical trial registration number, NCT04673149, NCT05085639 and NCT05182567)	GeneOne Life Science, Inc.	Phase I/II	ID (Gene-Derm)	0.6 or 1.2 mg	2	0+56
Providence Health & Services: CORVax12 Vaccine Type: DNA (Clinical trial registration	Providence Health & Services; OncoSec Medical Incorporated	Phase I/II	EP	/	/	0+28

number, NCT04627675)						
University of Sydney: COVIGEN (Clinical trial registration number, NCT04742842)	University of Sydney; Bionet Co., Ltd; Technovalia; Telethon Kids Institute; Institute for Clinical Pathology and Medical Research	Phase I	ID or IM	0.8 or 1mg (ID), 2 or 4 mg (IM)	2	0+28
The University of Hong Kong: SARS-CoV-2 DNA Vaccine (Clinical trial registration number, NCT05102643)	The University of Hong Kong; Immuno Cure 3 Limited	Phase I	IM followed by EP	1 and 2 mg	2	0+21
Symvivo: bacTRL-Spike (Clinical trial registration number, NCT04334980)	Symvivo Corporation	Phase I	Oral	1, 3 or 10 billion colony-forming-units of live Bifidobacterium longum	1	0
Imam Abdulrahman Bin Faisal University Almansour-001 (Clinical trial registration number, 001NCT05171946)	Imam Abdulrahman Bin Faisal University; ICON plc	Phase I	IM	1 mg, 2 mg or 4 mg	3	0+21+42
Scancell: COVIDITY (Clinical trial registration number, NCT05047445)	Scancell Ltd	Phase I	Needle-free ID (PharmaJet Tropis®) or IM (PharmaJet Stratis®)	0.2 mg or 0.8 mg (ID)/1 mg or 4 mg (IM)	2	0+28

EP: Electroporation; ID: Intradermal; IM: Intramuscular; RBD: Receptor-binding domain; S: Spike.

The 20th of August 2021, the first DNA vaccine for human use has been approved in India. It is a DNA vaccine against COVID-19, named ZyCoV-D, and the first needle-free plasmid DNA in the world. The vaccine is delivered in three doses of

2 mg as ID injections using the PharmaJet Tropis® Needle-Free Injection System. ZyCoV-D encodes SARS-CoV-2 spike (S) protein bearing the immunoglobulin E (IgE) signal sequence to promote secretion [60]. In clinical trials, ZyCoV-D was found to be 67% protective against symptomatic infection [61] and 100% effective at preventing moderate disease [60].

INO-4800, a synthetic DNA-based vaccine candidate, contains plasmid pGX9501 encoding the full length of the SARS-CoV-2 spike glycoprotein. The vaccine is a two-dose regimen (2 mg per dose) on days 0 and 28, administered by ID injection followed by EP using the CELLECTRA® 2000 device. INO-4800 is a non-frozen product that can be stored for more than 4 years at normal refrigerated temperatures, stable for more than one year at room temperature (RT), and more than 1 month at 37°C, showing great stability [62]. INO-4800 received FDA authorization for Phase III clinical trials in the United States on September 11, 2021. The vaccine has demonstrated its safety profile and was well tolerated in 38 participants with excellent immunogenicity by eliciting either or both humoral or cellular immune responses in phase I clinical trials [63]. Moreover, the immune response is durable for 6 months after the second dose, and a significant increase in the immune response was observed in 120 age-stratified healthy adults after receiving the booster shot [64]. In phase II clinical trials, INO-4800 maintained overall safety, tolerability and immunogenicity in a large population (approximately 400 subjects). Important finding was that neutralizing antibody levels and T-cell immune responses appeared to be higher in subjects who received the 2 mg dose than in subjects who received the 1 mg dose. Therefore, the 2 mg dose was selected to advance the Phase III efficacy evaluation [65]. Strikingly, T cell responses are consistently maintained against VOCs (including B.1.351 and P.1), suggesting the strong ability of INO-4800 to maintain one or both cellular and humoral immune responses even against emerging SARS-CoV-2 variants [66].

4. Delivery systems for DNA vaccines

Proper vaccine administration/delivery is a key factor in ensuring successful vaccination. Injections are the most common way of delivering vaccines. Classical methods of vaccine delivery are intramuscular (i.m.), intradermal (i.d.), and subcutaneous (s.c.) injections, targeting mainly myocytes and keratinocytes, as well as APCs located near the injected side and efficiently able to be drained to lymph nodes [67]. In DNA vaccination, it is critical to successfully deliver the DNA vaccine to the host's APC cells, where the foreign antigenic protein is expressed, processed, and presented in the context of both MHC class I and class II molecules to the immune system [58]. The table below shows the advantages and disadvantages of commonly used DNA vaccine delivery methods (Table 4). In addition to local intramuscular or intradermal injection, other delivery routes, including gene gun delivery, jet delivery, nanoparticle delivery, etc., have demonstrated to increase DNA uptake *in vivo* (Figure 9) [68]. In addition, adaptive electroporation technology increases transformation efficiency over needle and syringe delivery routes [69].

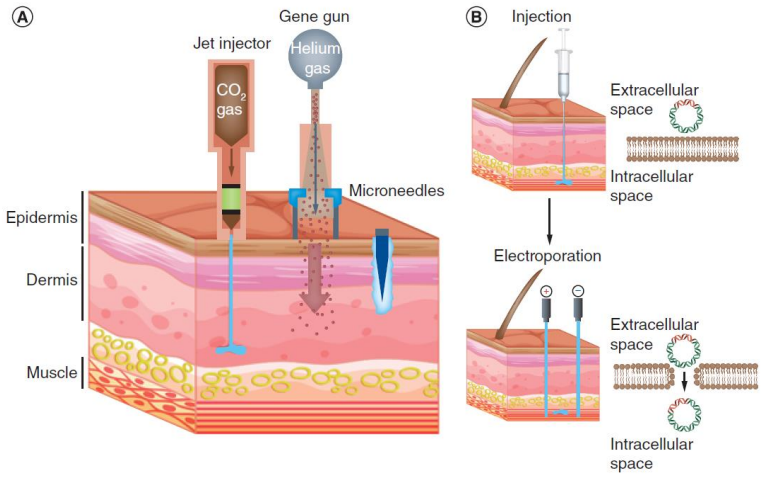

Figure 9. Overview of physical DNA vaccine delivery technologies. (A) Delivery of DNA vaccines into skin compartments using gene gun, jet injector and microneedles. These physical methods allow for delivery of DNA vaccines into the epidermis, dermis and subcutaneous compartments by providing enhanced efficacy and great safety than conventional needle methods. (B) The use of *in vivo* electroporation enhances the cellular uptake of injected DNA across the cell membrane [57].

Table 4. Advantages and disadvantages of commonly used DNA vaccine delivery systems.

Delivery methods	Advantage	Disadvantage
Needle injection (i.m.)	▪ Activate Th1 immune response ▪ pDNA spreads rapidly throughout the body	▪ Muscle pain
Electroporation (i.d, i.m.)	▪ High level of immune response ▪ Long duration of immune response	▪ Possible risk due to the high voltage
Gene gun (i.d.)	▪ DNA bombarded directly into cells ▪ A small amount of DNA needs to be injected	▪ Requires inert particles as carrier ▪ Low integrity of delivered DNA
Jet injection (i.d.)	▪ No particles required ▪ DNA can be delivered to cells mm to cm below skin surface	▪ Significant shearing of DNA after high-pressure expulsion ▪ Requires large amounts of DNA (up to 300 μg) ▪ Risk of cross-infection
Liposome-mediated delivery	▪ High levels of immune response can be generated ▪ Can increase transfection of intravenously delivered pDNA ▪ Intravenously delivered liposome-DNA complexes can potentially transfect all tissues ▪ Intranasally delivered liposome-DNA complexes can result in expression in distal mucosa as well as nasal muscosa and the generation of IgA antibodies	▪ Toxicity ▪ Ineffectiveness in serum ▪ Risk of disease or immune reactions

4.1 Intramuscular injection

Since 1990, intramuscular delivery of DNA vaccine successfully elicited an immune response and have become the most common method for immunization. The West Nile virus (WNV) vaccine was the first DNA vaccine administered in two intramuscular injections, was licensed for use in horses in 2005 [70]. There is another DNA vaccine that was approved in 2005 against infectious hematopoietic necrosis virus (IHNV) in salmon: the IHNV DNA (APEX-IHN®) vaccine, which encodes a viral glycoprotein and is administered by intramuscular injection [71]. Although i.m. injection yielded promising results in animals, naked plasmid DNA alone produces a low-specific immune response and was unsuccessful in human clinical trials.

To overcome these drawbacks, viruses which can infect mammals naturally were considered, once properly engineered, as an effective tool for gene delivery [72]. Viral entry occurs through the interaction of surface proteins on the viral particle with the

corresponding receptors on target cells, thereby triggering receptor-mediated endocytosis, protecting genetic material from degradation [73]. Despite viral vectors can induce high immunogenicity and long-lasting immune responses without the use of adjuvants, the safety concern is that the host's immune response may be directed against the vector rather than the antigen carried by the vector. As a result, viral transfection has not been considered the gold standard for gene delivery for many years.

4.2 Intramuscular electroporation

Electroporation (EP), the most appropriate physical delivery system for DNA vaccines, is the process of using an electric pulse to transfect cells with DNA (Figure 10). EP requires only purified plasmid DNA, that can be prepared quickly without the need to generate viral particles. Electroporation following intramuscular injection has been successful for *in vivo* [74] DNA delivery to tissues. Of note, EP mediated DNA delivery appears to have a dramatic impact on vaccine immunogenicity and efficacy, nearly 1000-fold enhancement of DNA delivery and antigen expression compared to naked DNA injection alone [75]. This promising delivery system is not only restricted to the preclinical phase, but now the system has been optimized to achieve enhanced immune responses also in human clinical trials [76]. On the other hand, potential cell damage and nonspecific transport of molecules into and out of the cell are the main drawbacks associated with EP. These limitations might be overcome by using advanced gene delivery technologies.

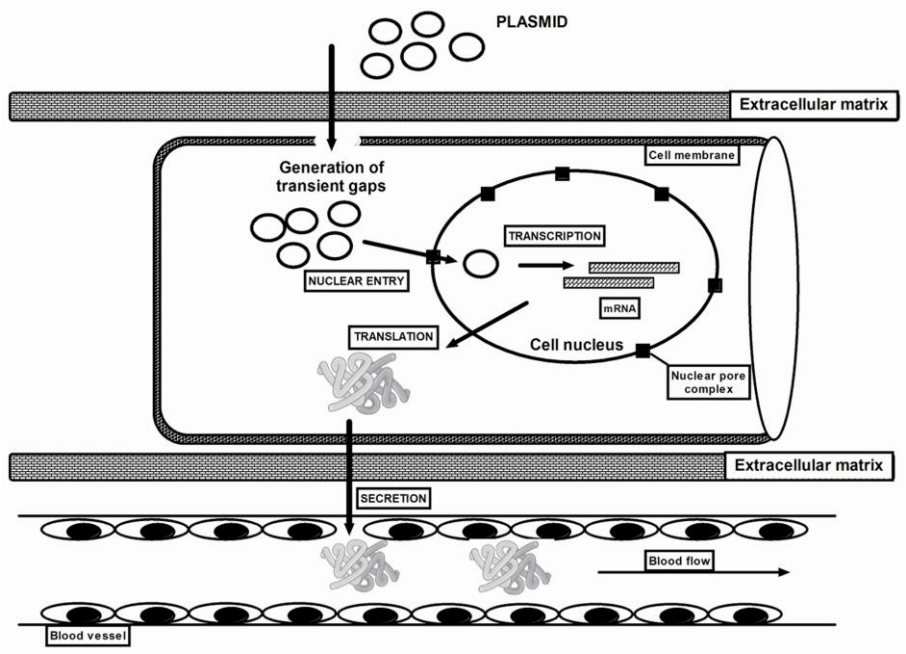

Figure 10. Schematic diagram of proposed plasmid DNA delivery with the use of electroporation. Plasmid DNA must overcome barriers, including extracellular matrix, cell membrane, cytoplasm and nuclear membrane before reaching the nucleus, where it is transcribed [77].

4.3 Gene gun

The gene gun, one of the physical delivery methods developed in 1987, laid the groundwork for DNA vaccine delivery [78]. This biolistic particle delivery system is an efficient and rapid tool for delivering foreign DNA (transgenes) into cells to achieve gene transfection. Particle-mediated epidermal delivery (PMED) system uses a high-pressure inert helium gas to fire DNA-coated gold microbeads into the epidermis (Figure 11). Regarding gold, it can be ionized to be positively charged so that it interacts well with negatively charged DNA. Efficacy and simplicity are representative advantages of gene gun delivery. When the transgene is administered by biolistic methods, its expression level is higher than intramuscular injection alone. A small amount of DNA is sufficient to trigger strong gene expression [22]. This delivery method was initially mainly used in plant cells [79, 80] and is now applied in animals and humans. Besides all these advantages, the efficiency of biolistic transfer may depend on cell type, cell growth conditions and setting appropriate parameters [81].

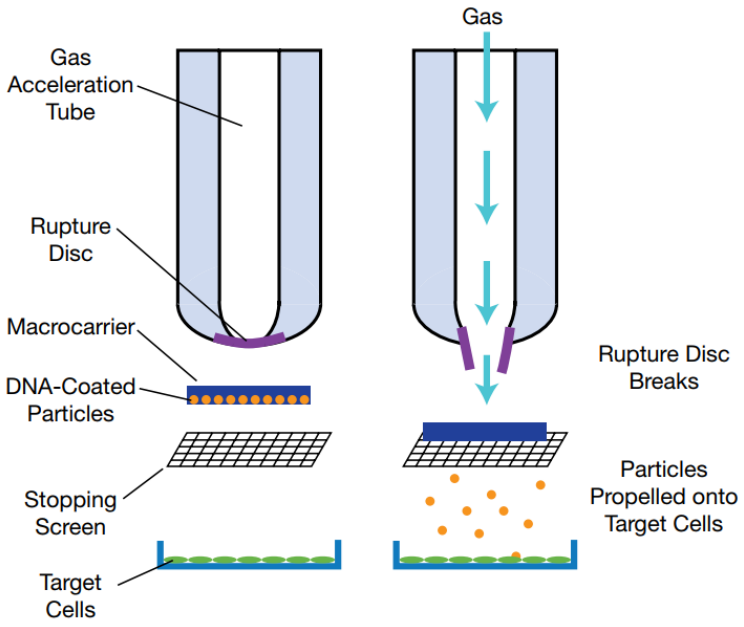

Figure 11. Gene gun or particle bombardment delivery device can deliver transgenes to cells. First, a macrocarrier is loaded with DNA-coated heavy-metal particles. Within the gene gun, gas pressure builds up against a rupture disk. The pressure eventually reaches a point that causes the rupture disc to break, and the pressure burst propels the macrocarrier into a stopping screen. The DNA-coated particles are propelled through the screen and hit the target cells [82].

4.4 Jet injection

Jet injection is a needle-free physical delivery method that uses a high-pressure jet of liquid medication to penetrate the skin and deliver a drug or vaccine under the skin. Various candidate DNA vaccines against SARS-COV-2 currently in clinical trials have opted to use needle-free jet injection systems. Two Scancell: COVIDITY DNA vaccines against SARS-COV-2, SCOV1 and SCOV2, delivered either by ID injection using the PharmaJet Tropis® Needle-Free Injection System or IM delivery using the PharmaJet Stratis® System, are currently in Phase I clinical trials and has generated excellent T-cell and antibody responses, PharmaJet chief executive announced on September 14, 2021. The use of jet injector as a DNA delivery system is not limited to COVIDITY DNA vaccine, but also applies to ZyCoV-D DNA vaccine delivery, the world's first FDA-approved DNA vaccine for emergency use. PharmaJet Tropis® injector that significantly reduces any side effects has been applied in ZyCoV-D DNA vaccine [42].

4.5 From liposomes to lipid nanoparticles (LNPs) mediated delivery

Liposome-mediated delivery, a chemical approach, is a well-known drug delivery systems applying nanotechnology with safety and compositional versatility for human use [83]. Liposomes were first discovered in the 1960s by the British hematologist Dr. Alec D. Bangham and collaborators at the Babraham Institute, University of Cambridge, and first reported in 1964 [84]. Liposomes are composed of hydrophobic lipid tail and hydrophilic lipid head, which constitute phospholipid bilayers (Figure 12). An aqueous fluid filled hydrophilic interior chamber surrounded by hydrophobic lipid hairs forms a spherical pore and hydrophilic tails face each other to form the hydrophobic region. This amphiphilic characteristic enables the loading of hydrophilic and/or hydrophobic molecules. Liposomes can be anionic, cationic, zwitterionic or nonionic depending on the overall charge carried by the polar head group [85].

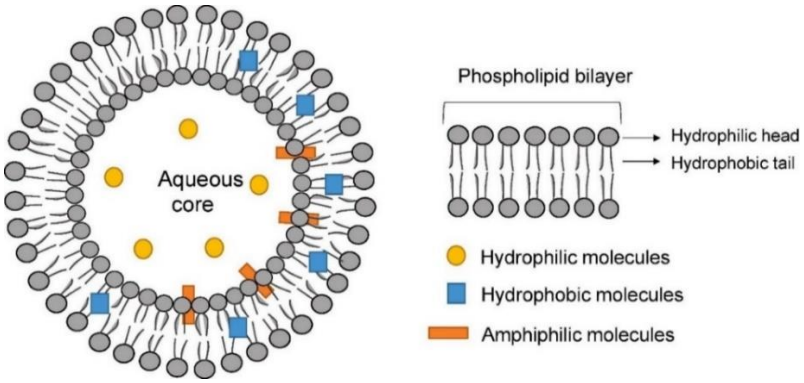

Figure 12. Representation of the general structure of liposomes [86].

Liposomes are classified based on their structures; 1) Multilamellar vesicles (MLVs), consists of many concentric double layers; 2) Unilamellar vesicles (ULVs), composed by a single layer lipid; 3) Oligolamellar vesicles (OLVs), comprised of 2 to 5 concentric bilayers. ULVs are further divided according to their size. Small unilamellar vesicles (SUVs) are typically below 100 nm in size, medium unilamellar vesicles (MUVs) are between 40 and 80 nm in size, large unilamellar vesicles (LUVs)

and giant unilamellar vesicles (GUVs) are larger than 100 nm (but below 1 μm), and 1 μm or larger, respectively [87]. ULVs containing a large aqueous core are more suitable for encapsulating water-soluble drugs. Contrastingly, MLVs, contain several concentric lipid bilayers befitting to carry lipid-soluble drugs [88].

Liposome can be categorized either into cationic liposomes and anionic liposomes. Thanks to the opposite surface charges, cationic liposomes can complex with negatively charged DNA molecules by electrostatic interaction to form a stable DNA-liposome complexes (lipoplexes). Neutral liposomes are widely used transfection helpers of cationic liposomes due to their nontoxicity and high stability in serum [89]. The neutral helper lipid 1, 2-dioleoyl-sn-glycero-3-phosphocholine (DOPC) or 1,2-dioleoyl-sn-glycero-3-phosphoethanolamine (DOPE) are mostly used neutral co-lipids for cationic liposomes to enhance transfection efficiency [90]. The overall net positively charged lipid complexes helps to bind negatively charged cell membrane, resulting in the lipoplexes entering the cells with high efficiency.

DNA-liposome complexes are internalized by targeted cells mainly by endocytosis (Figure 13). Then, DNA can escape from endosomes thanks to the fusion between lipoplexes and endosomal membranes, enabling gene transfection.

Cationic lipids are the most common class of molecules considered for liposome-mediated gene delivery. However, storage instability and relatively high levels of cytotoxicity both *in vitro* [91] and *in vivo* [92] are limitations that require improvement. In addition to cationic liposomes, anionic liposomes are also used as DNA carriers. Anionic liposomes exhibit higher stability in solution than cationic liposomes, and generally require divalent cations such as Ca^{2+}, Mg^{2+}, Mn^{2+}, and Ba^{2+} to neutralize mutual electrostatic repulsion. Among them, use of Ca^{2+} showed higher transfection efficiency due to its higher DNA binding affinity [93]. Anionic lipoplexes consisting of physiologically safe components for plasmid DNA delivery, including anionic lipids, divalent cations, and plasmid DNA, thus being explored as a potential gene delivery vehicle. However, inefficient DNA compaction and inadequate studies

on cytotoxicity are the drawback that needs to be overcome. Liposomes generally exhibit low DNA or mRNA encapsulation efficiency, which makes them impractical for *in vivo* delivery of nucleic acid vaccines.

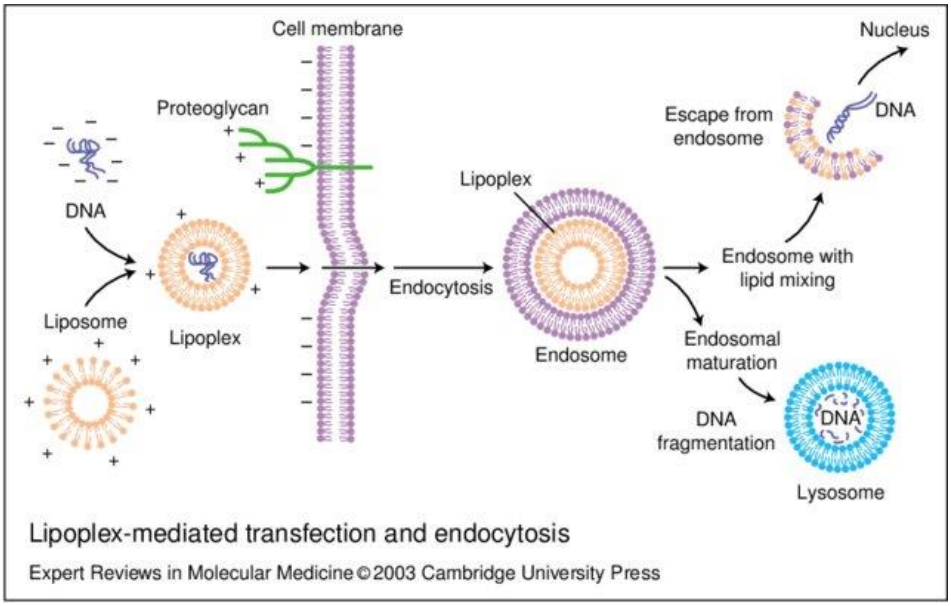

Figure 13. Lipoplex-mediated transfection and endocytosis. Cationic lipids forming micellar structures called liposomes are complexed with DNA to create lipoplexes. The structures fuse with the cell membrane, at least sometimes after interactions with surface proteoglycans. The complexes are internalised by endocytosis, resulting in the formation of a double-layer inverted micellar vesicle. During the maturation of the endosome into a lysosome, the endosomal wall might rupture, releasing the contained DNA into the cytoplasm and potentially towards the nucleus. DNA imported into the nucleus might result in gene expression [94].

Using the same type of components of lipoplexes, but mixing lipids and DNA by microfluidic technology (Figure 14), it is possible to obtain Lipid nanoparticles (LNPs), that can be considered advanced non-viral drug delivery systems, characterized by a higher transfection efficiency with respect to lipoplexes. LNPs have been initially used to encapsulate small non-coding RNAs. In particular, the first LNP-encapsulated siRNA drug Patisiran (Onpattro, Alnylam Pharmaceuticals) was approved by FDA in 2018 for the treatment of peripheral nerve disease caused by hereditary transthyretin-mediated amyloidosis (hATTR) [95]. As a new paradigm of delivery, LNPs are easy to formulate, self-assembled, and represents high biocompatibility and bioavailability [96]. The liposome-like structures of LNPs are feasible as vehicles for encapsulating nucleic acids (RNA and DNA). As a result, they

became the most popular non-viral gene delivery systems, and their importance is particularly evident in the recent Pfizer and Moderna COVID-19 vaccines that use LNPs as a vital component of mRNA vaccines. LNPs are generally composed of four main components: ionizable cationic lipids, that facilitate endosomal escape, phospholipids and cholesterol as stabilizers and PEGylated lipids act as a steric barrier to prevent aggregation during storage as well as increase bloodstream circulation lifetime [97]. LNPs offer many advantages over previous lipid-based nucleic acid delivery systems, including 1) High nucleic acid encapsulation efficiency; 2) Improved penetration into cells to deliver genetic materials followed by massive DNA release and potent transfection; 3) Low cytotoxicity. To surpass current technological paradigms, the development of targeted LNPs holds great promise. As mentioned above, DNA vaccines have shortcoming of relatively low immunogenicity. At this juncture, LNPs, a versatile delivery method in the limelight, as a potentially excellent candidate to overcome these limitations to deliver DNA vaccines to APC with improved transfection efficiency and enhanced immunogenicity. LNP formulated with DLin-KC2-DMA ionizable cationic lipid to encapsulate plasmid DNA, showed significant levels of DNA transfection efficiency and exhibited significantly higher *in vivo* protein production [98]. Yao *et al*. explored dendrigraft poly-l-lysines (DGL)-PEG-LNP as a gene vector to carry plasmid DNA encoding inhibitor of growth 4 (ING4) as a therapeutic gene; it possess excellent blood-brain barrier crossing efficiency and an anti-glioma effect in nude mice [99]. Elevated neutralizing antibodies produced in both rabbits and transchromosomic (Tc) bovine injected with LNP-formulated Andes virus or Zika virus DNA vaccines are over the unformulated vaccine [100]. Such promising results from numerous preclinical trials [101-104] point to LNPs to be effective DNA vaccine carrier, paving the way for the possibility of entering human clinical trials and further approval for their use in the near future. LNPs mediated gene delivery has opened up a new era for nucleic acid vaccine delivery routes.

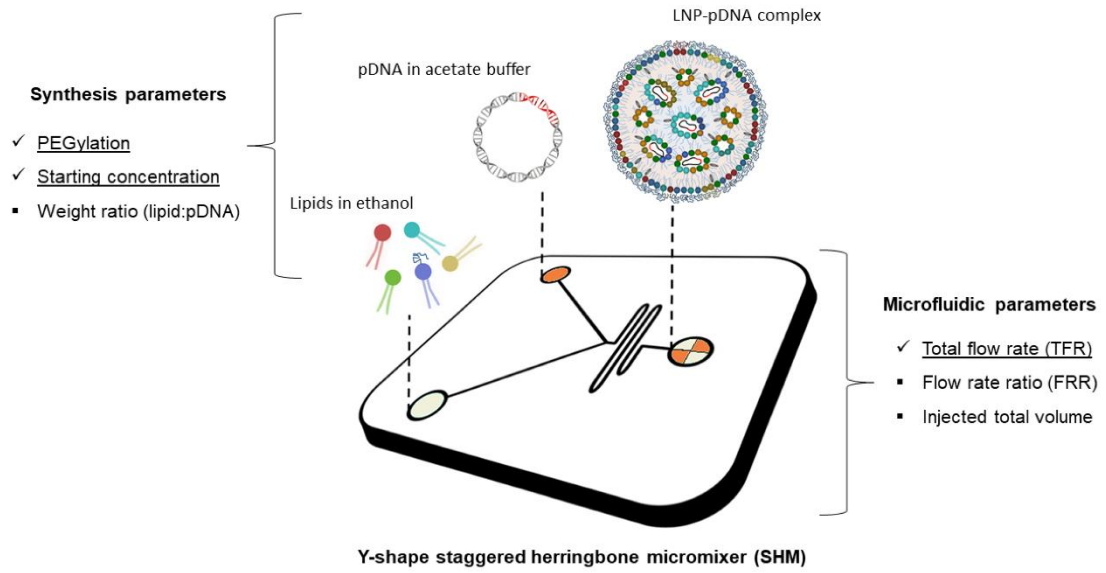

Figure 14. Schematic of lipid nanoparticle-plasmid DNA (LNP-pDNA) complex formulation strategy employing the staggered herringbone micromixer (SHM). Lipids in ethanol are injected in one inlet, while pDNA dissolved in acetate buffer solution is injected in the other inlet. The two solutions meet at the Y-junction of the SHM and undergo a chaotic mixing through the herringbone structure. This phenomenon leads to an increase of lipid solution polarity that generates LNPs encapsulating pDNA. On the sides of the image, two main categories of influential manufacturing factors are reported, i.e., synthesis and microfluidic parameters [105].

5. Age-related immune responses to vaccines

Immune memory is mediated by B- and T-cells and is important for long-term defense against pathogens. B cells and T follicular helper (T_{FH}) cells are responsible for producing high-affinity antibodies while inducing durable immune memory cells for effective recall immunity following reinfection [106]. In particular, T follicular helper (T_{FH}) cells indicate the maturation of humoral immune responses and the establishment of a repertoire of specific memory B cells [107]. Following vaccination, naïve vaccine-specific T cells will be greatly expanded while differentiating into two distinct subset of short-lived effector cells or memory precursor cells (MPECs). Among them, only a small subset of MPECs maintained stably to form long-lived memory T cells provide protection against infections (Figure 15). Therefore, in addition to the B cell receptor epitopes that play a decisive role in the ideal vaccine regimen, it also relies heavily on the stimulation of antigen-specific T_{FH} cells.

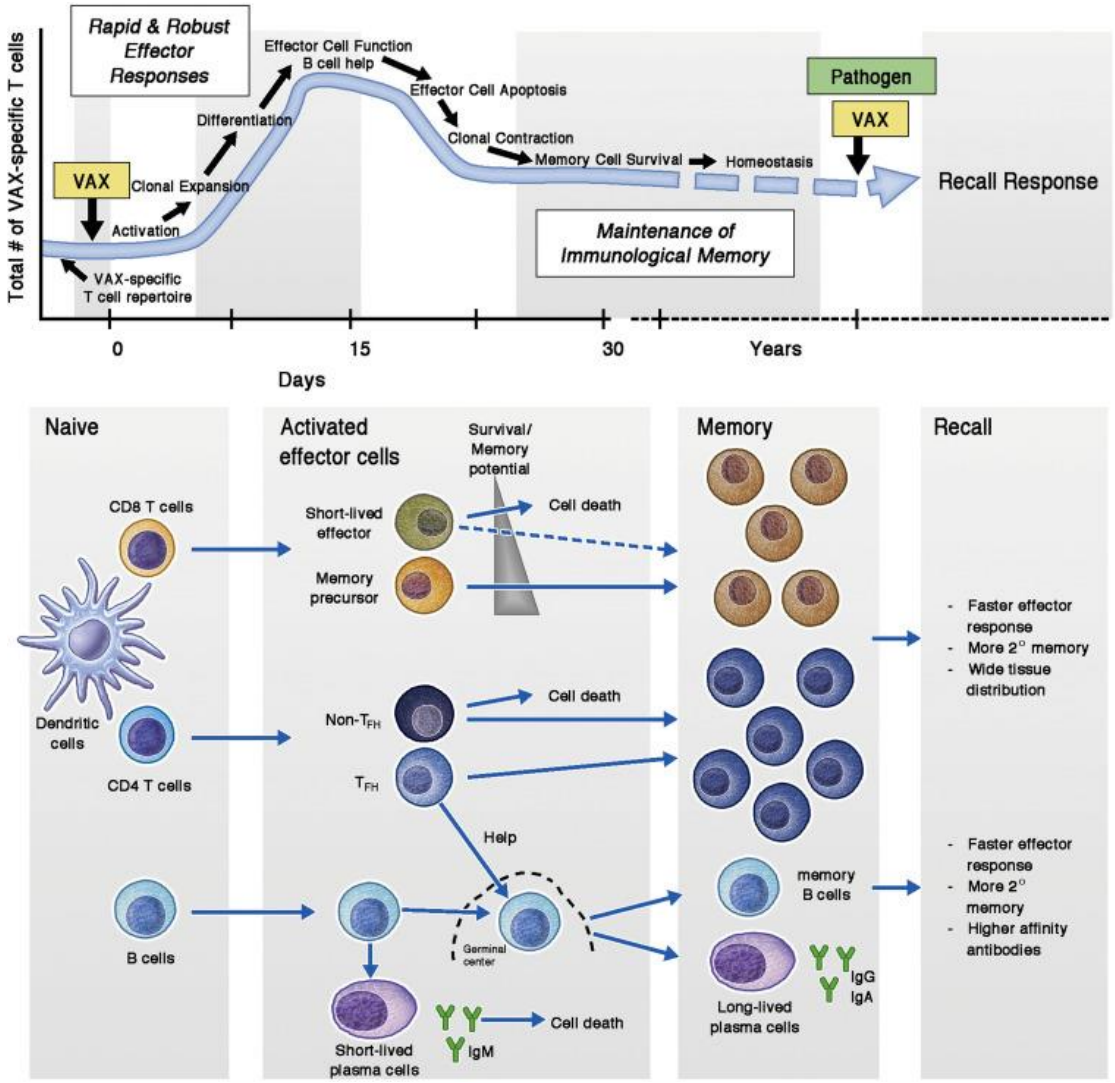

Figure 15. Key features of a primary T-cell response after vaccination. In the human T-cell repertoire, approximately 1 in every 10,000 naive cells will be a vaccine (VAX)-specific cell. Upon exposure to vaccination, these cells become activated through engagement of their TCR, and other costimulatory receptors, and undergo massive clonal expansion. During this expansion phase, activated naive cells differentiate into short-lived effector cells or memory precursor cells (MPECs). T_{FH} cells are generated, likely in a similar manner as MPECs, and provide critical help to B cells for the generation of high affinity vaccine specific antibodies. After resolution of vaccine antigen, most effector cells die. A small subset of MPECs survives to become long-lived memory T cells. These memory cells provide protection against subsequent infection or booster vaccination, possibly for decades, via a higher frequency of vaccine-specific cells, their poised effector state, and potential tissue localization. Recall responses after booster vaccination follow the same scheme, however, starting at higher initial frequency of VAX-specific T cells [106].

Aging is the leading cause of morbidity and mortality in the elderly population. Age-related immune dysfunction (immunosenescence) bears the greatest responsibility. With age, the function of innate and adaptive immune responses is

impaired, making it difficult to build effective long-term immune memory, resulting in a lower ability to respond to infections and vaccinations [108]. Booster shots can effectively re-raise antibody levels. Rescue of weakened immunity by booster doses relies on the ability of the adaptive immune system to maintain immune memory for long periods of time with high functional capacity of memory cells. Different mechanisms may lead to impaired responses to vaccines in elderly. Reasons for reduced recall responses during aging include i) loss of long-term memory, ii) impaired effector responses and iii) poor memory survival (Figure 16).

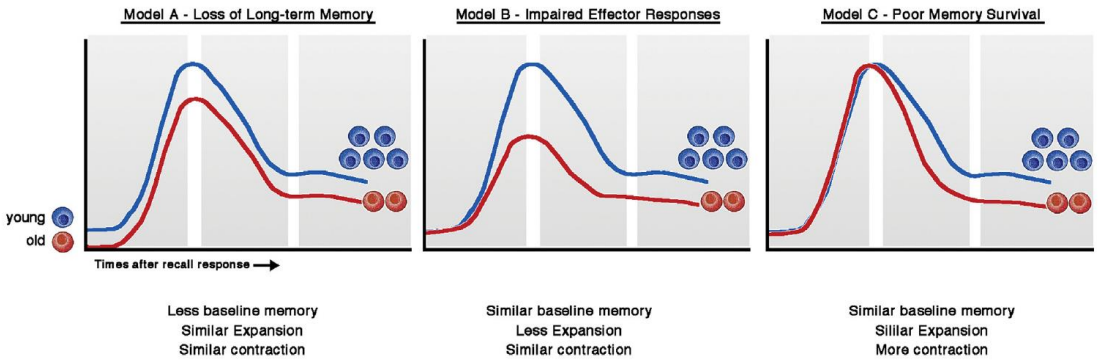

Figure 16. Potential models for reduced recall responses in aging. Loss of recall responses observed in older individuals could be contributed to 3, not mutually exclusive, scenarios: (Model A) reduced frequency of vaccine-specific memory cells for initial recall, (Model B) less expansion of vaccine-specific memory cells during recall, and (Model C) increased contraction, or poor survival, of vaccine-specific memory postrecall [106].

AIM OF THE THESIS

Severe Acute Respiratory Syndrome Coronavirus 2 (SARS-CoV-2) emerged in December 2019 and spread rapidly around the world. Subsequently, the World Health Organization (WHO) declared the COVID-19 outbreak a sixth public health emergency of international concern on 30 January 2020. WHO has classified five SARS-CoV-2 variants of concern (VOC) that pose a serious threat, including three of previously circulating variants of concerns, Alpha (B.1.1.7), Beta (B.1.351) and Gamma (P.1) plus two currently circulating variants of concerns, Delta (B.1.617.2) and Omicron (B.1.1.529).

Vaccines are well-studied methods that not only provide protection against severe syndromes, but also reduce the chance of getting infected. The Spike (S) glycoprotein of the SARS-CoV-2 is an ideal target for vaccine design, because it associates with the human angiotensin-converting enzyme 2 (ACE2) receptor to permit the viral entry. The S protein is made up of two subunits (S1 and S2). The S1 subunit can be further defined with two domains termed the N-terminal domain (NTD) and the C-terminal domain (CTD), that includes the receptor binding domain (RBD).

The high mutational variability of the spike protein (i.e., D614G mutation rate ≈1), might compromise the efficacy of existing COVID-19 vaccines [109]. Thus, the development of safe and effective vaccines, that can be adapted quickly to new SARS-CoV-2 mutants, represent an urgent global health priority.

DNA vaccines are simple circles of DNA, derived from bacterial plasmids, which contain cDNA coding for the target antigen, a strong viral promoter to drive the antigen expression in mammalian cells and a polyadenylation signal for transcription termination [110]. They are versatile and flexible, thus they can be quickly and easily modified and adapted in response to new variants. Moreover, considering the DNA vaccine's higher stability than RNA and proteins and their lower cost of production, they might be easily distributed even in low-income countries. In addition, DNA

vaccines can trigger both cellular and humoral arms of the adaptive immune system and this combined immunity may be more effective than either arm alone. Although DNA vaccines offer distinct advantages over other vaccine prototypes, there is only one DNA vaccine approved to use against COVID-19 in India. The difficulty of DNA vaccine delivery limits its development. Fortunately, with the evolution of technologies, nanotechnology opened a window in the delivery of genes.

Herein, we initially developed two candidate DNA vaccines against SARS-CoV-2; 1) pVAX-S1 encoding the S1 (1-660 aa) subunit of spike (S) glycoprotein and 2) pVAX-S1-TM encoding the S1 subunit of S protein anchored to the plasma membrane through the transmembrane region (TM), that permits the trimerization of the antigenic protein as predicted by *in silico* structure analysis. Facing the rapid spread of mutated viruses, three additional DNA vaccines were specifically conceived against emerging variants: the third vaccine, named pVAX-S1-TM-UK, includes the globally dominant D614G substitution in addition to two UK key mutations (N501Y and A570D) affecting amino acids in the receptor-binding site; the fourth vaccine, named pVAX-S1-TM-IND was generated against the Indian (B.1.617) lineage including the globally dominant D614G substitution in addition to two Indian (IND) key mutations (E484Q and L452R); and the last vaccine named pVAX-S1-TM-INDUK, is a chimeric DNA vaccine deriving from the combination of the UK and IND key mutations (INDUK). The indicated mutations were sequentially introduced into the previously obtained pVAX-S1-TM vaccine according to a site-directed plasmid mutagenesis protocol as described by Liu *et al* [111].

The expression and localization of the SARS-CoV-2 antigens expressed by the vaccines were investigated in transfected cells by immunofluorescence assay using commercial anti-SARS-CoV-2 antibodies. Furthermore, *in vivo* experiments were performed to evaluate the immunogenicity and duration of immune responses of pVAX-S1-TM-D614G and pVAX-S1-TM-INDUK DNA vaccines. Both young/adults and aged C57BL/6 mice used as preclinical models received 100 µg of DNA vaccines

intramuscularly followed by electroporation. The results show that these vaccines were able to elicit significant anti-Spike antibody production in both young and old immunized mice.

Moreover, with the aim to encapsulate our DNA vaccines into LNPs, to overcome the current limitations of electroporation-mediated vaccination, LNP-based delivery systems have been developed and their transfection efficiency and cytotoxicity were verified *in vitro*. The PEGylated lipid nanoparticle LNP15 was selected as the best candidate for gene delivery because LNP15 was most compatible with high transfection efficiency and low cytotoxicity. Therefore, preliminary *in vivo* experiments were performed using a prototype DNA vaccine (pVAX-hECTM) targeting the oncogene HER2, which was encapsulated in LNP15 to evaluate its gene delivery capacity. The encouraging results of the humoral response imply that the LNP15-mediated delivery route is efficient *in vivo* and thus represents an ideal delivery approach for encapsulating our COVID-19 DNA vaccine.

MATERIALS AND METHODS

1. Construction of pVAX-S1 DNA vaccine against SARS-CoV-2

pVAX vector (Invitrogen®, Carlsbad, CA) was chosen as the backbone plasmid for the construction of anti-SARS-CoV-2 vaccines, because it is specifically designed for the development of DNA vaccines and it is approved by FDA for use in humans.

In order to perform a directional cloning of the insert, pVAX plasmid, purified using QIAGEN® Plasmid Purification Maxi Kit according to manufacturer's instructions, was digested with *NheI* and *XhoI* restriction enzymes.

The sequence encoding the S1 region, corresponding to the N-terminal (1-660 aa) of the spike protein of SARS-CoV-2, was amplified by PCR, using pcDNA3.1-SARS2-Spike vector as template (Addgene plasmid # 145032 ; http://n2t.net/addgene:145032; RRID:Addgene_145032) (Figure 17) [112].

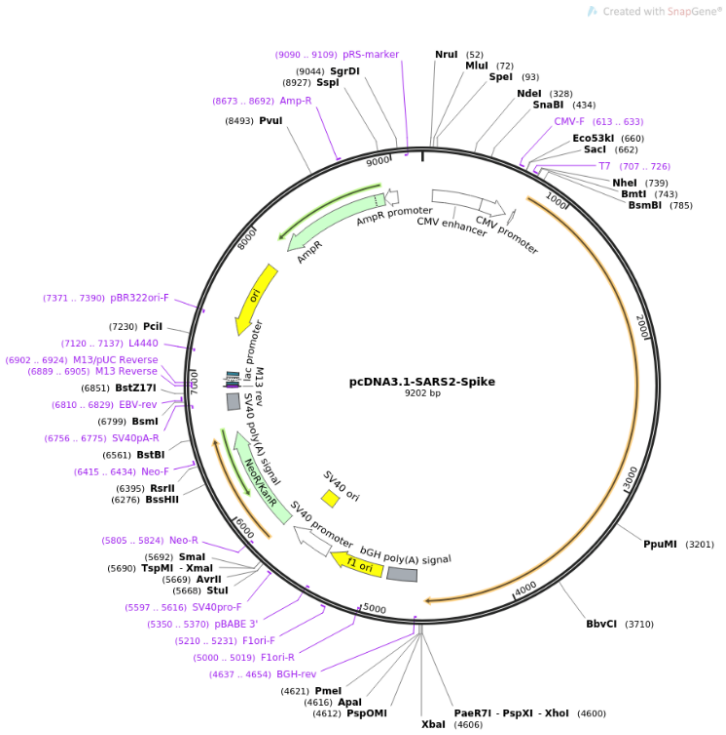

Figure 17. Vector map for pcDNA3.1-SARS2-Spike.

The Phusion™ High-Fidelity DNA Polymerase that, thanks to its proofreading activity (3'→5' exonuclease activity), has a very low error rate, and the primers indicated below:

Forward primer: 5'-ACT CAC TAT AGG GAG ACC CAA GCT G-3'
Reverse primer: 5'-CCG GCT CGA GCT AGT AGG AAT TGT TCA CGT G-3'

The forward primer anneals with a region in the template vector upstream the *NheI* restriction site, that in turn flanks the insert, so that, after the PCR reaction, the amplicon included *NheI* site and thus could be cut with this enzyme. On the contrary, the reverse primer is characterized by a hybridization sequence and by the *XhoI* restriction site at the 5' end (in red), so that it will be incorporated into the PCR product. Four extra bases on the 5' end of the primer assist with restriction enzyme digestion. Between the restriction site and the hybridization sequence, a stop codon (highlighted in green) has been inserted to ensure the proper translation of the S1 protein fragment.

PCR reactions were set up according to the manufacturer's instructions. The PCR product (S1 sequence, 2000 bp) was first purified with HiYield™ PCR Clean-Up Kit (Qiagen, Italy) and then cut with *NheI* and *XhoI*, and eventually used for ligation. The plasmid backbone (pVAX) and the DNA fragment obtained by PCR (S1), digested with the same restriction enzymes (*NheI/XhoI*), were mixed and sealed by ligation reaction to obtain the recombinant vector pVAX-S1. We used Thermo Scientific T4 DNA Ligase, that catalyzes the formation of a phosphodiester bond between juxtaposed 5'-phosphate and 3'-hydroxyl termini in duplex DNA. The ligation reactions were incubated at 22°C for one hour before being used to transform DH5α *E. coli* competent cells by heat shock method.

To identify the colonies containing the recombinant plasmids, the plasmid DNA vectors were isolated from bacterial cultures of different colonies and then analyzed by electrophoresis on 1% agarose gel and their dimension was compared: the recombinant plasmids (about 5000 bp) migrate slower than the empty vector (pVAX: 3000 bp) (Figure 18).

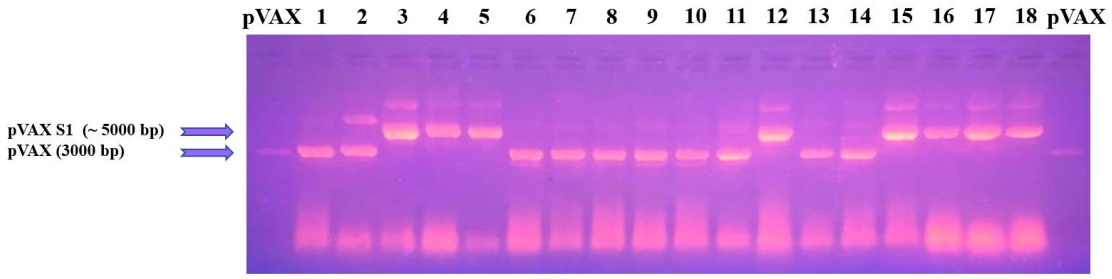

Figure 18. Analysis by agarose gel electrophoresis indicates that clones 3, 4, 5, 12, 15, 16, 17, 18 contained recombinant plasmids.

Moreover, the recombinant plasmids were cut with *NheI* and *XhoI*, to verify the dimension of the insert (S1 length: 1982 bp) once separated from the backbone (pVAX: 3000 bp) (Figure 19).

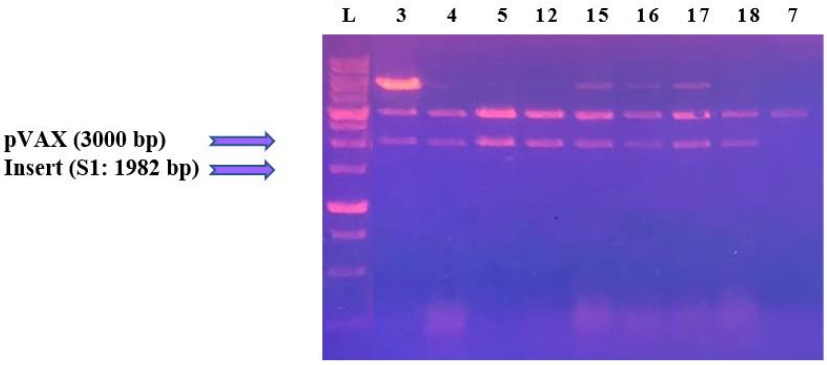

Figure 19. Recombinant plasmids, extracted from the selected clones, were cut with *NheI* and *XhoI* and the digestion product was analyzed by 1% agarose gel electrophoresis.

One of the recombinant pVAX-S1 plasmids was purified using the HiYield™ Plasmid Mini Kit and the sequence of the insert was analyzed (BMR Genomics (Padova)).

Sequencing was performed using the following oligonucleotides:

Primers	Sequence
Forw spike 561-580	5’ GAACCTGCGCGAGTTCGTGT 3’
Forw Spike 1151-1170	5’ CCACCAAGCTGAATGATCTG 3’
Forw spike 1351-1370	5’ TACCTGTACCGCCTGTTCCG 3’
Forw Spike 1751-1770	5’ TCCTGGATATCACCCCATGC 3’
Rev Spike 230-211	5’ TTGGTGCCATTGGTGCCGCT 3’
Rev Spike 1400-1381	5’ TCGCGCTCGAATGGCTTCAG 3’
T7 forward primer	5’ TAATACGACTCACTATAGGG 3’
BGH reverse primer	5’ TAGAAGGCACAGTCGAGG 3’

2. Construction of pVAX-S1-TM DNA vaccine against SARS-CoV-2

To obtain pVAX-S1-TM, the sequences encoding the S1 and TM regions were sequentially cloned into pVAX. First, S1 sequence was amplified (amino acids 1 to 660) using pcDNA3.1-SARS2-Spike plasmid (Addgene) as template and the following primers:

Forward primer (SPIKE-*NheI*): 5'-ACT CAC TAT AGG GAG ACC CAA GCT G-3'
Reverse primer (SPIKE FOR TM-*EcoRI*): 5'-GCG CGA ATT CGT AGG AAT TGT TCA CGT GCT CA-3'

The obtained PCR products were purified by the HiYield™ PCR Clean-Up Kit (Qiagen, Italy), digested with *NheI* and *EcoRI*, and cloned into pVAX cut with the same restriction enzymes.

After transformation, the pVAX-S1 recombinant plasmids were verified by electrophoresis on agarose gel then their dimension was compared: the recombinant plasmids (about 5000 bp), that migrate slower than the empty vector (3000 bp), were identified (Figure 20). One of the pVAX-S1 plasmids was used as a backbone to insert the TM sequence.

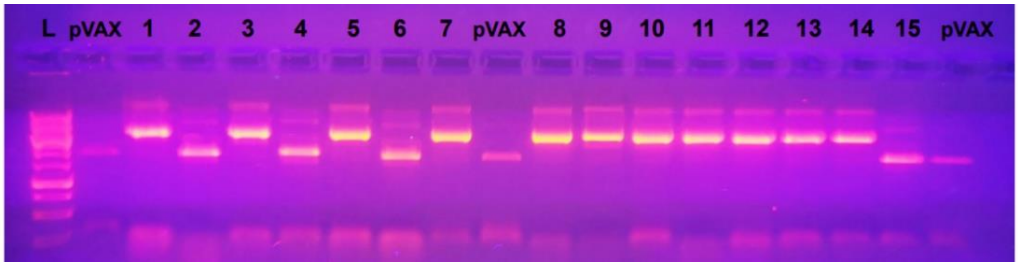

Figure 20. Analysis by 1% agarose gel electrophoresis, indicates that clones 1, 3, 5, 7, 8, 9, 10, 11, 12, 13 and 14 contained recombinant plasmids.

In detail, the sequence encoding the TM region of the S protein of SARS-CoV-2, was obtained by PCR using pcDNA3.1-SARS2-Spike vector (Addgene) as template and the following primers:

Forward primer (SPIKE FOR TM-*EcoRI*): 5'-GCG CGA ATT CTG GTA CAT CTG GCT GGG CTT C-3'
Reverse primer (SPIKE+TM+TAG-*XhoI*): 5'-CCG GCT CGA GCT AAG CGG GAG CGA CCT GGG A-3'

In the reverse primer, between the restriction site and the hybridization sequence, a stop codon (underlined) has been inserted.

The PCR product (TM sequence ~ 200 bp) was purified before to be cut with *EcoRI* and *XhoI*, and eventually used for ligation. Thermo Scientific T4 DNA ligase enzyme, in order to obtain the recombinant plasmid pVAX-S1-TM (Figure 21). The sequence of pVAX-S1-TM was verified by sequencing (BMR Genomics (Padova)).

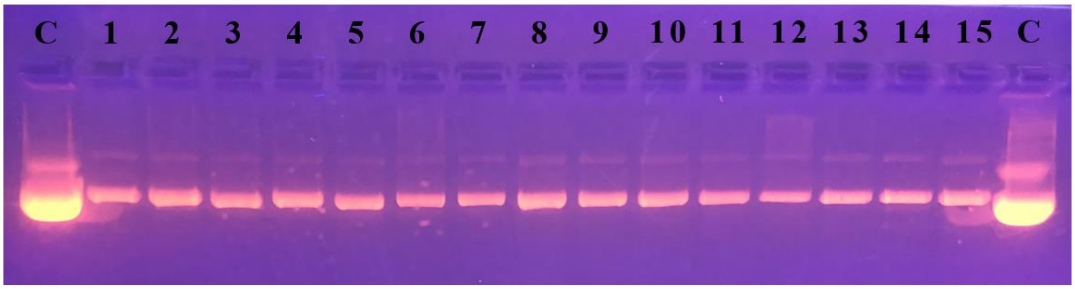

Figure 21. Analysis by agarose gel electrophoresis indicates that clones 1 to 15 contained recombinant plasmids.

2.1 Selection of S1 anchored to TM gene region based on in silico analysis

Since transmembrane facilitates the trimerization, for our DNA vaccine candidate, the target antigen amino acid sequence of SARS-CoV-2 S1-TM was analyzed *in silico* by our collaborators at Marche Polytechnic University. The 3D dimensional structure of the S1-TM portion of S protein was modelled using Iterative Threading ASSEmbly Refinement (I-TASSER) approach [113]. While its trimeric association was reconstructed using the trimeric assembly of Spike SARS-CoV-2 protein (6vxx pdb code). Both monomeric and trimeric macromolecular structure has been minimized with 10,000 cycles steepest descent followed by 5000 steps conjugate gradient, obtaining a convergence of maximum force to energy threshold of 1000 kJ/mol nm2, using AMBER99-SB-ILDN forces field within GROMACS 2020.2 software. In order to assess the conformational and association stability, the trimer underwent 100 ns MD simulation using Periodic Boundary Conditions (PBC) in explicit TIP3P water solvent and NPT ensemble.

3. Construction of DNA vaccines against SARS-CoV-2 variants

DNA vaccines against SARS-CoV-2 variants were obtained by introducing the selected mutations into pVAX-S1-TM using a PCR-based mutagenesis protocol, based on the Liu *et al.* One-step PCR-based Multiple Site-directed Plasmid Mutagenesis (Figure 22) [111].

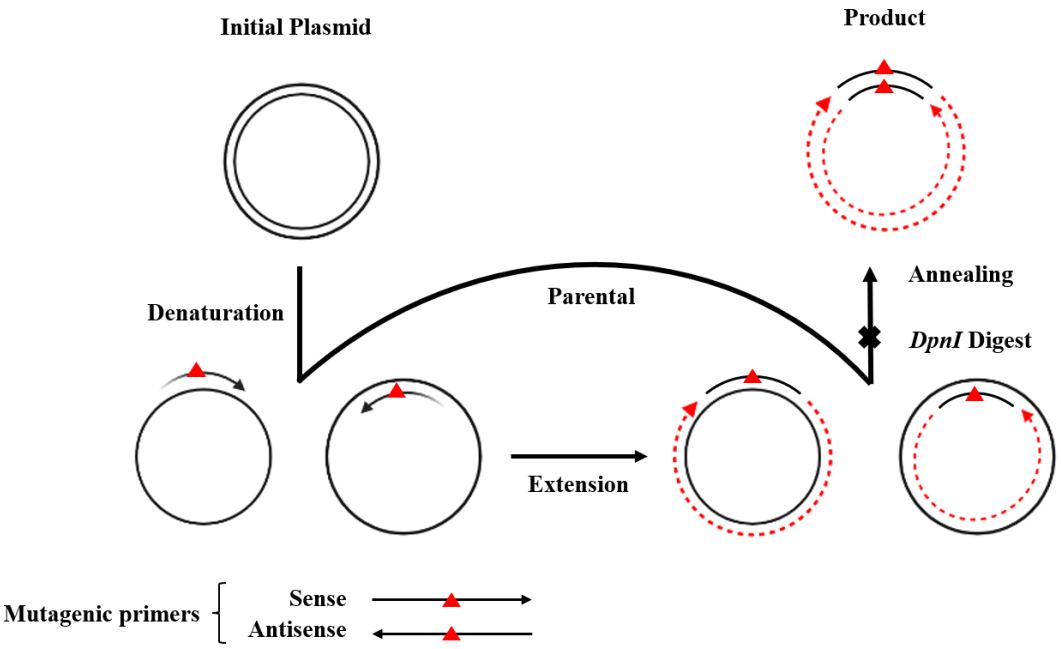

Figure 22. Schematic representation of PCR-based site directed mutagenesis strategy used to change DNA bases on a sequence of interest.

According to this approach, the mutation is introduced into a double-stranded plasmid with one pair of complementary primers containing the mutation of interest by a single-round PCR. Following the *DpnI* restriction enzyme digestion, the newly synthesized PCR product was then transformed into *E. coli* cells. In this approach, *DpnI* plays a crucial role, given that this enzyme is responsible to destroy the parental methylated DNA but not the newly synthesized unmethylated mutant DNA.

To eliminate the primer dimerization and permit the newly synthesized PCR product to be used as the template for the next round of amplification, Liu and Naismith developed a modified method by further extending the non-overlapping

sequence at the 3' end of the primers making the T_m of the non-overlapping sequences (T_{mno}) 5 to 10°C higher than the T_m of the primer-primer complementary sequences (T_{mpp}). In this method, T_{mno} - 5°C is used as the annealing temperature during the amplification cycle, and an additional annealing step at T_{mpp} - 5°C is added before the final extension step to increase the synthesis of the full-length plasmid. Each primer pair contains non-overlapping sequences at their 3' ends and primer-primer complementary (overlapping) sequences at their 5' ends [111]. Primers' information used for mutagenesis are list in the Table 5.

We optimized the protocol by increasing the concentration of DMSO (5%), facilitate strand separation in GC-rich regions of DNA reduce the propensity of the DNA to form secondary structures.

Table 5. Primers used in the mutagenesis.

Primers	Sequences	TM_{pp} (°C)	TM_{no} (°C)
D614G Forw	5'CTGTACCAGGGCGTGAATTGCACCGAG GTGCCAGTGGCTATCCAC 3'	56°C	65°C
D614G Rew	5'CAATTCACGCCCTGGTACAGCACGGCC ACCTGGTTGCTGGTATTG 3'	56°C	64.5°C
N501Y Forw	5'CCAGCCAACCTACGGAGTGGGATACCA GCCATACAGGGTGGTGGT 3'	61°C	62.2°C
N501Y Rew	5'CCACTCCGTAGGTTGGCTGGAAGCCGT AGCTCTGCAGGGGGAAGT 3'	59.6°C	65.8°C
A570D Forw	5'AAGGGACATCGATGATACCACCGACGC CGTGCGCGACCCACAGAC 3'	52.7°C	71.8°C
A570D Rew	5'TGGTATCATCGATGTCCCTTCCGAACTG CTGGAATGGCAGGAACT 3'	52.7°C	63.5°C
L452R Forw	5'ACAATTACCGGTACCGCCTGTTCCGCA AGTCCAATCTGAAGCCAT 3'	57.2°C	61.3°C
L452R Rew	5'CAGGCGGTACCGGTAATTGTAGTTGCC GCCCACTTTGCTATCCAG 3'	57.2°C	63.8°C
E484Q Forw	5'AATGGAGTGCAGGGCTTCAACTGCTAC TTCCCCCTGCAGAGCTAC 3'	56.9°C	62.7°C
E484Q Rew	5'TTGAAGCCCTGCACTCCATTGCATGGG GTGCTTCCAGCCTGGTAG 3'	56.9°C	65.6°C

N501Y leads to the change of asparagine (Asn or N) to tyrosine (Tyr or Y) at position 501 in the receptor binding domain; A570D leads to the change of alanine (Ale or A) to aspartic acid (Asp or D) at position 570 (near the RBD); D614G leads to the change of aspartic acid (Asp or D) to glycine (Gly or G) at position 614. E484Q

leads to the change of glutamic acid (Glu or E) to glutamine (Gln or Q) at position 484 in the receptor binding domain; L452R leads to the change of leucine (Leu or L) to arginine (Arg or R) at position 452.

According to the site-directed mutagenesis protocol, we used the Phusion™ High-Fidelity DNA Polymerase according to the protocol described below. In detail, the annealing temperature (T_{mno}) at 60°C, and an additional annealing step at 50°C (T_{mpp}), before the final extension step to increase the synthesis of the full-length plasmid were chosen.

Cycle step	Temperature	Time	Cycles
Initial Denaturation	98°C	5 min	1
Denaturation	98°C	1 min	12
Annealing (T_{mno})	60°C	1 min	
Extension	72°C	5 min	
Annealing (T_{mpp})	50°C	1 min	
Final extension	72°C	15 min	1
Hold	4°C	Hold	Hold

The purified PCR products were treated with 10 units of *DpnI* restriction enzyme at 37°C for 2 hours. *DpnI* is specific for methylated and hemimethylated DNA. Since DNA isolated from most *E. coli* strains is dam methylated, it is susceptible to *DpnI* digestion. Hence, *DpnI* incubation after a PCR reaction permits to digest the methylated parental DNA template and select for the newly synthesized DNA containing mutations. The digested products were used to transform *E. coli* DH5α competent cells by heat shock method.

D614G was the first mutation inserted into pVAX-S1-TM, since it is involved in both the United Kingdom (UK) (B.1.1.7) and the Indian (IND) (B.1.617) lineages. Other key mutations were subsequently introduced to construct the DNA vaccines against English, and Indian lineages. The vaccine pVAX-S1-TM-INDUK combined

the selected Indian and English mutations.

3.1 DNA vaccines specifically conceived against the United Kingdom (UK) (B.1.1.7): Insertion of key mutations into pVAX-S1-TM of SARS-CoV-2

3.1.1. Insertion of A570D mutation into pVAX-S1-TM (D614G)

pVAX-S1-TM carrying D614G mutation was used as template for A570D PCR mutagenesis. PCR running program was performed using primers including A570D mutation, with an annealing temperature (T_{mno}) of 58°C and an additional annealing step (T_{mpp}) of 48.7°C. Briefly, the PCR products were purified and treated with 10 units of *DpnI* at 37°C for 2 hours as described above. *DpnI* digested PCR product was used to transform *E. coli* cells.

3.1.2 Insertion of N501Y mutation into pVAX-S1-TM (including D614G and A570D)

The third mutation, N501Y, was inserted into pVAX-S1-TM already including D614G and A570D mutations. Thus, pVAX-S1-TM, including D614G and A570D, was used as template and a PCR was performed. 5X Phusion™ GC Buffer was chosen instead of 5X Phusion™ HF Buffer, to improve the performance of Phusion™ High-Fidelity DNA Polymerase, as suggested by the company in case of some difficulty or long templates, such as GC-rich templates or those with complex secondary structures; DMSO was increased to 5%.

According to the site-directed mutagenesis protocol, we used 62°C as annealing temperature (T_{mno}), and an additional annealing step at 55°C (T_{mpp}) before the final extension step to increase the synthesis of the full-length plasmid. After digestion with *DpnI*, the digested PCR products were used to transform *E. coli* DH5α competent cells by heat shock method.

3.1.3 Verification of pVAX-S1-TM-UK by sequencing

pVAX-S1-TM-UK vaccine, including D614G, A570D and N501Y mutations, specifically designed against the SARS-CoV-2 United Kingdom (UK) lineage (B.1.617), was isolated from *E. coli* DH5α cells using the HiYield™ Plasmid Mini Kit; the concentration was determined by using NanoDrop, and sequenced by BMR Genomics (Padova) using the following oligonucleotide:

Forw Spike 1151-1170

5’ CCACCAAGCTGAATGATCTG 3’

The three key mutations inserted by single-site mutagenesis into the pVAX-S1-TM sequence were identified: the two key English mutations (A570D and N501Y) plus D614G.

3.2 DNA vaccines specifically conceived against Indian (IND) lineage (B.1.617)

3.2.1 Insertion of E484Q and L452R mutations by single-site mutagenesis into pVAX-S1-TM including D614G mutation

pVAX-S1-TM vaccine carrying the D614G mutation was used as a template for E484Q PCR single-site mutagenesis, and the PCR running program was performed using primers including E484Q mutation. Then, L452R mutation was inserted into pVAX-S1-TM including D614G and E484Q, the PCR running program was performed using primers including L452R mutation. An annealing temperature (T_{mno}) of 59°C and an additional annealing step at 52°C (T_{mpp}) were used for insertion of E484Q and L452R mutations. The PCR product was purified, digested with *DpnI*, and used to transform *E. coli* DH5α competent cells.

3.2.3 Verification of pVAX-S1-TM-Indian by sequencing

pVAX-S1-TM-Indian including D614G, E484Q and L452R mutations,

specifically designed against the SARS-CoV-2 Indian (IND) lineage (B.1.617), was sequenced by BMR Genomics (Padova) using the same oligonucleotides as pVAX-S1-TM-UK. The three mutations inserted by single-site mutagenesis into the pVAX-S1-TM sequence were identified: the two key Indian mutations (E484Q and L452R) plus D614G.

3.3 A chimeric DNA vaccine designed against both the United Kingdom (UK) (B.1.1.7) and Indian (IND) lineage (B.1.617)

3.3.1 Insertion of E484Q and L452R mutations into pVAX-S1-TM-UK

pVAX-S1-TM-UK, carrying D614G, A570D, N501Y mutations, was used as template for E484Q PCR-based single-site mutagenesis and the PCR running program was performed with annealing (T_{mno}) 59°C and annealing (T_{mpp}) 52°C, using primers including E484Q mutation, as reported above. The L452R mutation was inserted into pVAX-S1-TM-UK carrying E484Q mutation, using primers including L452R mutation.

3.3.3 Verification of pVAX-S1-TM-INDUK by sequencing

pVAX-S1-TM-INDUK (including D614G, A570D, N501Y, E484Q and L452R mutations), specifically designed against both UK and Indian SARS-CoV-2 variants, was isolated from DH5α *E. coli* cells and the concentration was determined by using NanoDrop, then sequenced by BMR Genomics (Padova) using the same oligonucleotide as pVAX-S1-TM-UK. The five expected mutations inserted by single-site mutagenesis into the pVAX-S1-TM sequence were identified.

3.4 In vitro validation of SARS-CoV-2 DNA vaccines

3.4.1 Cell culture

Human embryonic kindney-293 (HEK-293) and Chinese hamster ovary (CHO) cells were obtained from American Type Culture Collection (ATCC, Rockville, MD, USA) and cultured in Dulbecco's Modified Essential Medium (DMEM, Gibco, Life Technologies, Carlsbad, CA, USA) supplemented with 10% fetal bovine serum (FBS, Gibco, Life Technologies) and 1% penicillin-streptomycin (Gibco, Life Technologies). Cells were cultured at 37°C under humidified atmosphere with 5% CO_2.

3.4.2 Immunofluorescence analysis for in vitro validation of candidate DNA vaccines

HEK-293 cells were plated in a 24-well plate ($2x10^5$ cells/well). One day after plating, 70-90% confluent cells were transiently transfected with vaccine candidates, pVAX and pcDNA3.1-SARS2-SPIKE (addgene) were used as negative and positive controls respectively, complexed with Lipofectamine®3000, according to the manufacturer's instructions. Forty-eight hours after transfection, cells were fixed for 10 minutes with phosphate-buffered saline (PBS)-4% paraformaldehyde (Sigma, St. Louis, MO). After incubation in blocking buffer (PBS-10% bovine serum albumin (BSA; Sigma, Milan, Italy) for 20 min, cells were incubated for 1 h at 37°C with the primary antibody SARS-CoV-2 (COVID-19) Spike S1 antibody [HL134] (GTX635671) (anti-rabbit, 1:100). After washing, cells were incubated with Goat anti-rabbit IgG Alex Fluor 488® secondary antibody (Invitrogen Molecular Probes, Eugene, OR, USA) diluted at 1:200 for 1 h at 37°C. Finally, cells were examined under Fluorescence Microscope (Carl Zeiss GmbH, Germany) to assess the expression of antigens.

3.4.3 Confocal microscopy analysis

To expression of S1+TM antigen on the cell membrane of HEK-293 cells transfected with pVAX-S1-TM DNA vaccine was assessed by confocal microscopy. The cells were plated on 18-mm round coverslips and incubated for 24h. Cells were transfected using Lipofectamine™ 2000 Transfection Reagent and, after 24 hours, were fixed using 4% paraformaldehyde, washed 3 times with PBS (5 min each), and then incubated with the pcDNA3.1-SARS2-SPIKE (addgene) primary antibody for 1 hour. Next, the sample was washed in PBS 3 times (10 min each) and incubated for 1 h with the secondary antibody (Alexa Fluor 488). Finally, the cells were washed 3 times with PBS and stained for Dapi for 10 min (dilution factor 1:1000). Cells were examined under Fluorescence Confocal Microscope (Carl Zeiss GmbH, Germany) with a 63X 1.4 NA oil immersion objective at 405 and 488 nm excitation. The XZ, YZ projections, and intensity plot profile were performed using Fiji, and plotted by Origin (OriginLab Corporation, Origin 2019b).

3.5 In vivo validation of SARS-CoV-2 DNA vaccines

3.5.1 Mice

C57BL/6 mice were housed under controlled temperature (20°C) and circadian cycle (12 hours light / 12 hours 165 dark). The animals were fed on a chow diet (Mucedola) and tap water *ad libitum.* Mice were treated in accordance with the U.K. Animals (Scientific Procedures) Act, 1986 and associated guidelines, EU Directive 2010/63/EU for animal experiments and with the 3Rs principles. All animal experiments were authorized by the Italian Ministry of Health (#708/2021-PR) and by the Animal Research Committee (OPBA) of the National Institute of Health and Science on Ageing (INRCA – Istituto Nazionale di Riposo e Cura per Anziani), Ancona (Italy).

3.5.2 SARS-CoV-2 DNA vaccines preparation

Escherichia coli strain DH5a was transformed with the different plasmids and then grown in Luria-Bertani medium with kanamycin (Sigma-Aldrich). Large-scale preparation of the plasmids was carried out by alkaline lysis using Endofree Qiagen Plasmid-Giga kit (Qiagen, Chatsworth, CA, USA) according to the manufacturer's instructions. Subsequently, DNA was resuspended in saline and stored in aliquots at -20°C, after concentration determination using NanoDrop spectrofotometer (Thermo Scientific).

3.5.3 Mice immunization with SARS-CoV-2 DNA vaccines

Young/adults (11 weeks of age) and aged (20 months of age) C57BL/6 mice were immunized by intramuscular (i.m.) injections into the tibial muscle followed by electroporation using T820 electroporator (BTX), 2 square-ware 25 ms, 375 V/cm pulse. Mice underwent two DNA vaccine boosts at three-week intervals with 100 μg of DNA vaccines or pVAX empty control vector. Blood was collected from the retro-orbital plexus under anesthesia before vaccination and two weeks after the last vaccination. In order to collect serum, whole blood samples were left to clot at room temperature for 30 minutes. Serum separation was accomplished by centrifugations at 6,000 rpm at 4°C.

3.5.4 Immunofluorescence analysis of antibody response

HEK-293 cells were plated in a 24-well plate ($2x10^5$ cells/well). One day after plating, 70-90% confluent cells were transiently transfected with pcDNA3.1-SARS2-SPIKE (addgene), complexed with Lipofectamine®3000, according to the manufacturer's instructions. Forty-eight hours after transfection, cells were fixed for 10 minutes with phosphate-buffered saline (PBS)-4% paraformaldehyde (Sigma, St. Louis, MO，USA). After incubation in blocking buffer ((PBS-10% bovine serum

albumin (BSA; Sigma, Milan, Italy) for 20 min, cells were incubated for 1 h at 37°C with sera of immunized mice. After washing, cells were incubated with Goat anti-mouse IgG Alex Fluor 488® secondary antibody (Invitrogen Molecular Probes, Eugene, OR) diluted at 1:200 for 1 h at 37°C. Finally, cells were examined under Fluorescence Microscope (Carl Zeiss GmbH, Germany).

3.5.5 Analysis of antibody response by flow cytometry

Sera from immunized mice collected two weeks after the last vaccination analyzed by flow cytometry (BD FACSCalibur), using HEK-293 cells transiently transfected with pcDNA3.1-SARS2-Spike vector (Plasmid#145032) from Addgene, as targeted cells. Briefly, subconfluent cells were detached and dispensed at a density of 10^6 cells per Falcon® 5 mL Round Bottom Polystyrene Test Tube. After 3 minutes centrifugation at 1,000 rpm at 4°C, the obtained cell pellet was resuspended and washed in staining buffer (2% FBS, 0.05% sodium azide-containing 1× PBS). Cells were incubated with sera of immunized mice for 1 hour on ice. After three washes, incubated with the Goat anti-mouse IgG Alex Fluor 488® secondary antibody (Invitrogen Molecular Probes, Eugene, OR) for 1 hour on ice. Cells were washed and resuspended in PBS before the analysis was performed using FACS equipped with Cell Quest software (BD Pharmingen, BD Life Sciences, San Jose, CA, USA). FlowJo software (BD Life Sciences, San Jose, CA, USA) was employed for data analysis.

4. Nanoparticles as possible delivery system for DNA vaccines

4.1 Microfluidic preparation of LNP-pDNA complexes

Cationic lipids 1,2-Dioleoyl-3-trimethyl-ammonium-propane (DOTAP) and (3-[N- (N0,N0-dimethyl-aminoethane)-carbamoyl])-cholesterol (DC-Chol, zwitterionic lipids: dioleoyl phosphatidylethanol-amine (DOPE), 1,2-Dioleoyl-sn-glycero-3-

phosphocholine (DOPC), Cholesterol and PEG-lipids: 1,2-dioleoyl-sn-glycero-3-phosphoethanolamine-N-[amino(polyethylene glycol)-2000] (DOPE-PEG) and 1,2-distearoyl-sn-glycero-3-phosphoethanolamine-N-[amino(polyethylene glycol)-2000] (DSPE-PEG) were purchased from Avanti Polar Lipids (Alabaster, AL, USA). Plasmid used for LNPs synthesis, pGL3 (Firefly luciferase encoding plasmid) was purchased from Promega (Fitchburg, WI, USA). Lipid nanoparticles (LNPs) were obtained through microfluidic mixing device (NanoAssemblr® Benchtop from Precision NanoSystems Inc., Vancouver, BC, Canada) with a Y-shape staggered herringbone micromixer (SHM) (Figure 23). All the formulations were prepared by dissolving lipids in different combinations and molar ratios (Table 6), in absolute ethanol to reach a final concentration of 12.5 mM. PmirGLO (Promega, Italy) was dissolved in 25 mM sodium acetate buffer (pH = 4), to 0.2 mg/mL. The organic solvent where lipids are dissolved in and pDNA aqueous solutions are pumped by syringes into the microfluidic device and at the Y-junction they interact forming LNPs complexes. Two different total flow rates (TFR; 2 mL/min and 8 mL/min), were explored to get LNPs complexes. The formulations were produced at different DNA/lipid weight ratio (Rw = 5, 10 and 20) corresponding to a nitrogen to phosphate charge ratio (N/P; nitrogen from the cationic lipid and phosphate from the nucleic acid) of 1.5, 3 and 6. After the micromixing process the ethanol concentration decreases until 25% of the final LNP suspension volume. LNPs complexes were subsequently loaded on Dialysis cassettes (0.5-3 mL, MWCO 3 kDa, Thermo Scientific, Rockford, MI, USA) and dialyzed for 19 h against 500 mL of phosphate buffered saline (PBS) at pH 7.4 to remove the residual ethanol.

Table 6. Lipid composition and mixing parameters for the preparation of the LNPs included in the library. In PEGylated formulations, the total percentage of lipid species yields 98.5%. The remaining 1.5% consists of PEGylated lipid.

N° of components	ID	DOTAP (%)	DC-Chol (%)	CHOL (%)	DOPC (%)	DOPE (%)	Surface Functionalization	Total Flow Rate (mL/min)	Rw
2 components	LNP1	50	0	50	0	0	Plain	2	10
	LNP2	50	0	0	0	50	Plain	2	10
	LNP3	0	50	50	0	0	Plain	2	10
	LNP4	0	50	0	0	50	Plain	2	10
3 components	LNP5	50	0	25	0	25	Plain	2	10
	LNP6	0	50	25	0	25	Plain	2	10
	LNP7	50	0	38.5	0	11.5	Plain	2	10
	LNP8	50	0	38.5	0	10	PEGylated	2	10
4 components	LNP9	12.5	37.5	12.5	0	37.5	Plain	2	10
	LNP10	25	25	0	25	25	Plain	2	5
	LNP11	25	25	0	25	25	Plain	2	10
	LNP12	25	25	0	25	25	Plain	2	20
	LNP13	25	25	0	25	23,5	PEGylated	2	10
	LNP14	13.3	40	0	13.3	32	PEGylated	2	10
	LNP15	13.3	40	13.3	0	32	PEGylated	2	10
	LNP16	13.3	40	13.3	0	32	PEGylated	8	10

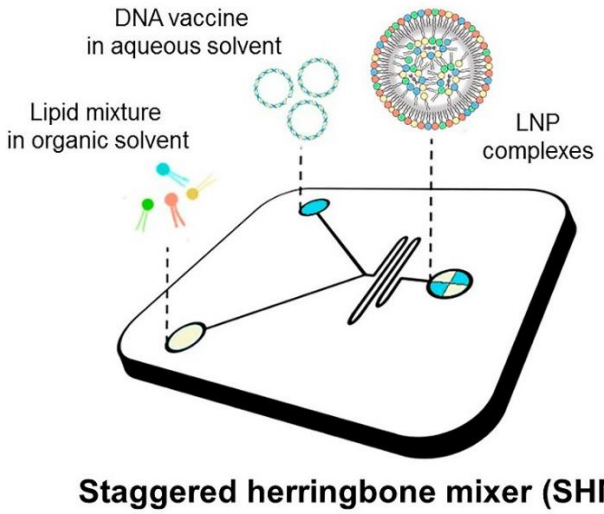

Figure 23. Schematic representation of synthesis procedure of LNP DNA vaccines. Lipids in ethanol are injected in one inlet, while pDNA in acetate buffer solution is injected in the other inlet. The two solutions meet at the Y-junction of the SHM and undergo a chaotic mixing through the herringbone structure. This phenomenon leads to an increase of lipid solution polarity that generates LNP-pDNA complexes.

4.2 Transfection efficiency experiments for evaluate LNPs

In transfection experiments, HEK-293 cells were seeded on 24-well plates (40,000 cells per well). Cells were treated with 1 μg (LNP) formulated pDNA (pGL3), on the base of encapsulated DNA quantification. Three different DNA amounts 1 μg, 2 μg and 5 μg per well was explored for LNP15. Lipofectamine™3000 was used as positive control at 1 μg DNA per well following the standardized protocol (Life Technologies, Carlsbad, CA, USA). Cells were treated in Opti-MEM™ medium (Life Technologies, Carlsbad, CA, USA), with selected LNPs (LNP8, LNP9, LNP11, LNP12, LNP13, LNP14, LNP15, LNP16) or Lipofectamine™3000 and then incubated for 3 h. After treatment, appropriate medium supplemented by 20% FBS was added to each well to reach a final FBS concentration of 10%, then cells were incubated at 37°C. Luciferase expression was measured after 48 h, through Luciferase Assay System (Promega, Madison, WI, USA).

Briefly, cells were washed in a phosphate saline buffer and 60 μL of lysis buffer 1X (Promega) were added to each well. Then, 30 μL of the cell lysate was placed in 3 wells of white Corning® 96 Well Solid Polystyrene Microplate (Sigma-Aldrich, Milan, Italy). The 10 μL present in each well were diluted with 100 μL per well of luciferase substrate (Promega) while the remaining 30 μL were divided into 3 wells (10 μL per well) and used for BCA assay. The transfection efficiency (TE) is expressed as Relative Light Units (RLU) per mg of cell proteins, while the protein amount was determined by Pierce BCA Assay Protein Kit (Thermo Fisher Scientific, Waltham, MA, USA).

4.3 Cell viability assay

The effects of LNPs with respect to Lipofectamine® 3000 (Invitrogen, Waltham, MA, USA) on cell viability were evaluated by seeding 8,000 HEK-293 cells/well in 96 wells plates in complete medium. The day after, appropriate concentrations of

plasmid DNA encapsulated in LNPs or complexed with lipofectamine were added. After 48 h, cell viability was determined using MTT assay (Sigma Aldrich, St. Louis, MO, USA), which is based on the conversion of tetrazolium salt [3-(4,5-dimethylthiazol-2-yl)-2,5-diphenyl-2H-tetrazolium bromide] into formazan by means of mitochondrial enzymes. The formazan crystals were dissolved using dimethyl sulfoxide (DMSO) and the absorbance was measured at 540 nm using Multiskan Ascent 96/384 Plate Reader. Each sample was tested with eight replicates, and the experiments were performed in triplicate. The cell viability was reported as percentage of viable cells in respect to control cells.

4.4 LNPs encapsulated pVAX-hECTM DNA vaccine preparation

pVAX Vector (Life Technologies) and the DNA vaccine pVAX-hECTM (encoding the human extracellular and transmembrane domains of the human HER2 receptor; about 5000 bp) were transformed into *Escherichia coli* strain DH5a and grown in Luria-Bertani medium with kanamycin (Sigma-Aldrich). DNA plasmids were purified using a Maxiprep kit (Qiagen) for *in vitro* transfections and an EndoFree Plasmid-Giga kit (Qiagen, Chatsworth, CA, USA) for *in vivo* immunization and their concentration was determined spectrophotometrically at 260 nm. pVAX and pVAX-hECTM were encapsulated in LNPs by microfluidics.

4.5 Immunofluorescence analysis of LNPs encapsulated pVAX-hECTM

HEK-293 cells were plated in a 24-well plate (2 x 10^5 cells/well). One day after plating, 70-90% of confluent cells were transiently transfected with 1 μg pVAX-hECTM encapsulated in LNPs or complexed with Lipofectamine®3000, according to the manufacturer's instructions. Forty-eight hours after transfection, cells were fixed for 10 minutes with phosphate-buffered saline (PBS)-4% paraformaldehyde (Sigma, St. Louis, MO, USA). After incubation in blocking buffer (PBS-10% bovine serum albumin (BSA; Sigma, Milan, Italy) for 20 min, cells were incubated for 1 h at 37°C

with the primary antibody trastuzumab (anti-human HER2 antibody, 1:50). After washing, cells were incubated with Alexa Fluor 488-conjugated anti-human IgG secondary antibody (Invitrogen Molecular Probes, Eugene, OR, USA) at a dilution of 1:200 for 1 h at 37°C. Finally, cells were examined under Fluorescence Microscope (Carl Zeiss GmbH, Munich, Germany) to assess membrane expression of the oncoantigen HER2.

4.6 Immunization of mice with LNP15 encapsulated pVAX- hECTM DNA vaccine

C57BL/6 male mice (11 weeks of age) were immunized by intramuscular (i.m.) injections into the tibial muscle two times at 3 weeks interval with 100 μg of hECTM DNA vaccine or pVAX empty control vector encapsulated in LNP15 (4 mice/ experimental groups). Two weeks after the last vaccination, blood was collected from the retro-orbital plexus under anesthesia. To collect serum, whole blood samples were left to clot at room temperature for 30 minutes. Serum separation was accomplished by centrifugations at 6.000 rpm at 4°C.

4.7 Analysis of antibody response elicited by LNP15 encapsulated pVAX-hECTM vaccinated mice

Sera from immunized mice were analyzed by flow cytometry (BD FACSCalibur), using human HER-2 overexpressing SK-BR-3 cells as target cells. SK-BR-3 cells were obtained from American Type Culture Collection (Rockville, MD) and cultured in Dulbecco's Modified Essential Medium (DMEM, Gibco, Life Technologies) supplemented with 10% fetal bovine serum (FBS, Gibco, Life Technologies) and 1% penicillin-streptomycin (P/S) (Gibco, Life Technologies). Cells were maintained at 37°C in an atmosphere of 5% CO_2. Briefly, subconfluent cells were detached and dispensed at a density of 10^6 cells per Falcon® 5 mL Round Bottom Polystyrene Test Tube. After a 3 minutes centrifugation at 1.000 rpm at 4°C, the obtained cell pellet was resuspended in staining buffer (0.05% NaN_3, 2% FBS in 1x PBS) and incubated

with sera of vaccinated mice (1:40 dilution in staining buffer) for 1 hour at 4°C. After incubation, cells were washed three times and incubated with Alexa Fluor® 488 goat anti-mouse IgG secondary antibody (1:200 dilution in staining buffer) for 1 hour, at 4°C. Samples were washed three times with staining buffer, and resuspended in 1x PBS, ready for analysis with BD FACSCalibur. Cell Quest Pro (version 6.0.2) and FlowJo (version 8.7) were used as acquisition and analysis software, respectively.

4.8 Statistical analysis

Each experiment was performed at least three times independently. Quantitative data are presented as means ± SEM from three independent experiments. The significance of differences was evaluated with two-tailed Student's t-test, or one way ANOVA. Statistical analysis was carried out with GraphPad Prism 9 software (San Diego, CA, USA). $p \leq 0.05$ was used as the critical level of significance. P-value is indicated in Figure Legends.

RESULTS

1. Generation and in vitro validation of pVAX-S1 DNA vaccine

1.1 pVAX-S1 DNA vaccine

Recombinant DNA technologies were applied to construct a DNA vaccine expressing the S1 region of the SARS-CoV-2 Spike protein, including the RBD. The cDNA (about 2 kb) that encodes the S1 region (660 aa) of the S protein of the SARS-CoV-2 was cloned into pVAX, chosen as a backbone, using *NheI* and *XhoI* restriction enzymes, as described in the Methods section (Figure 24). The DNA sequence encoding for the antigen was verified by sequencing (BMR genomics) and by pairwise sequence alignment tool (EMBL-EBI). The nucleotide sequence of SARS-CoV-2 S1 (reported below) is shown in black, the sequence encoding the signal peptide (13 aa) is shown in orange, and the stop codon is indicated in blue.

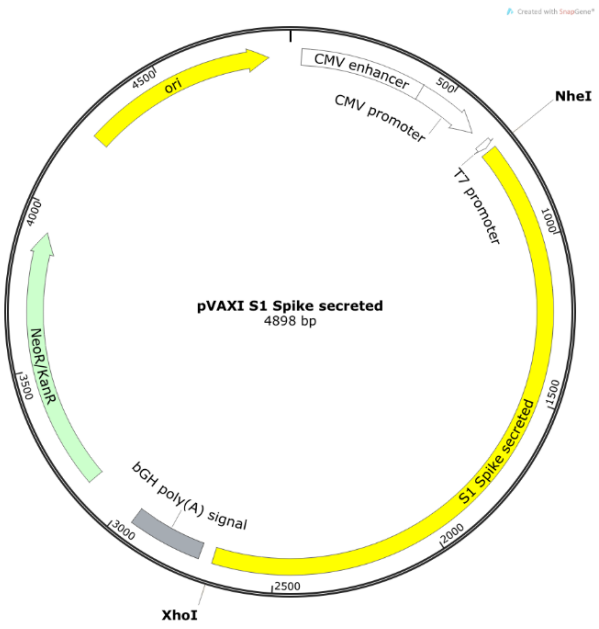

Figure 24. Map of pVAX-S1, a DNA vaccine encoding the S1 subunit of the SARS-CoV-2 spike protein.

Nucleotide sequence of secreted S1 spike:

ATGTTTGTCTTCCTGGTCCTGCTGCCTCTGGTCTCGTCTCAGTGCGTGAACCTGACTACTAGAACCCAGCTGCCTCCT
GCCTATACTAACTCCTTCACCCGCGGCGTGTACTACCCAGACAAGGTGTTCCGCAGCTCCGTGCTGCACTCCACCCA
GGATCTGTTCCTGCCCTTCTTCAGCAACGTGACCTGGTTCCACGCCATCCACGTGAGCGGCACCAATGGCACCAAG
CGGTTCGACAATCCCGTGCTGCCATTCAACGATGGCGTGTACTTCGCCTCCACCGAGAAGAGCAACATCATCCGCGG
CTGGATCTTCGGCACCACCCTGGACTCCAAGACCCAGAGCCTGCTGATCGTGAACAATGCCACCAACGTGGTCATC
AAGGTGTGCGAGTTCCAGTTCTGCAATGATCCATTCCTGGGCGTGTACTACCACAAGAACAATAAGTCCTGGATGGA
GAGCGAGTTCCGCGTGTACAGCTCCGCCAACAATTGCACCTTCGAGTACGTGTCCCAGCCCTTCCTGATGGACCTGG
AGGGCAAGCAGGGCAATTTCAAGAACCTGCGCGAGTTCGTGTTCAAGAATATCGATGGCTACTTCAAGATCTACTCC
AAGCACACCCCCATCAACCTGGTGCGCGACCTGCCACAGGGCTTCAGCGCCCTGGAGCCACTGGTGGATCTGCCAA
TCGGCATCAACATCACCAGGTTCCAGACCCTGCTGGCCCTGCACCGCAGCTACCTGACCCCAGGCGACAGCTCCAG
CGGATGGACCGCTGGAGCTGCTGCCTACTACGTGGGCTACCTGCAGCCCCGCACCTTCCTGCTGAAGTACAACGAG
AATGGCACCATCACCGACGCCGTGGATTGCGCCCTGGATCCACTGTCCGAGACAAAGTGCACCCTGAAGAGCTTCA
CCGTGGAGAAGGGCATCTACCAGACCTCCAATTTCCGCGTGCAGCCAACCGAGAGCATCGTGCGCTTCCCCAATATC
ACCAACCTGTGCCCATTCGGCGAGGTGTTCAACGCTACCAGGTTCGCCAGCGTGTACGCTTGGAATCGCAAGCGCA
TCTCCAACTGCGTGGCCGACTACAGCGTGCTGTACAACTCCGCCAGCTTCTCCACCTTCAAGTGCTACGGCGTGTCC
CCCACCAAGCTGAATGATCTGTGCTTCACCAACGTGTACGCCGATAGCTTCGTGATCAGGGGCGACGAGGTGCGCC
AGATCGCTCCAGGACAGACCGGCAAGATCGCTGACTACAATTACAAGCTGCCCGACGATTTCACCGGCTGCGTGAT
CGCCTGGAACTCCAACAATCTGGATAGCAAAGTGGGCGGCAACTACAATTACCTGTACCGCCTGTTCCGCAAGTCC
AATCTGAAGCCATTCGAGCGCGACATCTCCACCGAGATCTACCAGGCTGGAAGCACCCCATGCAATGGAGTGGAGG
GCTTCAACTGCTACTTCCCCCTGCAGAGCTACGGCTTCCAGCCAACCAACGGAGTGGGATACCAGCCATACAGGGT
GGTGGTGCTGTCCTTCGAGCTGCTGCACGCTCCAGCTACCGTGTGCGGACCAAAGAAGAGCACCAATCTGGTGAAG
AACAAGTGCGTGAACTTCAATTTCAACGGCCTGACCGGAACCGGCGTGCTGACCGAGTCCAACAAGAAGTTCCTG
CCATTCCAGCAGTTCGGAAGGGACATCGCTGATACCACCGACGCCGTGCGCGACCCACAGACCCTGGAGATCCTGG
ATATCACCCCATGCTCCTTCGGCGGCGTGAGCGTGATCACCCCAGGAACCAATACCAGCAACCAGGTGGCCGTGCT
GTACCAGGACGTGAATTGCACCGAGGTGCCAGTGGCTATCCACGCTGATCAGCTGACCCCAACCTGGCGCGTGTAC
AGCACCGGATCCAACGTGTTCCAGACCCGCGCCGGATGCCTGATCGGAGCTGAGCACGTGAACAATTCCTACTAG

1.2 In vitro validation of pVAX-S1: antigen is expressed in transfected HEK-293 cells

The expression of the antigenic viral protein (S1) was assessed by immunofluorescence assay on HEK-293 cells transiently transfected with pVAX-S1, using a commercial anti-SARS-CoV-2 (COVID-19) Spike S1 antibody.

The immunofluorescence assay revealed that pVAX-S1 candidate DNA vaccine expresses the S1 antigen, as expected. The obtained fluorescent signal was comparable in pVAX-S1-transfected and pcDNA 3.1-SARS2-Spike-transfected

(positive control) HEK-293 cells, whereas fluorescent signal was not detected in the HEK-293 cells transfected with empty pVAX (negative control) (Figure 25).

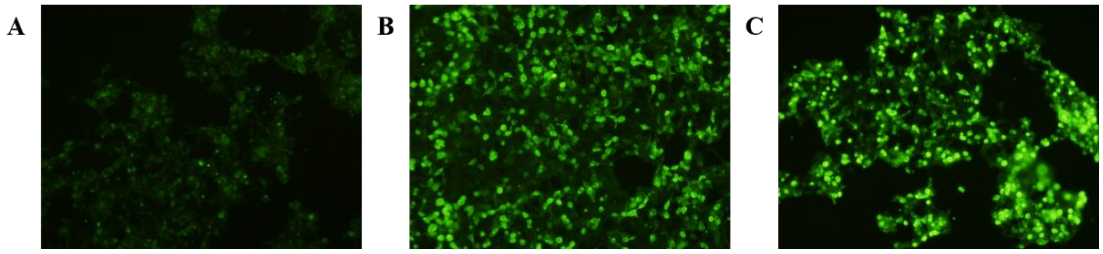

Figure 25. Immunofluorescence analysis to verify the expression of S1 in HEK-293 cells transiently transfected with pVAX-S1. Cells were transfected with (A) empty plasmid pVAX (Control); (B) pcDNA 3.1-SARS2-Spike as positive control; (C) or pVAX-S1 encoding the S1 region of S protein. Cells were treated with Brefeldin A, fixed and permeabilized. Expression of S protein was measured with monoclonal rabbit anti-SARS-CoV-2 spike S1 Protein IgG and Alexa Fluor® 488 goat anti-rabbit IgG secondary antibody (green). Images were captured using inverted fluorescence microscope at 10X Magnification.

2. Generation and in vitro validation of pVAX-S1-TM DNA vaccine

2.1 pVAX-S1-TM DNA vaccine

A recent study reported that SARS-CoV-2 transmembrane domain (TM) is sufficient to mediate trimerization of the spike RBD. Thus, TM domain seems to play a critical role in the induction of the native trimeric conformation of spike protein [114]. Considering these previously reported data, we decided to construct a DNA vaccine, called pVAX-S1-TM, against SARS-CoV-2, encoding the S1 subunit of the spike protein anchored to the plasma membrane through the transmembrane region (TM). The encoded antigen should be expressed on the plasma membrane of transfected cells, maintaining the trimeric conformation. We obtained the DNA vaccine pVAX-S1-TM by cloning into the pVAX vector the sequence encoding the S1 region (1-660 aa), using *NheI* and *EcoRI* restriction enzymes, and then by inserting the sequence encoding the TM region (ending with a stop codon) downstream and in frame with the S1, using *EcoRI* and *XhoI* restriction enzymes, as described in the Methods section. Figure 26 shows the map of pVAX-S1-TM, the second anti-SARS-

CoV-2 DNA vaccine that we constructed. The DNA sequence encoding for the S1-TM antigen was verified by sequencing (BMR Genomics) and by pairwise sequence alignment tool (EMBL-EBI).

Figure 26. Map of pVAX-S1-TM, a DNA vaccine against SARS-CoV-2 encoding the SARS-CoV-2 spike S1 region in fusion with the transmembrane region.

The nucleotide sequence of SARS-CoV-2 S1-TM is reported below. The nucleotide sequence encoding the signal peptide (13 aa) is indicated in orange, the sequence encoding the transmembrane region is indicated in blue, *EcoRI* restriction site is indicated in green, the stop codon is indicated in bold.

Nucleotide sequence of S1-TM spike:

ATGTTTGTCTTCCTGGTCCTGCTGCCTCTGGTCTCGTCTCAGTGCGTGAACCTGACTACTAGAACCCAGCTGCCTCCT
GCCTATACTAACTCCTTCACCCGCGGCGTGTACTACCCAGACAAGGTGTTCCGCAGCTCCGTGCTGCACTCCACCCA
GGATCTGTTCCTGCCCTTCTTCAGCAACGTGACCTGGTTCCACGCCATCCACGTGAGCGGCACCAATGGCACCAAG
CGGTTCGACAATCCCGTGCTGCCATTCAACGATGGCGTGTACTTCGCCTCCACCGAGAAGAGCAACATCATCCGCGG
CTGGATCTTCGGCACCACCCTGGACTCCAAGACCCAGAGCCTGCTGATCGTGAACAATGCCACCAACGTGGTCATC
AAGGTGTGCGAGTTCCAGTTCTGCAATGATCCATTCCTGGGCGTGTACTACCACAAGAACAATAAGTCCTGGATGGA
GAGCGAGTTCCGCGTGTACAGCTCCGCCAACAATTGCACCTTCGAGTACGTGTCCCAGCCCTTCCTGATGGACCTGG
AGGGCAAGCAGGGCAATTTCAAGAACCTGCGCGAGTTCGTGTTCAAGAATATCGATGGCTACTTCAAGATCTACTCC
AAGCACACCCCCATCAACCTGGTGCGCGACCTGCCACAGGGCTTCAGCGCCCTGGAGCCACTGGTGGATCTGCCAA

TCGGCATCAACATCACCAGGTTCCAGACCCTGCTGGCCCTGCACCGCAGCTACCTGACCCCAGGCGACAGCTCCAG
CGGATGGACCGCTGGAGCTGCTGCCTACTACGTGGGCTACCTGCAGCCCCGCACCTTCCTGCTGAAGTACAACGAG
AATGGCACCATCACCGACGCCGTGGATTGCGCCCTGGATCCACTGTCCGAGACAAAGTGCACCCTGAAGAGCTTCA
CCGTGGAGAAGGGCATCTACCAGACCTCCAATTTCCGCGTGCAGCCAACCGAGAGCATCGTGCGCTTCCCCAATATC
ACCAACCTGTGCCCATTCGGCGAGGTGTTCAACGCTACCAGGTTCGCCAGCGTGTACGCTTGGAATCGCAAGCGCA
TCTCCAACTGCGTGGCCGACTACAGCGTGCTGTACAACTCCGCCAGCTTCTCCACCTTCAAGTGCTACGGCGTGTCC
CCCACCAAGCTGAATGATCTGTGCTTCACCAACGTGTACGCCGATAGCTTCGTGATCAGGGGCGACGAGGTGCGCC
AGATCGCTCCAGGACAGACCGGCAAGATCGCTGACTACAATTACAAGCTGCCCGACGATTTCACCGGCTGCGTGAT
CGCCTGGAACTCCAACAATCTGGATAGCAAAGTGGGCGGCAACTACAATTACCTGTACCGCCTGTTCCGCAAGTCC
AATCTGAAGCCATTCGAGCGCGACATCTCCACCGAGATCTACCAGGCTGGAAGCACCCCATGCAATGGAGTGGAGG
GCTTCAACTGCTACTTCCCCCTGCAGAGCTACGGCTTCCAGCCAACCAACGGAGTGGGATACCAGCCATACAGGGT
GGTGGTGCTGTCCTTCGAGCTGCTGCACGCTCCAGCTACCGTGTGCGGACCAAAGAAGAGCACCAATCTGGTGAAG
AACAAGTGCGTGAACTTCAATTTCAACGGCCTGACCGGAACCGGCGTGCTGACCGAGTCCAACAAGAAGTTCCTG
CCATTCCAGCAGTTCGGAAGGGACATCGCTGATACCACCGACGCCGTGCGCGACCCACAGACCCTGGAGATCCTGG
ATATCACCCCATGCTCCTTCGGCGGCGTGAGCGTGATCACCCCAGGAACCAATACCAGCAACCAGGTGGCCGTGCT
GTACCAGGACGTGAATTGCACCGAGGTGCCAGTGGCTATCCACGCTGATCAGCTGACCCCAACCTGGCGCGTGTAC
AGCACCGGATCCAACGTGTTCCAGACCCGCGCCGGATGCCTGATCGGAGCTGAGCACGTGAACAATTCCTACGAAT
TCTGGTACATCTGGCTGGGCTTCATCGCCGGCCTGATCGCCATCGTGATGGTGACCATCATGCTGTGCTGCATGACCT
CCTGCTGCAGCTGCCTGAAGGGCTGCTGCTCCTGCGGCAGCTGCTGCAAGTTCGATGAGGACGATAGCGAGCCCGT
GCTGAAGGGCGTCAAACTGCACTATACAGGCTCCACCGAGACATCCCAGGTCGCTCCCGCT**TAG**

2.2 In silico analysis of the antigen encoded by pVAX-S1-TM

In silico analysis (performed by prof. Roberta Galeazzi at UNIVPM as described in the Methods section), confirmed that the transmembrane region associated to the S1 subunit of the SARS-CoV-2 spike protein permits the trimerization of the antigen, reproducing the conformation of the native Spike protein exposed as a trimer on the surface of the virus. The overall structure is stable and associates in close conformation to complete SARS-CoV-2 protein in closed state. Thus, the exposed epitopes on the RBD of the S1-TM antigen can be potentially recognized by neutralizing antibodies (Figure 27).

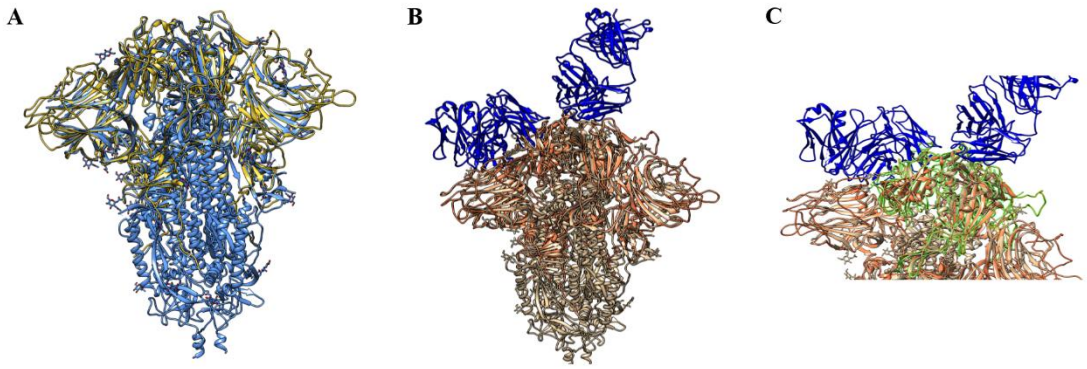

Figure 27. *In silico* three-dimensional (3D) structure of S1-TM spike protein. (A) 3D model of the selected S1-TM spike protein in its trimeric association (gold ribbons), superimposed with trimeric model of full SARS-CoV-2 spike protein in its closed state (pdb code 6vxx; blue ribbons); (B) 3D model of the selected S1-TM spike protein in its trimeric association (coral ribbons), superimposed with trimeric model of full SARS-CoV-2 spike protein in its closed state (pdb code 6vxx; tan ribbons) and the Fab fragments of two neutralizing antibodies targeting RBD domain (6xdg pdb code); (C) same as above but with RBD highlighted. The 3D dimensional structure of the S1-TM portion of S-protein was modeled using Iterative Threading ASSEmbly Refinement (I-TASSER) approach (Harracha M.F. and Drossel B. J. Chem. Phys. 2014;140,174501).

2.3 In vitro validation of pVAX-S1-TM: Spike S1-TM antigen is successfully expressed in HEK-293 cells

In order to assess the expression of the antigen encoded by pVAX-S1-TM and its proper localization in transfected cells, an immunofluorescence assay was performed on HEK-293 cells transiently transfected with the pVAX-S1-TM DNA vaccine.

The Immunofluorescence assay revealed a strong fluorescent signal in the HEK-293 cells transfected pVAX-S1-TM DNA vaccine candidate, mainly localized at the level of the plasma membrane and visible even in not permeabilized cells. This result demonstrates the ability of the pVAX-S1-TM DNA vaccine to express the antigen on the cell membrane of transfected mammalian cells (Figure 28).

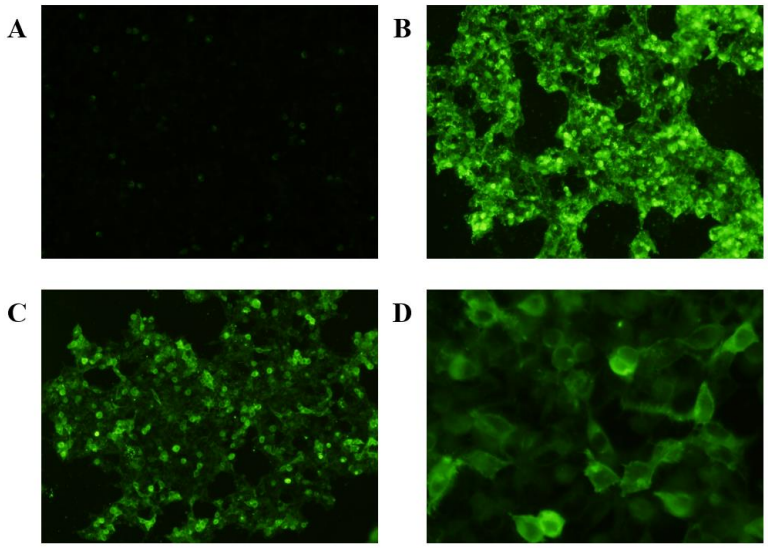

Figure 28. Immunofluorescence analysis to verify the expression of S1-TM in transfected HEK-293 cells. Cells were transfected with (A) empty plasmid pVAX (Control); (B) pcDNA 3.1-SARS2-Spike as positive control; (C&D) or pVAX-S1-TM encoding the S1 protein anchored to the plasma membrane through the transmembrane region. Expression of S protein was analyzed on not permeabilized cells using a monoclonal rabbit anti-SARS-CoV-2 spike S1 Protein IgG and Alexa Fluor® 488 goat anti-rabbit IgG secondary antibody (green). Images were captured using inverted fluorescence microscope at 10X (A, B and C) and 40X (D) Magnifications.

3. Generation and in vitro validation of pVAX-S1-TM-D614G DNA vaccine

The mutation at amino acid position 614 (aspartic acid-to-glycine substitution), localized in the exterior part of the RBD (receptor binding domain) region of the spike glycoprotein, became predominant across the world within a brief period (by April–May 2020). The D614G mutation is present in all significant variants of this virus and confers higher infectivity and transmissibility. For these reasons, this mutation was selected to be introduced into pVAX-S1-TM DNA vaccine by using a PCR-based mutagenesis protocol, according to Liu *et al.* [111] as described in the Methods section. Briefly, the mutation is introduced into a double-stranded plasmid with one pair of complementary primers containing the mutation of interest by a single-round PCR. The proper insertion of the D614G mutation in the sequence for S1-TM antigen was verified by sequencing (BMR Genomics). The expression of the D614G mutant

was verified on both HEK-293 and CHO (Chinese hamster ovary) cells transiently transfected with pVAX-S1-TM-D614G by immunofluorescence analysis (Figure 29). The antigen appears localized on the cell membrane.

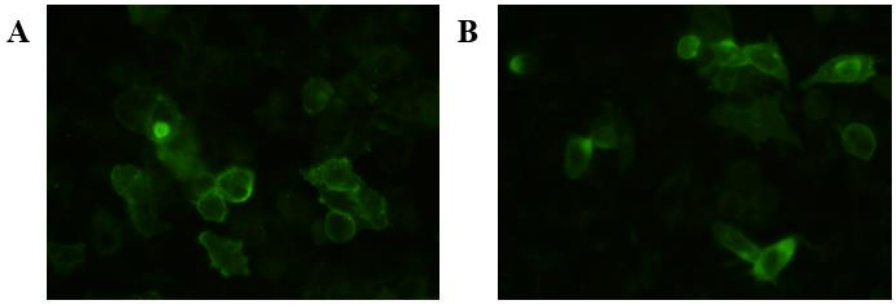

Figure 29. Immunofluorescence analysis of the expression of antigenic portions of Spike protein after transient transfection of (A) HEK-293 and (B) CHO cells with pVAX-S1-TM-D614G. Spike protein expression was detected with a monoclonal rabbit anti-SARS-CoV-2 Spike S1 Protein IgG and Goat anti-rabbit IgG Alex Fluor 488® secondary antibody (green). Images were captured using inverted fluorescence microscope at 40X Magnification.

Confocal microscopy analysis was also performed to obtain further evidence that pVAX-S1-TM-D614G encodes an antigen strongly expressed on the plasma membrane of transfected cells. Figure 30 shows the results of immunofluorescence staining by confocal microscopy.

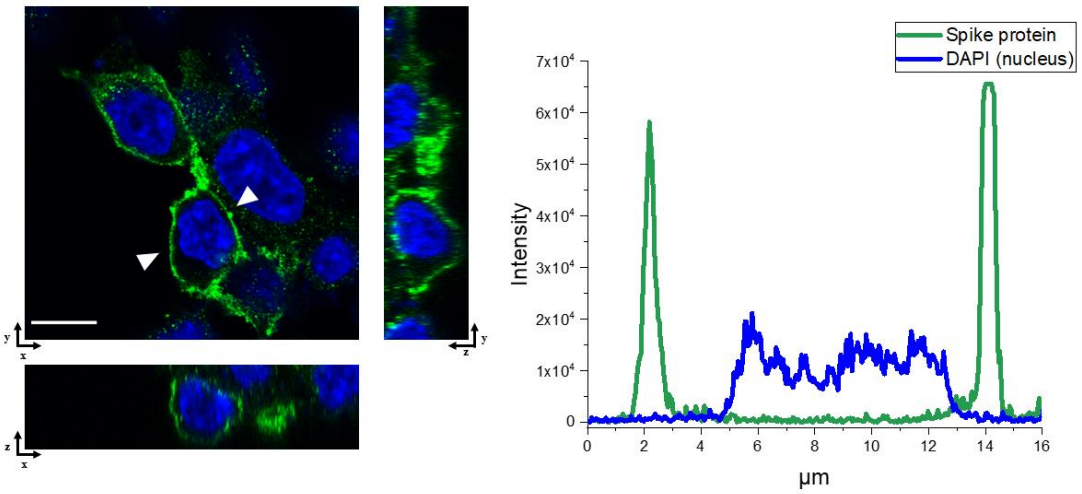

Figure 30. Representative confocal microscopy images of HEK-293 cells transiently transfected with pVAX-S1-TM-D614G DNA vaccine. Profile of the fluorescence intensity of stained HEK-293 cells expressing SARS-CoV-2 spike protein (green line) and labeled for DAPI (blue line), taken along the white arrows. For imaging, a Leica SP5 confocal microscope (Leica Microsystems AG, Wetzlar, Germany) was used. Objective lens 63X/NA1.4; excitation light 405 and 488 nm. Scale bar 10 µm.

3.1 pVAX-S1-TM-D614G elicited a better anti-SARS-CoV-2 immune reaction in mice with respect to pVAX-S1

In vivo experiments were performed to compare the immunogenicity of pVAX-S1-TM-D614G with that of pVAX-S1. For this purpose, C57BL/6 mice (4 mice/groups; 11 weeks of age) were vaccinated two times at 21-day intervals with 100 μg of naked DNA plasmids via intramuscular injection followed by electroporation. Blood samples were collected the day before the first vaccination and two weeks after the last vaccination to allow the subsequent evaluation of the antibody titer (Figure 31).

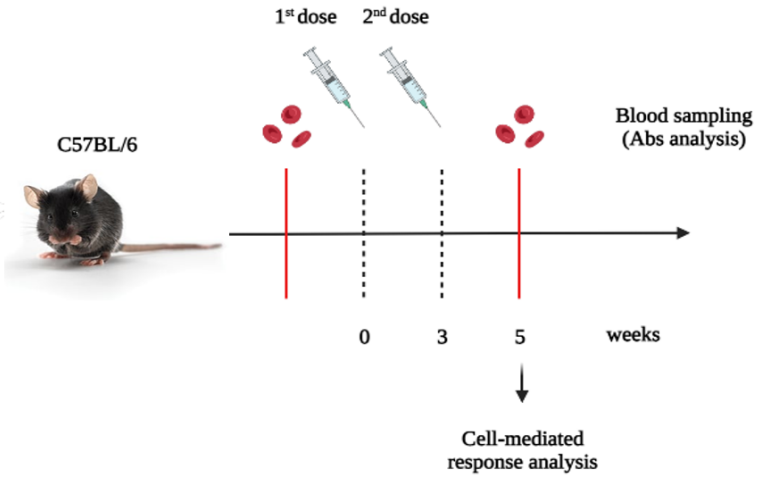

Figure 31. Schematic representation of DNA vaccination experiment. pVAX-S1-TM-D614G and pVAX-S1 DNA vaccines (100 μg/mouse) were administered in two doses, at three-week interval, by intramuscular injection (i.m.) followed by electroporation, to young/adult (11 weeks old) C57BL/6 mice (n=4 mice/group). Bleeding occurred before vaccination and two weeks after the last booster for sera analysis of anti-Spike-antibody titer.

Flow cytometric analysis was performed to detect the presence of anti-Spike antibodies in the sera from vaccinated mice. These obtained results are shown in Figure 32 and indicate that both vaccines are immunogenic and able to elicit a statistically significant antibody response, although the pVAX-S1-TM-D614G vaccine appears to be more effective than pVAX-S1.

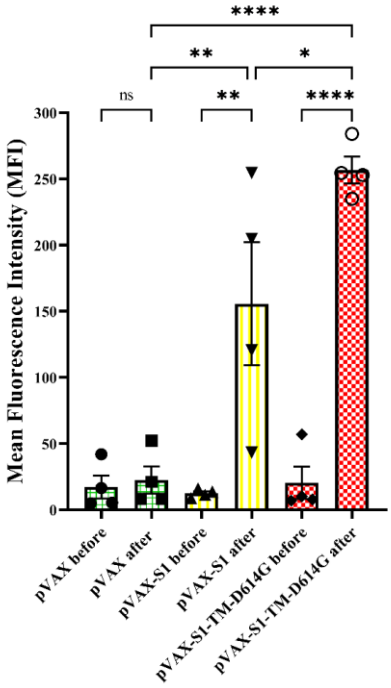

Figure 32. pVAX-S1-TM-D614G induced a higher level of anti-Spike antibodies with respect to pVAX-S1 in C57BL/6 mice. Antibody titer was measured by flow cytometry on HEK-293 cells ectopically expressing SARS-CoV-2-Spike protein. Bars, Mean +/- SEM. * p<0.05; ** p<0.01; *** p<0.001; **** p<0.0001; Two-way ANOVA followed by Tukey's multiple comparisons test.

The presence of specific anti-S1 antibodies in immune sera was confirmed by immunofluorescence analysis. In particular, sera from mice vaccinated with pVAX-S1 or pVAX-S1-TM-D614G were tested on HEK-293 cells transiently transfected with pcDNA3.1 SARS2-Spike, which express the S protein. The most representative images are shown below (Figure 33).

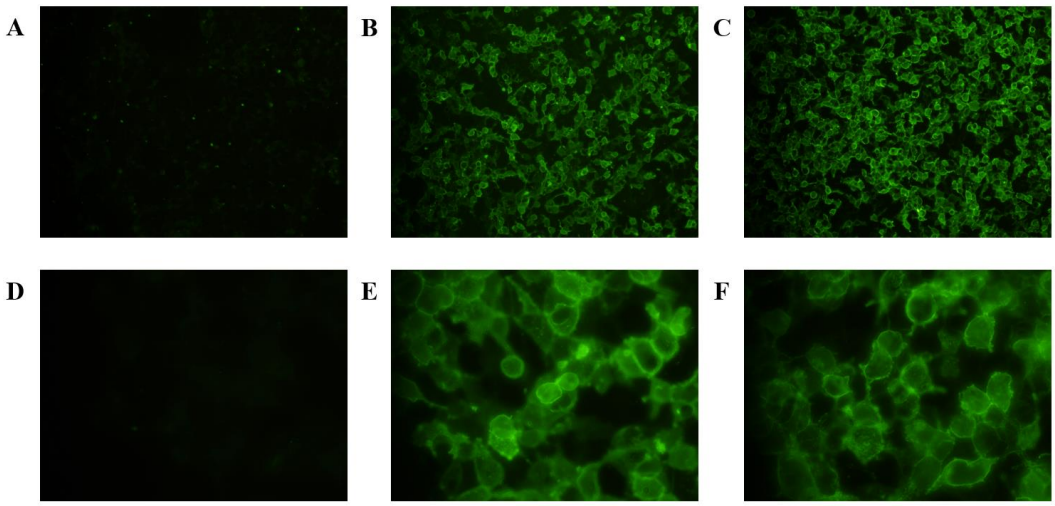

Figure 33. Immune sera of mice immunized with (A&D) empty plasmid pVAX (Control); (B&E) pVAX-S1 and (C&F) pVAX-SI-TM-D614G vaccines were tested on HEK-293 cells transiently transfected with pcDNA3.1 SARS2-Spike, to analyze the antibody response against SARS-CoV-2 spike protein. Alexa Fluor® 488 goat anti-mouse IgG was used as secondary antibody (green). Images were captured using inverted fluorescence microscope at 10X (A, B and C) and 40X (D, E and F) Magnifications.

4. DNA vaccines against the SARS-CoV-2 variants

Positive evolutionary selection of mutations within the spike protein has led to the genesis of new SARS-CoV-2 variants with greatly enhanced overall fitness. The rate at which mutations occur in the SARS-CoV-2 is about 10^{-4} nucleotide substitutions per site per year [115]. As of March 2022, five SARS-CoV-2 strains were defined "variants of concern" by the World Health Organization: The Alpha, Beta, Gamma, Delta, and Omicron variants [116]. Thus, we decided to construct three additional DNA vaccines against SARS-CoV-2 variants of concern: the first one was specifically conceived against the English (UK) variant (Alpha variant; B.1.1.7), the second was developed against the Indian (Delta variant; B.1.617) variant, and the last is a chimeric DNA vaccine (INDUK), that combines the UK and IND main mutations. In particular, the key mutations (A570D, and N501Y) of UK lineage or key mutations (E484Q and L452R) of Indian lineage (IND) or their combination were inserted in the pVAX-S1-TM-D614G DNA vaccine, which already included the global dominant D614G mutation and was validated both *in vitro* and *in vivo*, using the PCR-based mutagenesis protocol [111] described in the Methods section.

4.1 pVAX-S1-TM-UK: the DNA vaccine against the United Kingdom (UK) (B.1.1.7) variant

The pVAX-S1-TM-UK vaccine was obtained by inserting three key mutations that characterize the Alpha variant (B.1.1.7): N501Y, A570D and D614G. Of note, N501Y has been identified as one the mutations that not only contribute to reduce the neutralization of the mutant viruses by post-vaccinated sera (vaccines against the

original Wuhan lineage), but also confer increased binding affinity of Spike for ACE2. The nucleotide sequence and the presence of the selected UK mutations was analyzed by sequencing (BMR Genomics) and the results are reported below:

D614G leads to the change of aspartic acid (Asp or D) to glycine (Gly or G) at position 614, GGC replaces GAC as indicated in red; N501Y leads to the change of asparagine (Asn or N) to tyrosine (Tyr or Y) at position 501, TAC replaces AAC as indicated in green; A570D leads to the change of alanine (Ale or A) to aspartic acid (Asp or D) at position 570, GAT replaces GCT as indicated in blue.

ATGTTTGTCTTCCTGGTCCTGCTGCCTCTGGTCTCGTCTCAGTGCGTGAACCTGACTACTAGAACCCAGCTGCCTCCT
GCCTATACTAACTCCTTCACCCGCGGCGTGTACTACCCAGACAAGGTGTTCCGCAGCTCCGTGCTGCACTCCACCCA
GGATCTGTTCCTGCCCTTCTTCAGCAACGTGACCTGGTTCCACGCCATCCACGTGAGCGGCACCAATGGCACCAAG
CGGTTCGACAATCCCGTGCTGCCATTCAACGATGGCGTGTACTTCGCCTCCACCGAGAAGAGCAACATCATCCGCGG
CTGGATCTTCGGCACCACCCTGGACTCCAAGACCCAGAGCCTGCTGATCGTGAACAATGCCACCAACGTGGTCATC
AAGGTGTGCGAGTTCCAGTTCTGCAATGATCCATTCCTGGGCGTGTACTACCACAAGAACAATAAGTCCTGGATGGA
GAGCGAGTTCCGCGTGTACAGCTCCGCCAACAATTGCACCTTCGAGTACGTGTCCCAGCCCTTCCTGATGGACCTGG
AGGGCAAGCAGGGCAATTTCAAGAACCTGCGCGAGTTCGTGTTCAAGAATATCGATGGCTACTTCAAGATCTACTCC
AAGCACACCCCCATCAACCTGGTGCGCGACCTGCCACAGGGCTTCAGCGCCCTGGAGCCACTGGTGGATCTGCCAA
TCGGCATCAACATCACCAGGTTCCAGACCCTGCTGGCCCTGCACCGCAGCTACCTGACCCCAGGCGACAGCTCCAG
CGGATGGACCGCTGGAGCTGCTGCCTACTACGTGGGCTACCTGCAGCCCCGCACCTTCCTGCTGAAGTACAACGAG
AATGGCACCATCACCGACGCCGTGGATTGCGCCCTGGATCCACTGTCCGAGACAAAGTGCACCCTGAAGAGCTTCA
CCGTGGAGAAGGGCATCTACCAGACCTCCAATTTCCGCGTGCAGCCAACCGAGAGCATCGTGCGCTTCCCCAATATC
ACCAACCTGTGCCCATTCGGCGAGGTGTTCAACGCTACCAGGTTCGCCAGCGTGTACGCTTGGAATCGCAAGCGCA
TCTCCAACTGCGTGGCCGACTACAGCGTGCTGTACAACTCCGCCAGCTTCTCCACCTTCAAGTGCTACGGCGTGTCC
CCCACCAAGCTGAATGATCTGTGCTTCACCAACGTGTACGCCGATAGCTTCGTGATCAGGGGCGACGAGGTGCGCC
AGATCGCTCCAGGACAGACCGGCAAGATCGCTGACTACAATTACAAGCTGCCCGACGATTTCACCGGCTGCGTGAT
CGCCTGGAACTCCAACAATCTGGATAGCAAAGTGGGCGGCAACTACAATTACCTGTACCGCCTGTTCCGCAAGTCC
AATCTGAAGCCATTCGAGCGCGACATCTCCACCGAGATCTACCAGGCTGGAAGCACCCCATGCAATGGAGTGGAGG
GCTTCAACTGCTACTTCCCCCTGCAGAGCTACGGCTTCCAGCCAACCTACGGAGTGGGATACCAGCCATACAGGGTG
GTGGTGCTGTCCTTCGAGCTGCTGCACGCTCCAGCTACCGTGTGCGGACCAAAGAAGAGCACCAATCTGGTGAAGA
ACAAGTGCGTGAACTTCAATTTCAACGGCCTGACCGGAACCGGCGTGCTGACCGAGTCCAACAAGAAGTTCCTGCC
CATTCCAGCAGTTCGGAAGGGACATCGATGATACCACCGACGCCGTGCGCGACCCACAGACCCTGGAGATCCTGGA
TATCACCCCATGCTCCTTCGGCGGCGTGAGCGTGATCACCCCAGGAACCAATACCAGCAACCAGGTGGCCGTGCTGT
ACCAGGGCGTGAATTGCACCGAGGTGCCAGTGGCTATCCACGCTGATCAGCTGACCCCAACCTGGCGCGTGTACAG
CACCGGATCCAACGTGTTCCAGACCCGCGCCGGATGCCTGATCGGAGCTGAGCACGTGAACAATTCCTACGAATTC
TGGTACATCTGGCTGGGCTTCATCGCCGGCCTGATCGCCATCGTGATGGTGACCATCATGCTGTGCTGCATGACCTCC
TGCTGCAGCTGCCTGAAGGGCTGCTGCTCCTGCGGCAGCTGCTGCAAGTTCGATGAGGACGATAGCGAGCCCGTGC
TGAAGGGCGTCAAACTGCACTATACAGGCTCCACCGAGACATCCCAGGTCGCTCCCGCTTAG

4.2 pVAX-S1-TM-Indian: the DNA vaccine against the Indian (IND) variant (B.1.617)

The pVAX-S1-TM-Indian vaccine was obtained by inserting three key mutations that characterize the Delta (B.1.617) variant: E484Q and L452R and D614G.

Actually, a first attempt to obtain pVAX-S1-TM-Indian vaccine failed. In fact, thanks to pairwise sequence alignment tool (EMBL-EBI), an unwanted mutation was discovered in the antigen sequence (Figure 34). In detail, a nonsense mutation was introduced during the PCR amplification process (cytosine (C) was substituted by thymine (T)), leading to the appearance of a stop codon, as highlighted in red. The appearance of the stop codon gives rise to premature termination of translation and truncated polypeptides. Thus, the antigenic protein encoded by pVAX-S1-TM-Indian vaccine could not be expressed.

The nucleotide sequence of pVAX-S1-TM-Indian:

ATGTTTGTCTTCCTGGTCCTGCTGCCTCTGGTCTCGTCTCAGTGCGTGAACCTGACTACTAGAACCCAGCTGCCTCCT
GCCTATACTAACTCCTTCACCCGCGGCGTGTACTACCCAGACAAGGTGTTCCGCAGCTCCGTGCTGCACTCCACCTA
GGATCTGTTCCTGCCCTTCTTCAGCAACGTGACCTGGTTCCACGCCATCCACGTGAGCGGCACCAATGGCACCAAG
CGGTTCGACAATCCCGTGCTGCCATTCAACGATGGCGTGTACTTCGCCTCCACCGAGAAGAGCAACATCATCCGCG
GCTGGATCTTCGGCACCACCCTGGACTCCAAGACCCAGAGCCTGCTGATCGTGAACAATGCCACCAACGTGGTCAT
CAAGGTGTGCGAGTTCCAGTTCTGCAATGATCCATTCCTGGGCGTGTACTACCACAAGAACAATAAGTCCTGGATGG
AGAGCGAGTTCCGCGTGTACAGCTCCGCCAACAATTGCACCTTCGAGTACGTGTCCCAGCCCTTCCTGATGGACCT
GGAGGGCAAGCAGGGCAATTTCAAGAACCTGCGCGAGTTCGTGTTCAAGAATATCGATGGCTACTTCAAGATCTAC
TCCAAGCACACCCCCATCAACCTGGTGCGCGACCTGCCACAGGGCTTCAGCGCCCTGGAGCCACTGGTGGATCTGC
CAATCGGCATCAACATCACCAGGTTCCAGACCCTGCTGGCCCTGCACCGCAGCTACCTGACCCCAGGCGACAGCTC
CAGCGGATGGACCGCTGGAGCTGCTGCCTACTACGTGGGCTACCTGCAGCCCCGCACCTTCCTGCTGAAGTACAAC
GAGAATGGCACCATCACCGACGCCGTGGATTGCGCCCTGGATCCACTGTCCGAGACAAAGTGCACCCTGAAGAGCT
TCACCGTGGAGAAGGGCATCTACCAGACCTCCAATTTCCGCGTGCAGCCAACCGAGAGCATCGTGCGCTTCCCCAA
TATCACCAACCTGTGCCCATTCGGCGAGGTGTTCAACGCTACCAGGTTCGCCAGCGTGTACGCTTGGAATCGCAAGC
GCATCTCCAACTGCGTGGCCGACTACAGCGTGCTGTACAACTCCGCCAGCTTCTCCACCTTCAAGTGCTACGGCGTG
TCCCCCACCAAGCTGAATGATCTGTGCTTCACCAACGTGTACGCCGATAGCTTCGTGATCAGGGGCGACGAGGTGC
GCCAGATCGCTCCAGGACAGACCGGCAAGATCGCTGACTACAATTACAAGCTGCCCGACGATTTCACCGGCTGCGT
GATCGCCTGGAACTCCAACAATCTGGATAGCAAAGTGGGCGGCAACTACAATTACCTGTACCGCCTGTTCCGCAAGT
CCAATCTGAAGCCATTCGAGCGCGACATCTCCACCGAGATCTACCAGGCTGGAAGCACCCCATGCAATGGAGTGGA

GGGCTTCAACTGCTACTTCCCCCTGCAGAGCTACGGCTTCCAGCCAACCAACGGAGTGGGATACCAGCCATACAGG
GTGGTGGTGCTGTCCTTCGAGCTGCTGCACGCTCCAGCTACCGTGTGCGGACCAAAGAAGAGCACCAATCTGGTGA
AGAACAAGTGCGTGAACTTCAATTTCAACGGCCTGACCGGAACCGGCGTGCTGACCGAGTCCAACAAGAAGTTCC
TGCCATTCCAGCAGTTCGGAAGGGACATCGCTGATACCACCGACGCCGTGCGCGACCCACAGACCCTGGAGATCCT
GGATATCACCCCATGCTCCTTCGGCGGCGTGAGCGTGATCACCCCAGGAACCAATACCAGCAACCAGGTGGCCGTG
CTGTACCAGGGCGTGAATTGCACCGAGGTGCCAGTGGCTATCCACGCTGATCAGCTGACCCCAACCTGGCGCGTGT
ACAGCACCGGATCCAACGTGTTCCAGACCCGCGCCGGATGCCTGATCGGAGCTGAGCACGTGAACAATTCCTACGA
ATTCTGGTACATCTGGCTGGGCTTCATCGCCGGCCTGATCGCCATCGTGATGGTGACCATCATGCTGTGCTGCATGAC
CTCCTGCTGCAGCTGCCTGAAGGGCTGCTGCTCCTGCGGCAGCTGCTGCAAGTTCGATGAGGACGATAGCGAGCCC
GTGCTGAAGGGCGTCAAACTGCACTATACAGGCTCCACCGAGACATCCCAGGTCGCTCCCGCTTAG

Figure 34. Pairwise sequence alignment between the reconstructed plasmid and the expected pVAX-S1-TM-Indian including E484Q and L452R mutants: in the first version of pVAX-S1-TM-Indian an unwanted mutation introduced a stop codon in the sequence resulting in premature termination of translation.

Due to the unwanted mutation in the sequence of previously obtained pVAX-S1-TM-IND, the vaccine was again constructed and successfully obtained. The nucleotide sequence was verified by sequencing (BMR Genomics) to examine the presence of the key mutations in the pVAX-S1-TM-Indian vaccine. The sequence below shows the three selected mutations (E484Q and L452R and D614G) inserted into the S1-TM sequence. D614G leads to the change of aspartic acid (Asp or D) to glycine (Gly or G) at position 614, GGC replaces GAC as indicated in red; E484Q leads to the change of glutamic acid (Glu or E) to glutamine (Gln or G) at position 484, CAG replaces GAG as indicated in purple; L452R leads to the change of leucine

(Leu or L) to arginine (Arg or R) at position 452, CGG replaces CTG as indicated in yellow.

The nucleotide sequence of pVAX-S1-TM-Indian:

ATGTTTGTCTTCCTGGTCCTGCTGCCTCTGGTCTCGTCTCAGTGCGTGAACCTGACTACTAGAACCCAGCTGCCTCCT
GCCTATACTAACTCCTTCACCCGCGGCGTGTACTACCCAGACAAGGTGTTCCGCAGCTCCGTGCTGCACTCCACCCA
GGATCTGTTCCTGCCCTTCTTCAGCAACGTGACCTGGTTCCACGCCATCCACGTGAGCGGCACCAATGGCACCAAG
CGGTTCGACAATCCCGTGCTGCCATTCAACGATGGCGTGTACTTCGCCTCCACCGAGAAGAGCAACATCATCCGCGG
CTGGATCTTCGGCACCACCCTGGACTCCAAGACCCAGAGCCTGCTGATCGTGAACAATGCCACCAACGTGGTCATC
AAGGTGTGCGAGTTCCAGTTCTGCAATGATCCATTCCTGGGCGTGTACTACCACAAGAACAATAAGTCCTGGATGGA
GAGCGAGTTCCGCGTGTACAGCTCCGCCAACAATTGCACCTTCGAGTACGTGTCCCAGCCCTTCCTGATGGACCTGG
AGGGCAAGCAGGGCAATTTCAAGAACCTGCGCGAGTTCGTGTTCAAGAATATCGATGGCTACTTCAAGATCTACTCC
AAGCACACCCCCATCAACCTGGTGCGCGACCTGCCACAGGGCTTCAGCGCCCTGGAGCCACTGGTGGATCTGCCAA
TCGGCATCAACATCACCAGGTTCCAGACCCTGCTGGCCCTGCACCGCAGCTACCTGACCCCAGGCGACAGCTCCAG
CGGATGGACCGCTGGAGCTGCTGCCTACTACGTGGGCTACCTGCAGCCCCGCACCTTCCTGCTGAAGTACAACGAG
AATGGCACCATCACCGACGCCGTGGATTGCGCCCTGGATCCACTGTCCGAGACAAAGTGCACCCTGAAGAGCTTCA
CCGTGGAGAAGGGCATCTACCAGACCTCCAATTTCCGCGTGCAGCCAACCGAGAGCATCGTGCGCTTCCCCAATATC
ACCAACCTGTGCCCATTCGGCGAGGTGTTCAACGCTACCAGGTTCGCCAGCGTGTACGCTTGGAATCGCAAGCGCA
TCTCCAACTGCGTGGCCGACTACAGCGTGCTGTACAACTCCGCCAGCTTCTCCACCTTCAAGTGCTACGGCGTGTCC
CCCACCAAGCTGAATGATCTGTGCTTCACCAACGTGTACGCCGATAGCTTCGTGATCAGGGGCGACGAGGTGCGCC
AGATCGCTCCAGGACAGACCGGCAAGATCGCTGACTACAATTACAAGCTGCCCGACGATTTCACCGGCTGCGTGAT
CGCCTGGAACTCCAACAATCTGGATAGCAAAGTGGGCGGCAACTACAATTACCGGTACCGCCTGTTCCGCAAGTCC
AATCTGAAGCCATTCGAGCGCGACATCTCCACCGAGATCTACCAGGCTGGAAGCACCCCATGCAATGGAGTGCAGG
GCTTCAACTGCTACTTCCCCCTGCAGAGCTACGGCTTCCAGCCAACCAACGGAGTGGGATACCAGCCATACAGGGT
GGTGGTGCTGTCCTTCGAGCTGCTGCACGCTCCAGCTACCGTGTGCGGACCAAAGAAGAGCACCAATCTGGTGAAG
AACAAGTGCGTGAACTTCAATTTCAACGGCCTGACCGGAACCGGCGTGCTGACCGAGTCCAACAAGAAGTTCCTG
CCATTCCAGCAGTTCGGAAGGGACATCGCTGATACCACCGACGCCGTGCGCGACCCACAGACCCTGGAGATCCTGG
ATATCACCCCATGCTCCTTCGGCGGCGTGAGCGTGATCACCCCAGGAACCAATACCAGCAACCAGGTGGCCGTGCT
GTACCAGGGCGTGAATTGCACCGAGGTGCCAGTGGCTATCCACGCTGATCAGCTGACCCCAACCTGGCGCGTGTAC
AGCACCGGATCCAACGTGTTCCAGACCCGCGCCGGATGCCTGATCGGAGCTGAGCACGTGAACAATTCCTACGAAT
TCTGGTACATCTGGCTGGGCTTCATCGCCGGCCTGATCGCCATCGTGATGGTGACCATCATGCTGTGCTGCATGACCT
CCTGCTGCAGCTGCCTGAAGGGCTGCTGCTCCTGCGGCAGCTGCTGCAAGTTCGATGAGGACGATAGCGAGCCCGT
GCTGAAGGGCGTCAAACTGCACTATACAGGCTCCACCGAGACATCCCAGGTCGCTCCCGCTTAG

4.3 pVAX-S1-TM-INDUK: the chimeric DNA vaccine

pVAX-S1-TM-INDUK was generated by introducing in the sequence of S1-TM a combination of UK and IND main selected mutations. Gene sequencing analysis of pVAX-S1-TM-INDUK plasmid is reported below: the global mutation D614G (in red)

together with the key mutations involved in the U.K (B.1.1.7) variant (N501Y (in green) and A570D (in blue)) and in the Indian (B.1.617) variant (E484Q (in purple) and L452R (in yellow)) are indicated. Pairwise sequence alignments assure that CAG replaces GAG, leading to the change of glutamic acid (Glu or E) to glutamine (Gln or Q) at position 484, and CGG substitutes CTG, leading to the change of leucine (Leu or L) to arginine (Arg or R) at position 452.

The nucleotide sequence of pVAX-S1-TM-INDUK:

ATGTTTGTCTTCCTGGTCCTGCTGCCTCTGGTCTCGTCTCAGTGCGTGAACCTGACTACTAGAACCCAGCTGCCTCCT
GCCTATACTAACTCCTTCACCCGCGGCGTGTACTACCCAGACAAGGTGTTCCGCAGCTCCGTGCTGCACTCCACCCA
GGATCTGTTCCTGCCCTTCTTCAGCAACGTGACCTGGTTCCACGCCATCCACGTGAGCGGCACCAATGGCACCAAG
CGGTTCGACAATCCCGTGCTGCCATTCAACGATGGCGTGTACTTCGCCTCCACCGAGAAGAGCAACATCATCCGCG
GCTGGATCTTCGGCACCACCCTGGACTCCAAGACCCAGAGCCTGCTGATCGTGAACAATGCCACCAACGTGGTCAT
CAAGGTGTGCGAGTTCCAGTTCTGCAATGATCCATTCCTGGGCGTGTACTACCACAAGAACAATAAGTCCTGGATGG
AGAGCGAGTTCCGCGTGTACAGCTCCGCCAACAATTGCACCTTCGAGTACGTGTCCCAGCCCTTCCTGATGGACCT
GGAGGGCAAGCAGGGCAATTTCAAGAACCTGCGCGAGTTCGTGTTCAAGAATATCGATGGCTACTTCAAGATCTAC
TCCAAGCACACCCCCATCAACCTGGTGCGCGACCTGCCACAGGGCTTCAGCGCCCTGGAGCCACTGGTGGATCTGC
CAATCGGCATCAACATCACCAGGTTCCAGACCCTGCTGGCCCTGCACCGCAGCTACCTGACCCCAGGCGACAGCTC
CAGCGGATGGACCGCTGGAGCTGCTGCCTACTACGTGGGCTACCTGCAGCCCCGCACCTTCCTGCTGAAGTACAAC
GAGAATGGCACCATCACCGACGCCGTGGATTGCGCCCTGGATCCACTGTCCGAGACAAAGTGCACCCTGAAGAGCT
TCACCGTGGAGAAGGGCATCTACCAGACCTCCAATTTCCGCGTGCAGCCAACCGAGAGCATCGTGCGCTTCCCCAA
TATCACCAACCTGTGCCCATTCGGCGAGGTGTTCAACGCTACCAGGTTCGCCAGCGTGTACGCTTGGAATCGCAAGC
GCATCTCCAACTGCGTGGCCGACTACAGCGTGCTGTACAACTCCGCCAGCTTCTCCACCTTCAAGTGCTACGGCGTG
TCCCCCACCAAGCTGAATGATCTGTGCTTCACCAACGTGTACGCCGATAGCTTCGTGATCAGGGGCGACGAGGTGC
GCCAGATCGCTCCAGGACAGACCGGCAAGATCGCTGACTACAATTACAAGCTGCCCGACGATTTCACCGGCTGCGT
GATCGCCTGGAACTCCAACAATCTGGATAGCAAAGTGGGCGGCAACTACAATTACCGGTACCGCCTGTTCCGCAAG
TCCAATCTGAAGCCATTCGAGCGCGACATCTCCACCGAGATCTACCAGGCTGGAAGCACCCCATGCAATGGAGTGC
AGGGCTTCAACTGCTACTTCCCCCTGCAGAGCTACGGCTTCCAGCCAACCTACGGAGTGGGATACCAGCCATACAG
GGTGGTGGTGCTGTCCTTCGAGCTGCTGCACGCTCCAGCTACCGTGTGCGGACCAAAGAAGAGCACCAATCTGGTG
AAGAACAAGTGCGTGAACTTCAATTTCAACGGCCTGACCGGAACCGGCGTGCTGACCGAGTCCAACAAGAAGTTC
CTGCCATTCCAGCAGTTCGGAAGGGACATCGATGATACCACCGACGCCGTGCGCGACCCACAGACCCTGGAGATCC
TGGATATCACCCCATGCTCCTTCGGCGGCGTGAGCGTGATCACCCCAGGAACCAATACCAGCAACCAGGTGGCCGT
GCTGTACCAGGGCGTGAATTGCACCGAGGTGCCAGTGGCTATCCACGCTGATCAGCTGACCCCAACCTGGCGCGTG
TACAGCACCGGATCCAACGTGTTCCAGACCCGCGCCGGATGCCTGATCGGAGCTGAGCACGTGAACAATTCCTACG
AATTCTGGTACATCTGGCTGGGCTTCATCGCCGGCCTGATCGCCATCGTGATGGTGACCATCATGCTGTGCTGCATGA
CCTCCTGCTGCAGCTGCCTGAAGGGCTGCTGCTCCTGCGGCAGCTGCTGCAAGTTCGATGAGGACGATAGCGAGCC
TGTGCTGAAGGGCGTCAAACTGCACTATACAGGCTCCACCGAGACATCCCAGGTCGCTCCCGCTTAG

4.4. In vitro validation of DNA vaccines against the SARS-CoV-2 variants

4.4.1 Strong expression of antigenic sequences on mammalian cells

An immunofluorescence assay was carried out to verify the expression of the antigenic sequences on HEK-293 cells transiently transfected with anti-SARS-CoV-2 DNA vaccines. As shown in Figure 35, HEK-293 cells transfected with pVAX-S1-TM-UK, pVAX-S1-TM-INDIAN or pVAX-S1-TM-INDUK DNA vaccines, properly expressed the target antigens on their membranes, as demonstrated by a strong fluorescent signal mainly localized at the level of the plasma membrane and visible even without cell permeabilization.

Figure 35. Immunofluorescence analysis of the expression of antigenic portions of Spike protein after transient transfection of HEK-293 cells with (A) pVAX-SI-TM-UK: including D614G, A570D and N501Y mutations; (B) pVAX-S1-TM-INDIAN: including D614G, E484Q and L452R mutations; (C) pVAX-S1-TM-INDUK: including D614G, A570D, N501Y, E484Q and L452R mutations. Expression of Spike protein was detected 48 h after transfection with a monoclonal rabbit anti-SARS-CoV-2 Spike S1 Protein IgG and Goat anti-rabbit IgG Alex Fluor 488® secondary antibody (green). Images were captured using inverted fluorescence microscope at 40X Magnification.

4.5 Immunogenicity of pVAX-S1-TM-D614G and pVAX-S1-TM-INDUK DNA vaccines in C57BL/6 young and aged mice

Aging often results in a marked reduction in immune protection against infection in elderly, and it is known that SARS-CoV-2 infection leads to higher mortality rates in aged individuals than in younger ones [117]. A recent study reported that in C57BL/6N aged mice model, the serum neutralizing antibody titers in sera were significantly lower than that of the vaccinated young mice, and 2 out of 6 aged mice had no detectable neutralizing antibodies after two doses of vaccine. Even the highly

immunogenic BNT162b2 mRNA vaccine failed to induce satisfactory antibody responses in aged mice [118]. Thus, protecting older peoples from COVID-19 with an effective vaccine represents a high-priority goal. For this purpose, we decided to test pVAX-S1-TM-D614G and pVAX-S1-TM-INDUK DNA vaccines not only in young/adults C57BL/6 mice (11 weeks of age), but also in aged C57BL/6 mice (20 months of age) as a preclinical model for elderly humans, and immunogenicity of candidate DNA vaccines and duration of immune responses were evaluated. pVAX-S1-TM-D614G, pVAX-S1-TM-INDUK or empty pVAX vector as control (100 μg of naked plasmid DNA/mouse) were administered, via intramuscular injection followed by electroporation, in two doses at 21-day intervals; blood samples were collected the day before the first vaccination and two weeks after the last vaccination, and once a month (for a total period of 6 months) to measure the antibody response and to establish the duration of the immunoprotection (Figure 36).

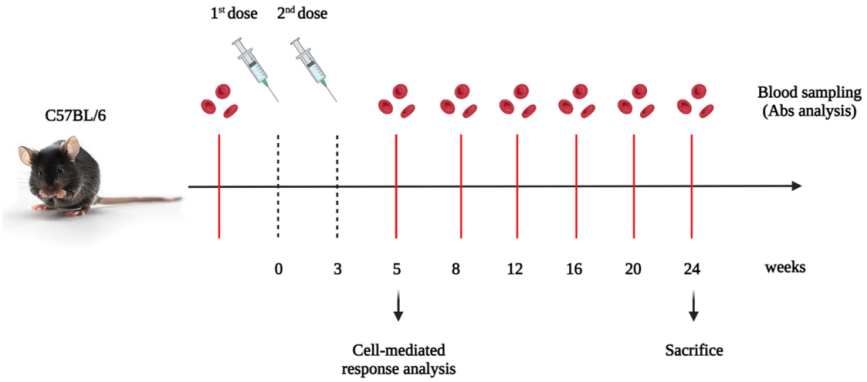

Figure 36. Vaccination regimen. Mice (n=8 mice/group) underwent a 3-week interval between two consecutive DNA vaccine boosts. Two weeks after the last vaccination, blood was harvested for antibody screening. In particular, pVAX-S1-TM-D614G and pVAX-S1-TM-INDUK Covid vaccines were administered by intramuscular injection (i.m.) followed by electroporation in both young and aged C57BL/6 mice.

The presence of anti-Spike antibodies in the sera of immunized mice was assessed by flow cytometry using HEK-293 cells ectopically expressing SARS-CoV-2-Spike protein as targeted cells. Both pVAX-S1-TM-D614G and pVAX-S1-TM-INDUK SARS-CoV-2 DNA vaccines elicited a statistically significant higher anti-Spike antibody titer in both young and old mice with respect to pVAX (control group

of mice), although a wide variation between individuals was observed, especially in the old mice group. On average, the antibody level elicited by our DNA vaccines was lower in old mice than in young mice (Figure 37). This result is in agreement with previous studies by other research groups, reporting that the quality of the humoral immune response declines with age, as aged B cells display a diminished potential to undergo somatic hypermutation, which could prevent aged individuals from generating robust neutralizing antibody titers to aid the clearance of natural infection and generate effective immunity against reinfections [106, 119, 120]. This decline in immune function (immunosenescence) limits also the effectiveness of vaccinations in older adults. Nevertheless, the obtained results indicate that pVAX-S1-TM-D614G and pVAX-S1-TM-INDUK are immunogenic not only in young mice, but also in aged animals.

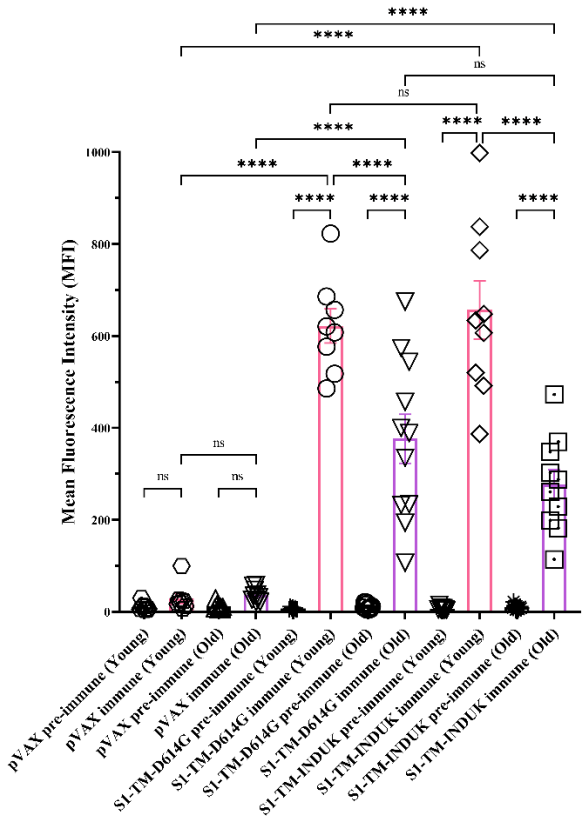

Figure 37. Antibody responses to pVAX-S1-TM-D614G, pVAX-S1-TM-INDUK or pVAX (control) in young and old C57BL/6 mice. Sera were harvested from immunized mice after two doses of DNA vaccines and antibody levels were measured by flow cytometry. Bars, Mean +/- SEM. * p<0.05; ** p<0.01; *** p<0.001; **** p<0.0001; Two-way ANOVA followed by Tukey's multiple comparisons test.

Numerous studies have reported a marked decline in antibody levels 6 months after the second vaccination against SARS-CoV-2 [121-123]. The persistence of antibodies in immunized mice is a key factor that cannot be ignored. Therefore, we assessed antibody levels for 6 months after a two-dose DNA vaccine regimen in both young and aged C57BL/6 mice. Flow cytometry analysis showed a significant and time-dependent decrease in antibody levels already fifty days after the second vaccination (23/03/2022), however, reasonable levels of antibodies in the young group of mice immunized with pVAX-S1-TM-INDUK DNA vaccine persisted until week 20 and showed statistical significance as far as 3 months after the second vaccination (Figure 38).

Thus, pVAX-S1-TM-INDUK DNA vaccine elicited robust and more persistent antibody response in young animals with respect to pVAX-S1-TM-D614G. Unfortunately, both DNA vaccines were not able to elicit a persistent antibody response in aged mice, in which the antibody levels dropped down within two months from the last vaccination.

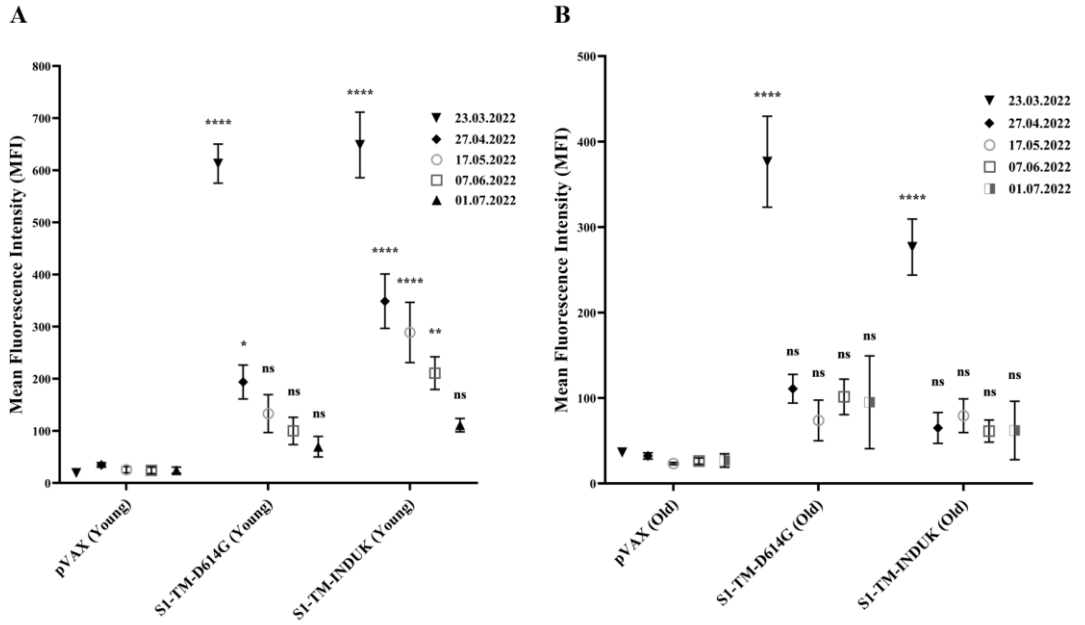

Figure 38. Antibody persistency and post-vaccination trend in both (A) young and (B) aged C57BL/6 mice. Antibody levels in the sera of immunized mice were evaluated via flow cytometry on HEK-293 cells transfected with pcDNA3.1-SARS2-Spike. The blood was taken at three weeks intervals for 6 months for antibody monitoring. dots, Mean +/- SEM. * $p<0.05$; ** $p<0.01$; *** $p<0.001$; **** $p<0.0001$; Two-way ANOVA followed by Tukey's multiple comparisons test.

Boosting strategies have been reported to significantly increase immune responses and raised the level of protection against symptomatic disease, hospitalization and death [124, 125]. To address whether a booster dose can restore waning immunity in young and older mice, we gave a third dose of pVAX-S1-TM-D614G and pVAX-S1-TM-INDUK DNA vaccines to groups of young and old mice who had completed their vaccination cycle by receiving a second dose six months earlier. Blood was collected two weeks after the third vaccination to assess their antibody response after the booster dose (Figure 39).

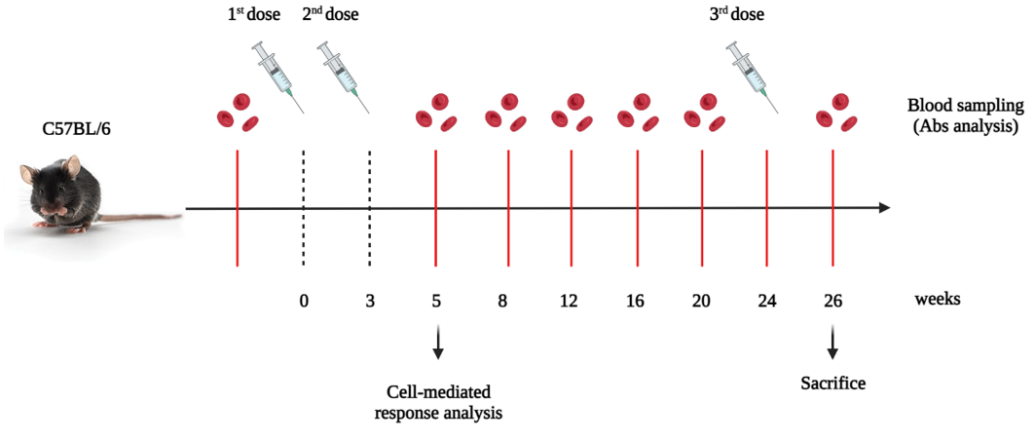

Figure 39. Vaccination regimen. Mice (n=8 mice/group) underwent a 3-week interval between two consecutive DNA vaccine boosts plus booster (3rd) dose. Two weeks after the booster dose, blood was harvested for antibody screening. In particular, pVAX-S1-TM-D614G and pVAX-S1-TM-INDUK Covid vaccines were administered by intramuscular injection (i.m.) followed by electroporation in both young and aged C57BL/6 mice.

Flow cytometry results showed that the booster doses of pVAX-S1-TM-D614G and pVAX-S1-TM-INDUK DNA vaccines significantly increased the magnitude of antibody titers in young and aged mice, suggesting that our vaccines can provide a long-lasting immunity if the vaccination schedule is optimized. Of note, 26-month-old mice displayed a non-inferior spike-specific antibody responses compared to younger mice after receiving a booster dose (Figure 40). No signs of toxicity were observed in vaccinated mice. Autoptic examination of old mice performed at the end of the experiment confirmed that our DNA vaccines do not cause any organ damage.

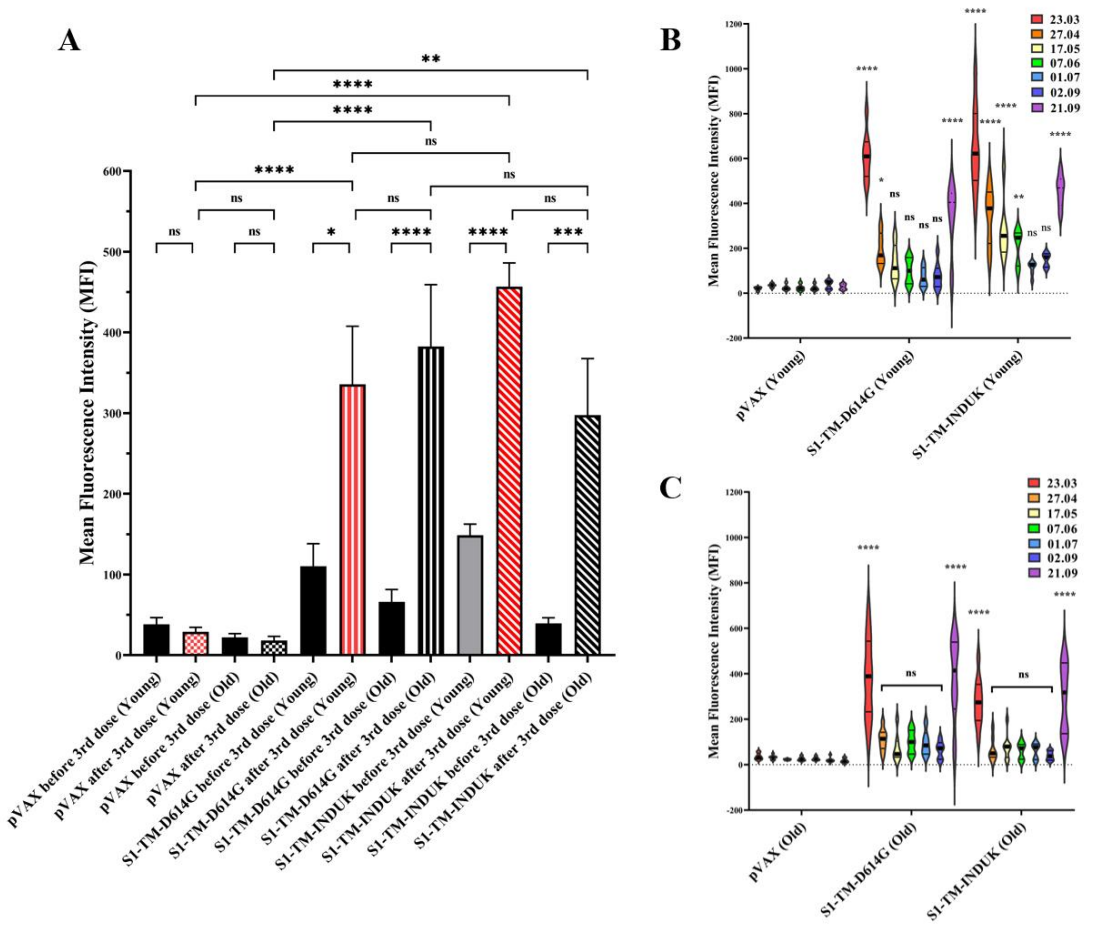

Figure 40. Booster doses increased the magnitude of antibody titers. Bar graph (A) represents antibody titers in sera of both young and old mice before and after receiving the third dose of vaccines. Violin plots (B&C) show antibody response elicited by two doses of vaccines, its decline during the following six month, and its recall by booster doses in young and aged mice, measured by flow cytometry. Violin plot, the center thick line represents the median, the thin lines the interquartile range and violin width kernel density estimates. Mean +/- SEM. * p<0.05; ** p<0.01; *** p<0.001; **** p<0.0001; Two-way ANOVA followed by Tukey's multiple comparisons test.

5. Generation and validation of multicomponent LNPs for DNA vaccination

Lipid nanoparticles (LNPs) represent a promising alternative to electroporation for DNA vaccine delivery. They depict the ideal carrier for DNA vaccines as it offers a higher safety profile compared with electroporation and ensure high cell transfection efficiency reducing off-target accumulation and extracellular DNA degradation. Multicomponent LNPs, conceived to deliver anti-SARS-CoV-2 DNA vaccines, were obtained by Prof. Giulio Caracciolo (Sapienza University of Rome).

5.1 Transfection efficiency and cell toxicity of LNPs: LNP15 displays optimal characteristics

Following the screening procedure (i.e., chemical-physical characterization), eight out of sixteen LNPs with the required characteristics for *in vitro* validation were tested on HEK-293 cells. According to their smaller than the threshold (200 nm), with average size = 130 nm and average polydispersity index (PdI) = 0.235. In Figure 41a, negative controls are reported as blue histograms having 100% cell viability and no luciferase expression (TE= 0), while positive controls are represented as red histograms and exhibited average TE= 4 and about 50% cell viability. Results for all the tested formulations are depicted as green histograms. The identification of the best candidate among the LNPs included in the library can be easily achieved by coupling TE and cell viability values in a scatter plot (Figure 41b). Each dot corresponds to a specific LNP, and its location is determined by the measured values of cell viability (x-axis) and TE (y-axis). Highly transfecting LNPs are generally cytotoxic, leading to cell viability values of about 50% (e.g., LNP12 and LNP14), whereas the most biocompatible system was the less performant as a transfecting agent (i.e., LNP13). LNP16, LNP8, and LNP15 exhibited comparable TE values, but increased cell viability, which read 40%, 75%, and 86%, respectively. Based on the results of Figure 41, LNP15 was identified as the most promising formulation for further validation, as it exhibited the best compromise between high TE (i.e., 3 order of magnitude higher than the negative control) and good biocompatibility (i.e., cell viability = 86%). Specifically, LNP15/pDNA complexes consisted of two cationic lipids, DOTAP and DC-Chol, and two helper lipids DOPE and DOPC, plus cholesterol and PEG-lipids: 1,2-dioleoyl-sn-glycero-3-phosphoethanolamine-N-[amino(polyethylene glycol)-2000] (DOPE-PEG) and 1,2-distearoyl-sn-glycero-3-phosphoethanolamine-N-[amino(polyethylene glycol)-2000] (DSPE-PEG) mixed with pGL3 (Firefly luciferase encoding plasmid).

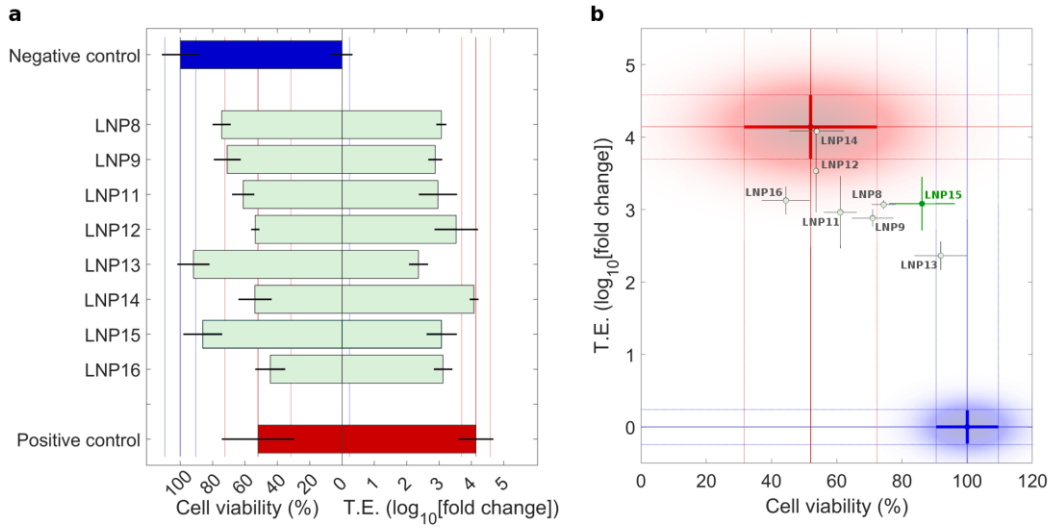

Figure 41. Transfection efficiency and cell viability of eight LNPs. (a) Histogram chart and (b) scatter plot of HEK-293 cell viability (with respect to non-treated cells) and transfection efficiency (expressed as fold-change with respect to non-treated cells) for LNPs.

5.2 In vitro and in vivo validation of LNP15 as DNA delivery system

The ability of LNPs to deliver DNA vaccines was evaluated *in vitro* and *in vivo*. Since LNP15 displayed an optimal compromise in terms of toxicity and transfection properties, it was chosen as formulation to encapsulate a prototype DNA vaccine: pVAX-hECTM, a DNA vaccine conceived against the oncogene HER2 and known to be able to elicit a protective immune response against HER2-positive breast cancer in preclinical model [126]. HER2 is a tyrosine kinase receptor overexpressed in roughly 20% of breast cancer patients and correlates with poor prognosis [127]. HER2 is considered an optimal target for cancer immunotherapies since it is expressed on the cell membrane, and thus it can be targeted by antibodies and cell-mediated immunity. HER2 comprises an extracellular (EC) domain of 654 amino acids, a single transmembrane-spanning domain (TM), and a long cytoplasmic tyrosine kinase domain (IC). pVAX-hECTM encodes a truncated version of the human HER2 protein, encoding the EC and TM domains but lacking the IC domain [126].

pVAX-hECTM encapsulated in LNP15 was validated *in vitro* to demonstrate that

transiently transfected cells can express the oncoantigen HER2 encoded by the DNA vaccine and can display it on the cell surface as required for inducing an effective humoral response (Figure 43A).

In vivo experiments were performed to evaluate the immunogenicity of LNP15 encapsulated pVAX-hECTM DNA vaccine. In particular, the ability of LNP15-hECTM to induce a specific antibody response in vaccinated mice was analyzed. C57BL/6 male mice (11 weeks of age) were administered by intramuscular (i.m.) injections into the tibial muscle two times at 3-week intervals with 100 μg of hECTM DNA vaccine or pVAX empty control vector encapsulated in LNP15 (4 mice/ experimental groups). Blood was collected two weeks after the last vaccination and analyzed by flow cytometry (BD FACSCalibur), using human HER-2 overexpressing SK-BR-3 cells as target cells (Figure 42).

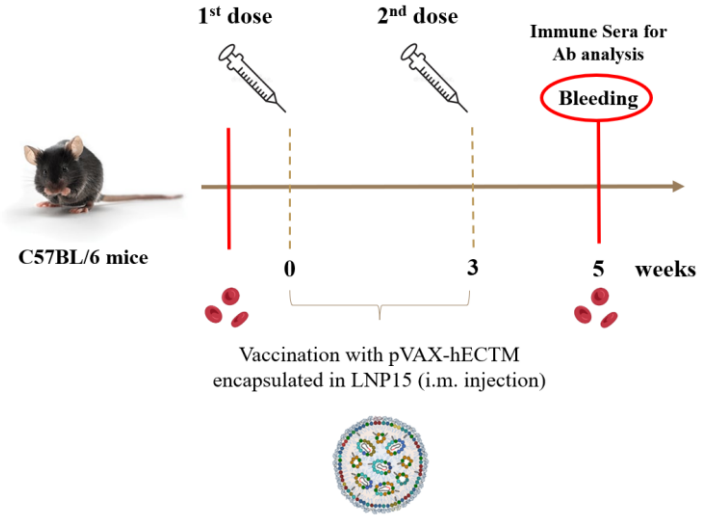

Figure 42. Vaccination regimen. C57BL/6 male mice (n=4 mice/group) underwent a 3-week interval between two consecutive DNA vaccine boosts. Two weeks after the last vaccination, blood was harvested for antibody screening. In particular, LNP15 encapsulated pVAX-hECTM DNA vaccines were administered by intramuscular injection.

Of note, mice immunization with LNP15-pVAX-hECTM triggered a significantly higher antibody titer with respect to encapsulated empty plasmids (LNP15-pVAX), which was used as controls (Figure 43b). Thus, pVAX-hECTM DNA vaccine, known to be effective against HER2-positive breast cancer when

administered by electroporation [126], was still immunogenic once encapsulated in LNP15. Such encouraging results shed light on this gene delivery approach. LNP15 formulation might be employed to develop a disruptive targeted nanoparticle DNA vaccine technology even against SARS-CoV-2 variants, overcoming the current limitations of electroporation-mediated vaccination.

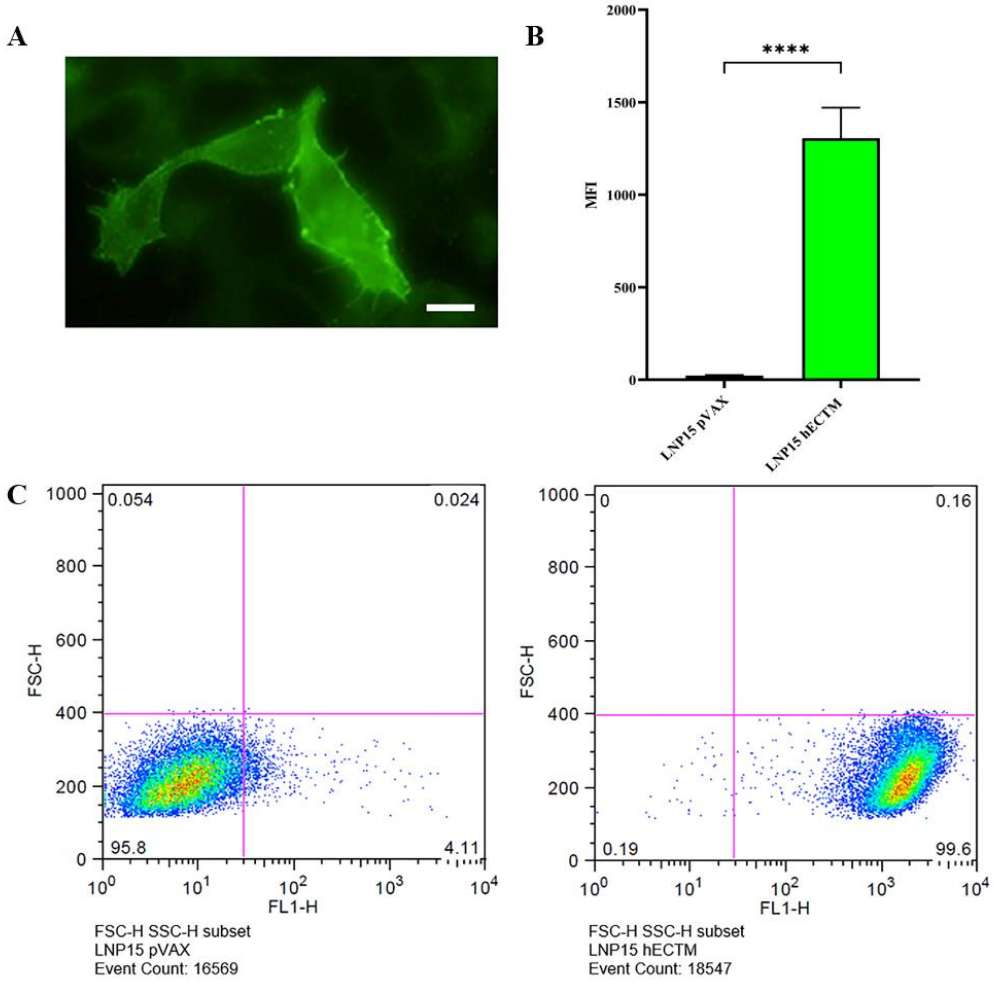

Figure 43. *In vitro* and *in vivo* validation of vaccine-loaded LNP15. (A) HEK-293 cells were transiently transfected with the pVAX-hECTM loaded LNP15 and analyzed under a fluorescence microscope 48 hours after transfection. To detect the expression of the HER2 antigen in the membrane, trastuzumab was used as the primary antibody and cells were stained using a secondary fluorescent antibody (Alexa-fluor 488). Magnification 40X (scalebar = 1 μm). (B) FACS analysis of the anti-HER2 antibody response induced in C57BL/6 mice (n=4/experimental group) by the pVAX-hECTM vaccine in comparison with pVAX empty vector (control), encapsulated in LNP15, administered by intramuscular (i.m.) injections into the tibial muscle two times at 3-week interval. Sera from immunized mice were harvested two weeks after the last booster and tested on SK-BR-3 target cells. (C) Representative dot plots (increasing dot density from blue to red). Data are shown as MFI ± SEM; t-test **** P <0.0001 LNP15 hECTM vs. LNP15 pVAX (control).

DISCUSSION

The World Health Organization declared a novel coronavirus (COVID-19) outbreak as the sixth public health emergency of international concern on 30 January 2020 [128]. In the midst of a global epidemic, it is imperative to create a safe and effective vaccine against SARS-CoV-2 and its variants. Genetic recombination technology has greatly accelerated our response to the variants that have emerged or are likely to emerge. DNA vaccines display several advantages over other vaccine prototypes, including ease of production, stability, low cost of production and transport, and the ability to vaccinate against multiple pathogens in a single vaccination. This is of great importance considering the high mutability of SARS-CoV-2. There are currently sixteen DNA-based vaccine candidates in the clinical trials (e.g., INO-4800 and AG0302-COVID19). In August 2021, the world's first DNA vaccine ZyCoV-D received an Emergency Use Authorization (EUA) in India, hinting that the success of the DNA vaccine will unlock the future of vaccinology. The vaccine was developed using the pVAX-1 vector, which is approved by the U.S. Food and Drug Administration (FDA) to be used in human trials [129].

Here in, we developed candidate DNA vaccines that potentially could be applied to this global pandemic. Starting from two DNA vaccines encoding the S1 subunit of the spike protein or the S1 in fusion with the TM region (pVAX-S1 and pVAX-S1-TM), we selected the second one because it was more immunogenic, probably due to the ability of the encoded antigen to form trimers. Then, crucial mutations of Alpha and Delta variants, or their combination, were introduced into S1-TM sequence, to obtain pVAX-S1-TM-D614G, pVAX-S1-TM-UK, pVAX-S1-TM-IND and pVAX-S1-TM-INDUK (D614G, A570D, N501Y, E484Q and L452R) DNA vaccines. After their validation *in vitro* by immunofluorescence assay and confocal microscopy analysis, we provided evidence that the target antigens are properly expressed in mammalian cells transfected with our DNA vaccines and are localized on the cell membrane, as

expected. The immunogenicity of pVAX-S1-TM-D614G and pVAX-S1-TM-INDUK was then tested *in vivo*.

The decline in the capacity of the immune system in the elderly is clinically evident, as aging is closely associated with a significant reduction in vaccine efficacy. The COVID-19 pandemic has emphasized the strong log-linear relationship between age and the risk of COVID-19-associated death in individuals 65 years of age and older [130]. A recent study reported that both innate and adaptive immune responses were significantly impaired in aged mice compared with younger mice [118]. Additionally, it's known that 95% of patients with a fatal outcome are over 60 years old. In this context, studying a strategy to trigger a protective immune response in elderly is crucial. For this reason, the immunogenicity of pVAX-S1-TM-D614G and pVAX-S1-TM-INDUK candidate DNA vaccines and duration of elicited immune responses were evaluated not only in young/adults C57BL/6 mice (11 weeks of age) but also in aged C57BL/6 mice (20 months of age), representing a preclinical model of elderly humans. Even though both innate and adaptive immune responses have been reported to be significantly impaired in aged mice compared to younger mice following infection with SARS-CoV-2 [118], statistically significant antibody responses were elicited in aged mice immunized with pVAX-S1-TM-D614G and pVAX-S1-TM-INDUK DNA vaccines. Although our DNA vaccines elicited lower levels of antibodies in older mice than in younger mice, the induced humoral response was relevant even in aged mice especially considering that lower B- and T-cell responses were reported in the elderly populations and in individuals over the age of 80, there is no neutralizing activity against the variants [131, 132].

While the vaccination campaign prompted most of the population to receive two doses of the COVID-19 vaccine, the emergence of a new Omicron variant ushered in a new wave of the pandemic. Rapidly declined antibody levels have been reported approximately two months after the second vaccination [133, 134]. To overcome

waning immunity, an additional dose of the vaccine (booster) might be a critical mitigation approach. On August 12, 2021, FDA authorized both the BNT162b2 [Pfizer-BioNTech] and mRNA-1273 [Moderna] COVID-19 vaccines to allow a third dose in certain immunocompromised individuals [135]. As of November 19, 2021, boosters are recommended for all adults 18 years of age and older [136]. A three-dose regimen of ZyCoV-D administered intradermally via a needle-free injection system was found to be 66 6% effective against COVID-19 at the peak of the second wave, mainly due to the B.1.617.2 (delta) variant [137]. Based on these studies, we decided to administer a third dose to mice that had been vaccinated with a second dose 6 months earlier and their antibody levels were found to be drastically reduced when analyzed by flow cytometry. Of note, we demonstrated that a booster dose with pVAX-S1-TM-D614G or pVAX-S1-TM-INDUK DNA vaccines strongly enhanced humoral responses in both young and aged mice.

Although DNA vaccines have the advantage to be quickly adapted to emerging variants of concern, in order to widely use them it is necessary to improve and facilitate their administration and develop delivery methods alternative to electroporation.

Lipid nanoparticles (LNPs) obtained by microfluidics are now considered one of the most advanced delivery technologies. Precise LNP size controllability, high reproducibility, high-throughput optimization of LNP formulation are just some of the advantages associated with LNPs. COVID-19 mRNA vaccines use ionizable lipid nanoparticles (80–100 nm in diameter) to deliver nucleoside-modified mRNA encoding the full-length spike protein of SARS-CoV-2. Both contain an ionizable lipid which is positively charged at low pH (enabling RNA complexation) and neutral at physiological pH (reducing the potential toxic effects and facilitating payload release). They also contain a PEGylated lipid to reduce clearance by phagocytes thus conferring longer systemic circulation. RNA vaccines are effective and the LNPs are

safe and stable delivery systems that protect the nucleic acid from degradation and that allow cellular uptake and mRNA release. However, mRNA vaccines are relatively unstable in a fridge or at room temperature and require cold-chain transportation.

On the contrary DNA vaccines are stable even at room temperature and thus they do not need the cold-chain transportation. In order to find out the best LNP formulation to encapsulate our DNA vaccines, we screened a library of 16 different LNPs and one of them, called LNP15, was selected thanks to its physico-chemical characteristics (positive charge and optimal dimension (130 nm in diameter)) and functional properties. LNP15 is a 4-component PEGylated formulation exhibiting high transfection efficiency and low cytotoxicity *in vitro*. Superior transfection efficiency correlated with the nanostructure of LNP15, which, once inside the cell, is more prone to destabilize the endosomal membrane and release the DNA (data not shown). In fact, to function *in vivo*, LNP formulations, used to deliver nucleic acid vaccines, need to overcome multiple extracellular and intracellular barriers. In particular, LNPs need to protect the nucleic acid payload from nuclease degradation in physiological fluids, reach target tissues, be internalized by target cells, that will express the antigen to trigger the immune responses.

First, LNP15 was used to encapsulate a prototype DNA vaccine, pVAX-hECTM, developed against the oncogene HER2 [126]. After *in vitro* validation, the immunogenicity of LNP15-pVAX-hECTM was verified *in vivo*. As expected, immunization of mice with LNP15-pVAX-hECTM elicited significantly high and specific anti-HER2 antibody responses, paving the way for using LNP15 to deliver DNA vaccines with a simple i.m. injection, without electroporation.

Currently, LNP15 has been used to encapsulate pVAX-S1-TM-INDUK, the anti-SARS-CoV-2 DNA vaccine that we developed against the Alpha and Delta variants of concern. *In vivo* experiments are ongoing to test if pVAX-S1-TM-INDUK remains immunogenic once administered within LNP15 by i.m. injection.

Further studies will help: (i) to determine the specificity of the antibody responses elicited by pVAX-S1-TM-INDUK against the Spike carrying the Delta variant mutations by an enzyme-linked immunosorbent assay (ELISA: Mouse Anti-SARS-CoV-2 (B.1.617.2) Antibody IgG Titer Serologic Assay Kit (Spike Trimer)); (ii) to analyze the presence of neutralizing antibodies on the sera of immunized mice by a ACE2:SARS-CoV-2 Spike S1 Inhibitor Screening Assay, designed for screening and profiling inhibitors of this interaction; (iii) to evaluate the cell-mediated immunity by standard enzyme-linked immunospot (ELISpot) assay and FACS analysis, in particular the ability of splenocytes from immunized mice to secrete interferon gamma (IFN-γ) after antigen-specific ex vivo restimulation with selected Spike protein peptides will be evaluated. The global cytokine profile of responding T cells will be also evaluated to determine its suitability for antiviral immunity.

CONCLUSIONS

COVID-19 is more severe in the elderly, while vaccines are less immunogenic in older individuals. mRNA COVID-19 vaccines from Pfizer-BioNTech (BNT162b2) and Moderna (mRNA-1273) initially showed high levels of efficacy across all age groups. However, the emergence of new variants with immune evasion capabilities led to diminished vaccine effectiveness and a corresponding resurgence of cases. In the present study, new DNA vaccines conceived against SARS-CoV-2 and its most aggressive variant have been developed and validated *in vivo,* in young and aged mice. The elicited immune responses after two doses of DNA vaccines, administered by electroporation, were monitored for 6 months. The obtained results demonstrate that both pVAX-S1-TM-D614G and pVAX-S1-TM-INDUK DNA vaccines, encoding the S1 region of the spike protein (bearing five selected mutations) in fusion with the TM domain, elicited a significant anti-Spike antibody response in both young and aged C57BL/6 mice models. pVAX-S1-TM-INDUK induced a quite persistent humoral response in young animals, although it declined within 6 months and dropped down much more quickly in aged mice. Of note, a booster dose at 6 months from the second dose was enough to increase again the antibody titer even in 26-month-old mice. These results indicate that pVAX-S1-TM-INDUK might represent a promising DNA vaccine against COVID-19 effective even in aged population, if the immunological memory is properly stimulated by booster doses. Moreover, we optimized a LNP formulation, we called LNP15, to encapsulate DNA vaccines and deliver them by i.m. injection without electroporation, making easier their administration without affecting their effectiveness and immunogenicity.

BIBLIOGRAPHY

1. Li, Q., et al., *Early Transmission Dynamics in Wuhan, China, of Novel Coronavirus-Infected Pneumonia.* N Engl J Med, 2020. 382(13): p. 1199-1207.
2. Lai, C.C., et al., *Severe acute respiratory syndrome coronavirus 2 (SARS-CoV-2) and coronavirus disease-2019 (COVID-19): The epidemic and the challenges.* Int J Antimicrob Agents, 2020. 55(3): p. 105924.
3. Wilder-Smith, A. and S. Osman, *Public health emergencies of international concern: a historic overview.* J Travel Med, 2020. 27(8).
4. Woo, P.C., et al., *Discovery of seven novel Mammalian and avian coronaviruses in the genus deltacoronavirus supports bat coronaviruses as the gene source of alphacoronavirus and betacoronavirus and avian coronaviruses as the gene source of gammacoronavirus and deltacoronavirus.* J Virol, 2012. 86(7): p. 3995-4008.
5. Cui, J., F. Li, and Z.L. Shi, *Origin and evolution of pathogenic coronaviruses.* Nat Rev Microbiol, 2019. 17(3): p. 181-192.
6. Letko, M., et al., *Bat-borne virus diversity, spillover and emergence.* Nat Rev Microbiol, 2020. 18(8): p. 461-471.
7. Dhar, M.S., Marwal, R., Vs, R., Ponnusamy, K., Jolly, B., Bhoyar, R. C., Sardana, V., Naushin, S., Rophina, M., Mellan, T. A., Mishra, S., Whittaker, C., Fatihi, S., Datta, M., Singh, P., Sharma, U., Ujjainiya, R., Bhatheja, N., Divakar, M. K., Singh, M. K., … Cherian, S. S., *Genomic characterization and epidemiology of an emerging SARS-CoV-2 variant in Delhi, India.* Genomic characterization and epidemiology of an emerging SARS-CoV-2 variant in Delhi, India., 2021. 374(6570): p. 995–999.
8. Lu, R., et al., *Genomic characterisation and epidemiology of 2019 novel coronavirus: implications for virus origins and receptor binding.* The Lancet, 2020. 395(10224): p. 565-574.
9. Wu, F., et al., *A new coronavirus associated with human respiratory disease in China.* Nature, 2020. 579(7798): p. 265-269.
10. Florindo, H.F., et al., *Immune-mediated approaches against COVID-19.* Nature Nanotechnology, 2020. 15(8): p. 630-645.
11. Huang, Y., et al., *Structural and functional properties of SARS-CoV-2 spike protein: potential antivirus drug development for COVID-19.* Acta Pharmacol Sin, 2020. 41(9): p. 1141-1149.
12. Wrapp, D., et al., *Cryo-EM structure of the 2019-nCoV spike in the prefusion conformation.* Science, 2020. 367(6483): p. 1260-1263.
13. Duan, L., et al., *The SARS-CoV-2 Spike Glycoprotein Biosynthesis, Structure, Function, and Antigenicity: Implications for the Design of Spike-Based Vaccine Immunogens.* Front Immunol, 2020. 11: p. 576622.
14. Rabaan, A.A., Al-Ahmed, S. H., Haque, S., Sah, R., Tiwari, R., Malik, Y. S., Dhama, K., Yatoo, M. I., Bonilla-Aldana, D. K., & Rodriguez-Morales, A. J., *SARS-CoV-2, SARS-CoV, and MERS-COV: A comparative overview.* Le infezioni in medicina, 2020. 28(2):

p. 174–184.
15. Jackson, C.B., et al., *Mechanisms of SARS-CoV-2 entry into cells.* Nat Rev Mol Cell Biol, 2022. 23(1): p. 3-20.
16. Wang, L., et al., *Importance of Neutralizing Monoclonal Antibodies Targeting Multiple Antigenic Sites on the Middle East Respiratory Syndrome Coronavirus Spike Glycoprotein To Avoid Neutralization Escape.* J Virol, 2018. 92(10).
17. Naqvi, A.A.T., et al., *Insights into SARS-CoV-2 genome, structure, evolution, pathogenesis and therapies: Structural genomics approach.* Biochim Biophys Acta Mol Basis Dis, 2020. 1866(10): p. 165878.
18. Korber, B., et al., *Tracking Changes in SARS-CoV-2 Spike: Evidence that D614G Increases Infectivity of the COVID-19 Virus.* Cell, 2020. 182(4): p. 812-827 e19.
19. Yurkovetskiy, L., et al., *Structural and Functional Analysis of the D614G SARS-CoV-2 Spike Protein Variant.* Cell, 2020. 183(3): p. 739-751 e8.
20. Pak, A.J., et al., *Cooperative multivalent receptor binding promotes exposure of the SARS-CoV-2 fusion machinery core.* Nat Commun, 2022. 13(1): p. 1002.
21. Plante, J.A., et al., *Spike mutation D614G alters SARS-CoV-2 fitness.* Nature, 2021. 592(7852): p. 116-121.
22. Lyngse, F.P., et al., *Increased transmissibility of SARS-CoV-2 lineage B.1.1.7 by age and viral load.* Nature Communications, 2021. 12(1): p. 7251.
23. Liu, Y., et al., *The N501Y spike substitution enhances SARS-CoV-2 infection and transmission.* Nature, 2022. 602(7896): p. 294-299.
24. Cheng, L., et al., *Impact of the N501Y substitution of SARS-CoV-2 Spike on neutralizing monoclonal antibodies targeting diverse epitopes.* Virology Journal, 2021. 18(1): p. 87.
25. Davies, N.G., et al., *Estimated transmissibility and impact of SARS-CoV-2 lineage B.1.1.7 in England.* Science, 2021. 372(6538).
26. Aleem, A., A.B. Akbar Samad, and A.K. Slenker, *Emerging Variants of SARS-CoV-2 And Novel Therapeutics Against Coronavirus (COVID-19)*, in *StatPearls*. 2022, StatPearls Publishing

27. Wang, P., et al., *Antibody resistance of SARS-CoV-2 variants B.1.351 and B.1.1.7.* Nature, 2021. 593(7857): p. 130-135.
28. Zhou, D., et al., *Evidence of escape of SARS-CoV-2 variant B.1.351 from natural and vaccine-induced sera.* Cell, 2021. 184(9): p. 2348-2361.e6.
29. Faria, N.R., et al., *Genomics and epidemiology of the P.1 SARS-CoV-2 lineage in Manaus, Brazil.* Science, 2021. 372(6544): p. 815-821.
30. Naveca, F.G., et al., *COVID-19 in Amazonas, Brazil, was driven by the persistence of endemic lineages and P.1 emergence.* Nat Med, 2021. 27(7): p. 1230-1238.
31. Khan, A., et al., *Higher infectivity of the SARS-CoV-2 new variants is associated with K417N/T, E484K, and N501Y mutants: An insight from structural data.* J Cell Physiol, 2021. 236(10): p. 7045-7057.
32. Jensen, B., et al., *Emergence of the E484K mutation in SARS-COV-2-infected*

immunocompromised patients treated with bamlanivimab in Germany. Lancet Reg Health Eur, 2021. 8: p. 100164.

33. Saito, A., et al., *Enhanced fusogenicity and pathogenicity of SARS-CoV-2 Delta P681R mutation.* Nature, 2022. 602(7896): p. 300-306.
34. Planas, D., et al., *Reduced sensitivity of SARS-CoV-2 variant Delta to antibody neutralization.* Nature, 2021. 596(7871): p. 276-280.
35. Cherian, S., et al., *SARS-CoV-2 Spike Mutations, L452R, T478K, E484Q and P681R, in the Second Wave of COVID-19 in Maharashtra, India.* Microorganisms, 2021. 9(7).
36. Karim, S.S.A. and Q.A. Karim, *Omicron SARS-CoV-2 variant: a new chapter in the COVID-19 pandemic.* The Lancet, 2021. 398(10317): p. 2126-2128.
37. Kandeel, M., et al., *Omicron variant genome evolution and phylogenetics.* J Med Virol, 2022. 94(4): p. 1627-1632.
38. Tian, D., et al., *The emergence and epidemic characteristics of the highly mutated SARS-CoV-2 Omicron variant.* J Med Virol, 2022. 94(6): p. 2376-2383.
39. Pulliam, J., van Schalkwyk, C., Govender, N., von Gottberg, A., Cohen, C., Groome, M. J., Dushoff, J., Mlisana, K., & Moultrie, H. , *Pulliam, J., van Schalkwyk, C., Govender, N., von Gottberg, A., Cohen, C., Groome, M. J., Dushoff, J., Mlisana, K., & Moultrie, H.* . Science (New York, N.Y.), 2022. 4947.
40. Abdullah, F., et al., *Decreased severity of disease during the first global omicron variant covid-19 outbreak in a large hospital in tshwane, south africa.* Int J Infect Dis, 2022. 116: p. 38-42.
41. Pollard, A.J. and E.M. Bijker, *A guide to vaccinology: from basic principles to new developments.* Nature Reviews Immunology, 2021. 21(2): p. 83-100.
42. Khoshnood, S., et al., *An overview on inactivated and live-attenuated SARS-CoV-2 vaccines.* J Clin Lab Anal, 2022. 36(5): p. e24418.
43. Negahdaripour, M., et al., *Administration of COVID-19 vaccines in immunocompromised patients.* Int Immunopharmacol, 2021. 99: p. 108021.
44. Cid, R. and J. Bolívar, *Platforms for Production of Protein-Based Vaccines: From Classical to Next-Generation Strategies.* Biomolecules, 2021. 11(8).
45. Custers, J., et al., *Vaccines based on replication incompetent Ad26 viral vectors: Standardized template with key considerations for a risk/benefit assessment.* Vaccine, 2021. 39(22): p. 3081-3101.
46. Folegatti, P.M., et al., *Safety and immunogenicity of the ChAdOx1 nCoV-19 vaccine against SARS-CoV-2: a preliminary report of a phase 1/2, single-blind, randomised controlled trial.* Lancet, 2020. 396(10249): p. 467-478.
47. Fejer, G., et al., *Adenovirus-triggered innate signalling pathways.* Eur J Microbiol Immunol (Bp), 2011. 1(4): p. 279-88.
48. Callaway, E., *Mix-and-match COVID vaccines ace the effectiveness test.* Nature, 2021.
49. Rashedi, R., et al., *COVID-19 vaccines mix-and-match: The concept, the efficacy and the doubts.* J Med Virol, 2022. 94(4): p. 1294-1299.
50. Fang, E., et al., *Advances in COVID-19 mRNA vaccine development.* Signal Transduction and Targeted Therapy, 2022. 7(1): p. 94.

51. Hou, X., et al., *Lipid nanoparticles for mRNA delivery.* Nature Reviews Materials, 2021. 6(12): p. 1078-1094.
52. Angeli, F., et al., *SARS-CoV-2 vaccines: Lights and shadows.* Eur J Intern Med, 2021. 88: p. 1-8.
53. Wolff, J.A., et al., *Direct Gene Transfer into Mouse Muscle in Vivo.* Science, 1990. 247(4949): p. 1465-1468.
54. Kennedy, N.J., et al., *DNA vaccines in sheep: CTLA-4 mediated targeting and CpG motifs enhance immunogenicity in a DNA prime/protein boost strategy.* Vaccine, 2006. 24(7): p. 970-9.
55. Widera, G., et al., *Increased DNA Vaccine Delivery and Immunogenicity by Electroporation In Vivo.* The Journal of Immunology, 2000. 164(9): p. 4635-4640.
56. O'Brien, J.A. and S.C.R. Lummis, *Nano-biolistics: a method of biolistic transfection of cells and tissues using a gene gun with novel nanometer-sized projectiles.* BMC Biotechnology, 2011. 11(1): p. 66.
57. Shafaati, M., et al., *A brief review on DNA vaccines in the era of COVID-19.* Future Virol, 2021.
58. Kutzler, M.A. and D.B. Weiner, *DNA vaccines: ready for prime time?* Nature Reviews Genetics, 2008. 9(10): p. 776-788.
59. Hobernik, D. and M. Bros, *DNA Vaccines—How Far From Clinical Use?* International Journal of Molecular Sciences, 2018. 19(11): p. 3605.
60. Sheridan, C., *First COVID-19 DNA vaccine approved, others in hot pursuit.* Nat Biotechnol, 2021. 39(12): p. 1479-1482.
61. Mallapaty, S., *India's DNA COVID vaccine is a world first - more are coming.* Nature, 2021. 597(7875): p. 161-162.
62. Smith, T.R.F., et al., *Immunogenicity of a DNA vaccine candidate for COVID-19.* Nat Commun, 2020. 11(1): p. 2601.
63. Tebas, P., et al., *Safety and immunogenicity of INO-4800 DNA vaccine against SARS-CoV-2: A preliminary report of an open-label, Phase 1 clinical trial.* EClinicalMedicine, 2021. 31: p. 100689.
64. Kraynyak, K.A., et al., *SARS-CoV-2 DNA Vaccine INO-4800 Induces Durable Immune Responses Capable of Being Boosted in a Phase 1 Open-Label Trial.* J Infect Dis, 2022. 225(11): p. 1923-1932.
65. Mammen, M.P., et al., *Safety and immunogenicity of INO-4800 DNA vaccine against SARS-CoV-2: a preliminary report of a randomized, blinded, placebo-controlled, Phase 2 clinical trial in adults at high risk of viral exposure.* medRxiv, 2021: p. 2021.05.07.21256652.
66. Andrade, V.M., et al., *INO-4800 DNA vaccine induces neutralizing antibodies and T cell activity against global SARS-CoV-2 variants.* npj Vaccines, 2021. 6(1): p. 121.
67. Hobernik, D. and M. Bros, *DNA Vaccines-How Far From Clinical Use?* Int J Mol Sci, 2018. 19(11).
68. Jorritsma, S.H.T., et al., *Delivery methods to increase cellular uptake and immunogenicity of DNA vaccines.* Vaccine, 2016. 34(46): p. 5488-5494.

69. Gary, E.N. and D.B. Weiner, *DNA vaccines: prime time is now.* Curr Opin Immunol, 2020. 65: p. 21-27.
70. De Filette, M., et al., *Recent progress in West Nile virus diagnosis and vaccination.* Veterinary Research, 2012. 43(1): p. 16.
71. Long, A., et al., *Transmission potential of infectious hematopoietic necrosis virus in APEX-IHN®-vaccinated Atlantic salmon.* Dis Aquat Organ, 2017. 122(3): p. 213-221.
72. Moss, B., et al., *Live recombinant vaccinia virus protects chimpanzees against hepatitis B.* Nature, 1984. 311(5981): p. 67-9.
73. Grove, J. and M. Marsh, *The cell biology of receptor-mediated virus entry.* J Cell Biol, 2011. 195(7): p. 1071-82.
74. Titomirov, A.V., S. Sukharev, and E. Kistanova, *In vivo electroporation and stable transformation of skin cells of newborn mice by plasmid DNA.* Biochim Biophys Acta, 1991. 1088(1): p. 131-4.
75. Sardesai, N.Y. and D.B. Weiner, *Electroporation delivery of DNA vaccines: prospects for success.* Curr Opin Immunol, 2011. 23(3): p. 421-9.
76. Heller, R. and L.C. Heller, *Gene electrotransfer clinical trials.* Adv Genet, 2015. 89: p. 235-262.
77. Sokołowska, E. and A.U. Błachnio-Zabielska, *A Critical Review of Electroporation as A Plasmid Delivery System in Mouse Skeletal Muscle.* Int J Mol Sci, 2019. 20(11).
78. Sanford, J.C., F.D. Smith, and J.A. Russell, *Optimizing the biolistic process for different biological applications.* Methods Enzymol, 1993. 217: p. 483-509.
79. Singsit, C., et al., *Expression of a Bacillus thuringiensis cryIA(c) gene in transgenic peanut plants and its efficacy against lesser cornstalk borer.* Transgenic Res, 1997. 6(2): p. 169-76.
80. Robertson, D., et al., *Genetic transformation of Norway spruce (Picea abies (L.) Karst) using somatic embryo explants by microprojectile bombardment.* Plant Mol Biol, 1992. 19(6): p. 925-35.
81. Katz, M.G., A.S. Fargnoli, and C.R. Bridges, *Myocardial gene transfer: routes and devices for regulation of transgene expression by modulation of cellular permeability.* Hum Gene Ther, 2013. 24(4): p. 375-92.
82. Demirer, G.S. and M.P. Landry, *Delivering genes to plants.* Chemical engineering progress, 2017. 113(4): p. 40-45.
83. Wen-Chi, T. and H. Leaf, *Liposome-based gene therapy.* Pharmaceutical Science & Technology Today, 1998. 1(5): p. 206-213.
84. Bangham, A.D. and R.W. Horne, *NEGATIVE STAINING OF PHOSPHOLIPIDS AND THEIR STRUCTURAL MODIFICATION BY SURFACE-ACTIVE AGENTS AS OBSERVED IN THE ELECTRON MICROSCOPE.* J Mol Biol, 1964. 8: p. 660-8.
85. Karmali, P.P. and A. Chaudhuri, *Cationic liposomes as non-viral carriers of gene medicines: resolved issues, open questions, and future promises.* Med Res Rev, 2007. 27(5): p. 696-722.
86. Diana, G., C.-P. Artur, and N. Eugénia, *Design of liposomes as drug delivery system for therapeutic applications.* International Journal of Pharmaceutics, 2021. 601: p. 120571.

87. Moghimi, S.M., *Liposomes,* in *Encyclopedia of Nanotechnology,* B. Bhushan, Editor. 2012, Springer Netherlands: Dordrecht. p. 1218-1223.
88. Immordino, M.L., F. Dosio, and L. Cattel, *Stealth liposomes: review of the basic science, rationale, and clinical applications, existing and potential.* Int J Nanomedicine, 2006. 1(3): p. 297-315.
89. Guido, A., et al., *Neutral liposomes containing crown ether-lipids as potential DNA vectors.* Biochimica et Biophysica Acta (BBA) - Biomembranes, 2013. 1828(11): p. 2506-2512.
90. Michela, P., M. Giovanna, and B. Paolo, *Neutral Liposomes and DNA Transfection.* 2011.
91. Lappalainen, K., et al., *Comparison of cell proliferation and toxicity assays using two cationic liposomes.* Pharm Res, 1994. 11(8): p. 1127-31.
92. Filion, M.C. and N.C. Phillips, *Toxicity and immunomodulatory activity of liposomal vectors formulated with cationic lipids toward immune effector cells.* Biochim Biophys Acta, 1997. 1329(2): p. 345-56.
93. Balazs, D.A. and W. Godbey, *Liposomes for use in gene delivery.* J Drug Deliv, 2011. 2011: p. 326497.
94. Parker, A.L., et al., *Nonviral gene delivery: techniques and implications for molecular medicine.* Expert Rev Mol Med, 2003. 5(22): p. 1-15.
95. Al Shaer, D., et al., *2018 FDA Tides Harvest.* Pharmaceuticals (Basel), 2019. 12(2).
96. Tenchov, R., et al., *Lipid Nanoparticles─From Liposomes to mRNA Vaccine Delivery, a Landscape of Research Diversity and Advancement.* ACS Nano, 2021. 15(11): p. 16982-17015.
97. Mitchell, M.J., et al., *Engineering precision nanoparticles for drug delivery.* Nature Reviews Drug Discovery, 2021. 20(2): p. 101-124.
98. Algarni, A., et al., *In vivo delivery of plasmid DNA by lipid nanoparticles: the influence of ionizable cationic lipids on organ-selective gene expression.* Biomater Sci, 2022. 10(11): p. 2940-2952.
99. Yao, H., et al., *Enhanced blood-brain barrier penetration and glioma therapy mediated by a new peptide modified gene delivery system.* Biomaterials, 2015. 37: p. 345-52.
100. Mucker, E.M., et al., *Lipid Nanoparticle Formulation Increases Efficiency of DNA-Vectored Vaccines/Immunoprophylaxis in Animals Including Transchromosomic Bovines.* Scientific Reports, 2020. 10(1): p. 8764.
101. Maeta, M., et al., *Vitamin E Scaffolds of pH-Responsive Lipid Nanoparticles as DNA Vaccines in Cancer and Protozoan Infection.* Mol Pharm, 2020. 17(4): p. 1237-1247.
102. Hasan, T., et al., *Toxoplasma gondii GRA15 DNA Vaccine with a Liposomal Nanocarrier Composed of an SS-Cleavable and pH-Activated Lipid-like Material Induces Protective Immunity against Toxoplasmosis in Mice.* Vaccines (Basel), 2021. 10(1).
103. Saljoughian, N., et al., *Cationic solid-lipid nanoparticles are as efficient as electroporation in DNA vaccination against visceral leishmaniasis in mice.* Parasite Immunol, 2013. 35(12): p. 397-408.

104. Aly, A.E., et al., *Intranasal Delivery of pGDNF DNA Nanoparticles Provides Neuroprotection in the Rat 6-Hydroxydopamine Model of Parkinson's Disease.* Mol Neurobiol, 2019. 56(1): p. 688-701.
105. Quagliarini, E., et al., *Microfluidic Formulation of DNA-Loaded Multicomponent Lipid Nanoparticles for Gene Delivery.* Pharmaceutics, 2021. 13(8).
106. Gustafson, C.E., et al., *Influence of immune aging on vaccine responses.* J Allergy Clin Immunol, 2020. 145(5): p. 1309-1321.
107. Cox, R.J. and K.A. Brokstad, *Not just antibodies: B cells and T cells mediate immunity to COVID-19.* Nature Reviews Immunology, 2020. 20(10): p. 581-582.
108. Borgoni, S., et al., *Targeting immune dysfunction in aging.* Ageing Res Rev, 2021. 70: p. 101410.
109. Vilar, S. and D.G. Isom, *One Year of SARS-CoV-2: How Much Has the Virus Changed?* Biology (Basel), 2021. 10(2).
110. Silveira, M.M., G. Moreira, and M. Mendonça, *DNA vaccines against COVID-19: Perspectives and challenges.* Life Sci, 2021. 267: p. 118919.
111. Liu, H. and J.H. Naismith, *An efficient one-step site-directed deletion, insertion, single and multiple-site plasmid mutagenesis protocol.* BMC Biotechnology, 2008. 8(1): p. 91.
112. Shang, J., et al., *Structural basis of receptor recognition by SARS-CoV-2.* Nature, 2020. 581(7807): p. 221-224.
113. Harrach, M.F. and B. Drossel, *Structure and dynamics of TIP3P, TIP4P, and TIP5P water near smooth and atomistic walls of different hydroaffinity.* J Chem Phys, 2014. 140(17): p. 174501.
114. Azad, T., et al., *Implications for SARS-CoV-2 Vaccine Design: Fusion of Spike Glycoprotein Transmembrane Domain to Receptor-Binding Domain Induces Trimerization.* Membranes (Basel), 2020. 10(9).
115. Scovino, A.M., et al., *SARS-CoV-2's Variants of Concern: A Brief Characterization.* Front Immunol, 2022. 13: p. 834098.
116. Magazine, N., et al., *Mutations and Evolution of the SARS-CoV-2 Spike Protein.* Viruses, 2022. 14(3).
117. Chen, Y., et al., *Aging in COVID-19: Vulnerability, immunity and intervention.* Ageing Res Rev, 2021. 65: p. 101205.
118. Chen, Y., et al., *Age-associated SARS-CoV-2 breakthrough infection and changes in immune response in a mouse model.* Emerg Microbes Infect, 2022. 11(1): p. 368-383.
119. Bartleson, J.M., et al., *SARS-CoV-2, COVID-19 and the aging immune system.* Nature Aging, 2021. 1(9): p. 769-782.
120. Yousefzadeh, M.J., et al., *An aged immune system drives senescence and ageing of solid organs.* Nature, 2021. 594(7861): p. 100-105.
121. Đaković Rode, O., et al., *Decline of Anti-SARS-CoV-2 IgG Antibody Levels 6 Months after Complete BNT162b2 Vaccination in Healthcare Workers to Levels Observed Following the First Vaccine Dose.* Vaccines (Basel), 2022. 10(2).
122. Naaber, P., et al., *Dynamics of antibody response to BNT162b2 vaccine after six months: a longitudinal prospective study.* Lancet Reg Health Eur, 2021. 10: p. 100208.

123. Bayart, J.L., et al., *Waning of IgG, Total and Neutralizing Antibodies 6 Months Post-Vaccination with BNT162b2 in Healthcare Workers*. Vaccines (Basel), 2021. 9(10).
124. Andrews, N., et al., *Effectiveness of COVID-19 booster vaccines against COVID-19-related symptoms, hospitalization and death in England.* Nat Med, 2022. 28(4): p. 831-837.
125. Vadrevu, K.M., et al., *Persistence of immunity and impact of third dose of inactivated COVID-19 vaccine against emerging variants.* Scientific Reports, 2022. 12(1): p. 12038.
126. Quaglino, E., et al., *A better immune reaction to Erbb-2 tumors is elicited in mice by DNA vaccines encoding rat/human chimeric proteins.* Cancer research, 2010. 70(7): p. 2604-2612.
127. Siegel, R.L., et al., *Cancer statistics, 2021.* CA: a cancer journal for clinicians, 2021. 71(1): p. 7-33.
128. Gao, Q., et al., *Development of an inactivated vaccine candidate for SARS-CoV-2.* Science, 2020. 369(6499): p. 77-81.
129. Li, Z.-x., et al., *Immunogenicity and protective efficacy of a DNA vaccine inducing optimal expression of the SARS-CoV-2 S gene in hACE2 mice.* Archives of Virology, 2022.
130. O'Driscoll, M., et al., *Age-specific mortality and immunity patterns of SARS-CoV-2.* Nature, 2021. 590(7844): p. 140-145.
131. Collier, D.A., et al., *Age-related immune response heterogeneity to SARS-CoV-2 vaccine BNT162b2.* Nature, 2021. 596(7872): p. 417-422.
132. Müller, L., et al., *Age-dependent Immune Response to the Biontech/Pfizer BNT162b2 Coronavirus Disease 2019 Vaccination.* Clin Infect Dis, 2021. 73(11): p. 2065-2072.
133. Harrington, W.E., et al., *Rapid decline of neutralizing antibodies is associated with decay of IgM in adults recovered from mild COVID-19.* Cell Rep Med, 2021. 2(4): p. 100253.
134. Erice, A., D. Varillas-Delgado, and C. Caballero, *Decline of antibody titres 3 months after two doses of BNT162b2 in non-immunocompromised adults.* Clin Microbiol Infect, 2022. 28(1): p. 139.e1-139.e4.
135. Barda, N., et al., *Effectiveness of a third dose of the BNT162b2 mRNA COVID-19 vaccine for preventing severe outcomes in Israel: an observational study.* Lancet, 2021. 398(10316): p. 2093-2100.
136. Tenforde, M.W., et al., *Effectiveness of a Third Dose of Pfizer-BioNTech and Moderna Vaccines in Preventing COVID-19 Hospitalization Among Immunocompetent and Immunocompromised Adults - United States, August-December 2021.* MMWR Morb Mortal Wkly Rep, 2022. 71(4): p. 118-124.
137. Khobragade, A., et al., *Efficacy, safety, and immunogenicity of the DNA SARS-CoV-2 vaccine (ZyCoV-D): the interim efficacy results of a phase 3, randomised, double-blind, placebo-controlled study in India*. Lancet, 2022. 399(10332): p. 1313-1321.

PATENT

1. P6315IT00_DOMANDA DI BREVETTO

   Inventors: Giulio Caracciolo, Daniela Pozzi, Erica Quagliarini, Serena Renzi, Luca Digiacomo, Augusto Amici, Cristina Marchini, **Lishan Cui**, Junbiao Wang, Francesco Cardarelli

   Title: Nanoparticelle lipidiche multicomponenti ad elevata fusogenicità cellulare per la veicolazione di acidi nucleici e relativo processo di preparazione

   Domanda numero: 812022000133749

   Data di presentazione: 19/09/2022

PUBLICATIONS

1. Quagliarini, E., Wang, J., Renzi, S., **Cui, L.**, Digiacomo, L., Ferri, G., Pesce, L., De Lorenzi, V., Matteoli, G., Amenitsch, H., Masuelli, L., Bei, R., Pozzi, D., Amici, A., Cardarelli, F., Marchini, C., & Caracciolo, G. (2022). Mechanistic Insights into the Superior DNA Delivery Efficiency of Multicomponent Lipid Nanoparticles: An In Vitro and In Vivo Study. *ACS applied materials & interfaces*, 10.1021/acsami.2c20019. Advance online publication. https://doi.org/10.1021/acsami.2c20019 Impact factor: 10.38
2. **Cui, L**., Quagliarini, E., Xiao, S., Giulimondi, F., Renzi, S., Digiacomo, L., Caracciolo, G., Wang, J., Amici, A., Marchini, C., & Pozzi, D. (2022). The protein corona reduces the anticancer effect of graphene oxide in HER-2-positive cancer cells. *Nanoscale advances*, *4*(18), 4009–4015. https://doi.org/10.1039/d2na00308b Impact factor: 5.598
3. **Cui, L**., Renzi, S., Quagliarini, E., Digiacomo, L., Amenitsch, H., Masuelli, L., Bei, R., Ferri, G., Cardarelli, F., Wang, J., Amici, A., Pozzi, D., Marchini, C., & Caracciolo, G. (2022). Efficient Delivery of DNA Using Lipid Nanoparticles. Pharmaceutics, 14(8), 1698. https://doi.org/10.3390/pharmaceutics14081698 Impact factor: 6.525
4. Wang, J., Lamolinara, A., Conti, L., Giangrossi, M., **Cui, L**., Morelli, M. B., Amantini, C., Falconi, M., Bartolacci, C., Andreani, C., Orlando, F., Provinciali, M., Del Pizzo, F. D., Russo, F., Belletti, B., Riccardo, F., Bolli, E., Quaglino, E., Cavallo, F., Amici, A., … Marchini, C. (2022). HER2-Displaying M13 Bacteriophages induce Therapeutic Immunity against Breast Cancer. *Cancers*, *14*(16), 4054. https://doi.org/10.3390/cancers14164054 Impact factor: 6.639
5. Galassi, R., Luciani, L., Wang, J., Vincenzetti, S., **Cui, L.**, Amici, A., Pucciarelli, S., & Marchini, C. (2022). Breast Cancer Treatment: The Case of Gold(I)-Based Compounds as a Promising Class of Bioactive Molecules. *Biomolecules*, *12*(1), 80. https://doi.org/10.3390/biom12010080 Impact factor: 5.88
6. Quagliarini, E., Renzi, S., Digiacomo, L., Giulimondi, F., Sartori, B., Amenitsch, H., Tassinari, V., Masuelli, L., Bei, R., **Cui, L.**, Wang, J., Amici, A., Marchini, C., Pozzi, D., & Caracciolo, G. (2021). Microfluidic Formulation of DNA-Loaded Multicomponent Lipid Nanoparticles for Gene Delivery. *Pharmaceutics*, *13*(8), 1292. https://doi.org/10.3390/pharmaceutics13081292 Impact factor: 6.525
7. Wang, J., Iannarelli, R., Pucciarelli, S., Laudadio, E., Galeazzi, R., Giangrossi, M., Falconi, M., **Cui, L.**, Navia, A. M., Buccioni, M., Marucci, G., Tomassoni, D., Serini, L., Sut, S., Maggi, F., Dall'Acqua, S., Marchini, C., & Amici, A. (2020). Acetylshikonin isolated from Lithospermum erythrorhizon roots inhibits dihydrofolate reductase and hampers autochthonous mammary carcinogenesis in Δ16HER2 transgenic mice. *Pharmacological research*, *161*, 105123. https://doi.org/10.1016/j.phrs.2020.105123 Impact factor: 10.334

Nanoscale Advances

ROYAL SOCIETY OF CHEMISTRY

PAPER

Cite this: *Nanoscale Adv.*, 2022, 4, 4009

The protein corona reduces the anticancer effect of graphene oxide in HER-2-positive cancer cells†

Lishan Cui,‡[a] Erica Quagliarini,‡[b] Siyao Xiao,[b] Francesca Giulimondi,[b] Serena Renzi,[b] Luca Digiacomo,[b] Giulio Caracciolo,[b] Junbiao Wang,[a] Augusto Amici,[a] Cristina Marchini*[a] and Daniela Pozzi*[b]

In the last decade, graphene oxide (GO)-based nanomaterials have attracted much attention for their potential anti-cancer properties against various cancer cell types. However, while *in vitro* studies are promising, following *in vivo* investigations fail to show any relevant efficacy. Recent research has clarified that the wide gap between benchtop discoveries and clinical practice is due to our limited knowledge about the physical–chemical transformation of nanomaterials *in vivo*. In physiological environments, nanomaterials are quickly coated by a complex dress of biological molecules referred to as the protein corona. Mediating the interaction between the pristine material and the biological system the protein corona controls the mechanisms of action of nanomaterials up to the sub-cellular level. Here we investigate the anticancer ability of GO in SK-BR-3 human breast cancer cells over-expressing the human epidermal growth factor receptor 2 (HER-2), which is functionally implicated in the cell growth and proliferation through the activation of downstream pathways, including the PI3K/AKT/mTOR and MAPK/ERK signaling cascades. Western blot analysis demonstrated that GO treatment resulted in a marked decrease in total HER-2, associated with a down-regulation of the expression and activation of protein kinase B (AKT) and extracellular signal-regulated kinase (ERK) thus indicating that GO may act as a potent HER-2 inhibitor. On the other side, the protein corona reverted the effects of GO on HER-2 expression and molecular downstream events to the control level. Our findings may suggest a mechanistic explanation of the reduced anticancer properties of GO-based nanomaterials *in vivo*. These results may also represent a good prediction strategy for the anticancer activity of nanomaterials designed for biomedical purposes, reaffirming the necessity of exploring their effectiveness under physiologically relevant conditions before moving on to the next *in vivo* studies.

Received 14th May 2022
Accepted 23rd August 2022

DOI: 10.1039/d2na00308b

rsc.li/nanoscale-advances

Introduction

To predict the effectiveness of a nanosystem designed for biological applications, it must be considered how it behaves within a biological system. First, its biological identity is governed by the interaction between the nanosystem and biological fluids.[1,2] In fact, due to their high surface free energy bare nanoparticles once immersed in biological media, are passed by several biomolecules that immediately interact with their surface, alter their synthetic identity and form a protein-enriched shell that is commonly referred to as a 'protein corona'.[3–5] This surface biotransformation has a strong impact on the pharmacological and toxicological profile of nanosystems in an unpredictable manner. As an example, it has been observed that only 0.7% of nanosystem doses reached the target tissue since the bio-nano interactions might perturb their primary function and influence cellular recognition and uptake.[6] With the growing application of nanomaterials in biomedicine and considering the increase in human exposure to nano-based therapies and treatments, this aspect is becoming a priority. Especially in the field of cancer therapy, the commercialization of nanoparticle-based anticancer therapeutics is increasing considerably with a rise in the number of available products on the market.[7] These include polymeric carriers[8,9] (*e.g.*, hydrogels, polymersomes, dendrimers, and nanofibers), lipid-based vehicles[10–12] (*e.g.*, liposomes, solid lipid nanoparticles, and micelles), metallic nanoparticles[13] (*e.g.*, gold, silver, and titanium), carbon structures (*e.g.*, nanotubes, nanohorns, nanodiamonds), and graphene.[14,15] However, less than 10% of such nanotherapeutics get translated into clinical applications, remaining with a large proportion of promising, but clinically ineffective, experimental therapies.[16] This makes translational research a long and expensive enterprise which

[a]*School of Biosciences and Veterinary Medicine, University of Camerino, 62032 Camerino, Italy. E-mail: cristina.marchini@unicam.it*
[b]*NanoDelivery Lab, Department of Molecular Medicine, Sapienza University of Rome, Viale Regina Elena 291, 00161 Rome, Italy. E-mail: daniela.pozzi@uniroma1.it*

† Electronic supplementary information (ESI) available. See https://doi.org/10.1039/d2na00308b

‡ These authors contributed equally.

pharmaceutics

MDPI

Article

Efficient Delivery of DNA Using Lipid Nanoparticles

Lishan Cui [1,†], Serena Renzi [2,†], Erica Quagliarini [2], Luca Digiacomo [2], Heinz Amenitsch [3], Laura Masuelli [4], Roberto Bei [5], Gianmarco Ferri [6], Francesco Cardarelli [6], Junbiao Wang [1], Augusto Amici [1], Daniela Pozzi [2], Cristina Marchini [1,*] and Giulio Caracciolo [2,*]

1 School of Biosciences and Veterinary Medicine, University of Camerino, 62032 Camerino, Italy
2 NanoDelivery Lab, Department of Molecular Medicine, Sapienza University of Rome, 00161 Rome, Italy
3 Institute of Inorganic Chemistry, Graz University of Technology, 8010 Graz, Austria
4 Department of Experimental Medicine, "Sapienza" University of Rome, 00161 Rome, Italy
5 Department of Clinical Sciences and Translational Medicine, University of Rome "Tor Vergata", 00133 Rome, Italy
6 National Enterprise for NanoScience and NanoTechnology (NEST), Scuola Normale Superiore, 56127 Pisa, Italy
* Correspondence: cristina.marchini@unicam.it (C.M.); giulio.caracciolo@uniroma1.it (G.C.)
† These authors contributed equally to this work.

Abstract: DNA vaccination has been extensively studied as a promising strategy for tumor treatment. Despite the efforts, the therapeutic efficacy of DNA vaccines has been limited by their intrinsic poor cellular internalization. Electroporation, which is based on the application of a controlled electric field to enhance DNA penetration into cells, has been the method of choice to produce acceptable levels of gene transfer in vivo. However, this method may cause cell damage or rupture, non-specific targeting, and even degradation of pDNA. Skin irritation, muscle contractions, pain, alterations in skin structure, and irreversible cell damage have been frequently reported. To overcome these limitations, in this work, we use a microfluidic platform to generate DNA-loaded lipid nanoparticles (LNPs) which are then characterized by a combination of dynamic light scattering (DLS), synchrotron small-angle X-ray scattering (SAXS), and transmission electron microscopy (TEM). Despite the clinical successes obtained by LNPs for mRNA and siRNA delivery, little is known about LNPs encapsulating bulkier DNA molecules, the clinical application of which remains challenging. For in vitro screening, LNPs were administered to human embryonic kidney 293 (HEK-293) and Chinese hamster ovary (CHO) cell lines and ranked for their transfection efficiency (TE) and cytotoxicity. The LNP formulation exhibiting the highest TE and the lowest cytotoxicity was then tested for the delivery of the DNA vaccine pVAX-hECTM targeting the human neoantigen HER2, an oncoprotein overexpressed in several cancer types. Using fluorescence-activated cell sorting (FACS), immunofluorescence assays and fluorescence confocal microscopy (FCS), we proved that pVAX-hECTM-loaded LNPs produce massive expression of the HER2 antigen on the cell membrane of HEK-293 cells. Our results provide new insights into the structure–activity relationship of DNA-loaded LNPs and pave the way for the access of this gene delivery technology to preclinical studies.

Keywords: DNA vaccines; lipid nanoparticles; HER2

Citation: Cui, L.; Renzi, S.; Quagliarini, E.; Digiacomo, L.; Amenitsch, H.; Masuelli, L.; Bei, R.; Ferri, G.; Cardarelli, F.; Wang, J.; et al. Efficient Delivery of DNA Using Lipid Nanoparticles. *Pharmaceutics* **2022**, *14*, 1698. https://doi.org/10.3390/pharmaceutics14081698

Academic Editor: Lídia Maria Diogo Gonçalves

Received: 7 July 2022
Accepted: 28 July 2022
Published: 15 August 2022

1. Introduction

Despite the massive involvement of resources in cancer studies and in the development of potential therapeutic strategies, cancer is still one of the main causes of death worldwide [1]. The conventional approaches in cancer therapy, such as chemotherapy, radiotherapy, and surgery, are often effective in early-stage tumors but not in those diagnosed in advanced stages. The temporary suspension of screening programs caused by the COVID-19 pandemic exacerbated this trend [2]. The non-specific targeting of both tumoral and healthy cells observed in traditional chemotherapies causes side effects that have significantly evolved over the last decades [3]. Recently, immunotherapy has been investigated

cancers

MDPI

Article

HER2-Displaying M13 Bacteriophages induce Therapeutic Immunity against Breast Cancer

Junbiao Wang [1,†], Alessia Lamolinara [2,†], Laura Conti [3], Mara Giangrossi [1], Lishan Cui [1], Maria Beatrice Morelli [4], Consuelo Amantini [1], Maurizio Falconi [1], Caterina Bartolacci [1], Cristina Andreani [1], Fiorenza Orlando [5], Mauro Provinciali [5], Francesco Domenico Del Pizzo [2], Francesca Russo [6,7], Barbara Belletti [6], Federica Riccardo [3], Elisabetta Bolli [3], Elena Quaglino [3], Federica Cavallo [3], Augusto Amici [1], Manuela Iezzi [2,*,‡] and Cristina Marchini [1,*,‡]

1 School of Biosciences and Veterinary Medicine, Biology Division, University of Camerino, via Gentile III da Varano, 62032 Camerino, Italy
2 Center for Advanced Studies and Technology, Department of Neurosciences, Imaging and Clinical Sciences, G. d'Annunzio University of Chieti-Pescara, 66013 Chieti, Italy
3 Department of Molecular Biotechnology and Health Sciences, Molecular Biotechnology Center "Guido Tarone", University of Torino, 10126 Torino, Italy
4 School of Pharmacy, University of Camerino, 62032 Camerino, Italy
5 Experimental Animal Models for Aging Unit, Scientific Technological Area, IRCCS INRCA, 60100 Ancona, Italy
6 Molecular Oncology Unit, Centro di Riferimento Oncologico di Aviano (CRO Aviano), IRCCS, National Cancer Institute, 33081 Aviano, Italy
7 Department of Life Sciences, University of Trieste, 34128 Trieste, Italy
* Correspondence: m.iezzi@unich.it (M.I.); cristina.marchini@unicam.it (C.M.); Tel.: +39-0737-403275 (C.M.)
† These authors contributed equally to this work.
‡ These authors contributed equally to this work.

check for updates

Citation: Wang, J.; Lamolinara, A.; Conti, L.; Giangrossi, M.; Cui, L.; Morelli, M.B.; Amantini, C.; Falconi, M.; Bartolacci, C.; Andreani, C.; et al. HER2-Displaying M13 Bacteriophages induce Therapeutic Immunity against Breast Cancer. *Cancers* **2022**, *14*, 4054. https://doi.org/10.3390/cancers14164054

Academic Editors: Paola Marcato and Suresh Gadde

Received: 30 July 2022
Accepted: 16 August 2022
Published: 22 August 2022

Simple Summary: The high incidence and death rates of breast cancer make the development of new therapies an urgent need. The introduction into the clinic of the anti-HER2 monoclonal antibody trastuzumab considerably improved the overall survival and time-to-disease progression of patients with HER2-positive breast cancer. However, many patients do not benefit from it because of resistance to therapy. Cancer vaccines, by inducing into the patient an anti-cancer specific immunity, might represent an alternative immunotherapeutic approach, but despite promises, so far no anti-HER2 cancer vaccine has been approved for human use. In this study, we propose therapeutic phage-based vaccines, against HER2 and its aggressive isoform Δ16HER2, able to elicit a protective immunity and potentially capable of preventing relapse in HER2-positive breast cancer patients, even in those who develop trastuzumab resistance.

Abstract: The advent of trastuzumab has significantly improved the prognosis of HER2-positive (HER2+) breast cancer patients; nevertheless, drug resistance limits its clinical benefit. Anti-HER2 active immunotherapy represents an attractive alternative strategy, but effective immunization needs to overcome the patient's immune tolerance against the self-HER2. Phage display technology, taking advantage of phage intrinsic immunogenicity, permits one to generate effective cancer vaccines able to break immune tolerance to self-antigens. In this study, we demonstrate that both preventive and therapeutic vaccination with M13 bacteriophages, displaying the extracellular (EC) and transmembrane (TM) domains of human HER2 or its Δ16HER2 splice variant on their surface (ECTM and Δ16ECTM phages), delayed mammary tumor onset and reduced tumor growth rate and multiplicity in Δ16HER2 transgenic mice, which are tolerant to human Δ16HER2. This antitumor protection correlated with anti-HER2 antibody production. The molecular mechanisms underlying the anticancer effect of vaccine-elicited anti-HER2 antibodies were analyzed in vitro against BT-474 human breast cancer cells, sensitive or resistant to trastuzumab. Immunoglobulins (IgG) purified from immune sera reduced cell viability mainly by impairing ERK phosphorylation and reactivating retinoblastoma

biomolecules

MDPI

Review

Breast Cancer Treatment: The Case of Gold(I)-Based Compounds as a Promising Class of Bioactive Molecules

Rossana Galassi [1,*], Lorenzo Luciani [1], Junbiao Wang [2], Silvia Vincenzetti [2], Lishan Cui [2], Augusto Amici [2], Stefania Pucciarelli [2,†] and Cristina Marchini [2,*,†]

[1] Chemistry Division, School of Science and Technology, University of Camerino, 62032 Camerino, Italy; lorenzo.luciani@unicam.it

[2] School of Biosciences and Veterinary Medicine, University of Camerino, 62032 Camerino, Italy; junbiao.wang@unicam.it (J.W.); silvia.vincenzetti@unicam.it (S.V.); lishan.cui@unicam.it (L.C.); augusto.amici@unicam.it (A.A.); stefania.pucciarelli@unicam.it (S.P.)

* Correspondence: rossana.galassi@unicam.it (R.G.); cristina.marchini@unicam.it (C.M.)

† These authors contributed equally to this work.

Abstract: Breast cancers (BCs) may present dramatic diagnoses, both for ineffective therapies and for the limited outcomes in terms of lifespan. For these types of tumors, the search for new drugs is a primary necessity. It is widely recognized that gold compounds are highly active and extremely potent as anticancer agents against many cancer cell lines. The presence of the metal plays an essential role in the activation of the cytotoxicity of these coordination compounds, whose activity, if restricted to the ligands alone, would be non-existent. On the other hand, gold exhibits a complex biochemistry, substantially variable depending on the chemical environments around the central metal. In this review, the scientific findings of the last 6–7 years on two classes of gold(I) compounds, containing phosphane or carbene ligands, are reviewed. In addition to this class of Au(I) compounds, the recent developments in the application of Auranofin in regards to BCs are reported. Auranofin is a triethylphosphine-thiosugar compound that, being a drug approved by the FDA—therefore extensively studied—is an interesting lead gold compound and a good comparison to understand the activities of structurally related Au(I) compounds.

Keywords: gold; breast cancer; Auranofin; phosphane compounds; carbene compounds; IC_{50}; in vivo; in vitro; metal-based drugs; molecular targets

Citation: Galassi, R.; Luciani, L.; Wang, J.; Vincenzetti, S.; Cui, L.; Amici, A.; Pucciarelli, S.; Marchini, C. Breast Cancer Treatment: The Case of Gold(I)-Based Compounds as a Promising Class of Bioactive Molecules. *Biomolecules* **2022**, *12*, 80. https://doi.org/10.3390/biom12010080

Academic Editors: Georgi Momekov and Vladimir N. Uversky

Received: 21 November 2021
Accepted: 30 December 2021
Published: 5 January 2022

1. Introduction

Breast cancer is one of the most common forms of tumors for women and some subtypes of breast cancers are still without efficacious therapy. The search for new drugs with improved and wider efficacy is a current challenge. The present review focuses on the most relevant results reported in the scientific literature published over the last 6–7 years about the in vitro and/or in vivo treatment of breast cancers by two classes of gold(I)-based drugs, phosphane and N-Heterocyclic Carbene (NHC) compounds, and on the main mechanism of actions thereby disclosed. The results are discussed comparatively to the classic metal-based drug, cisplatin, and to Auranofin.

2. Breast Cancer: An Introduction to the Disease

Breast Cancers, Current and Potential Metal-Based Alternative Therapies

Breast cancer is the most common cancer in women worldwide. Advances in early detection and therapy have resulted in significant improvement in breast cancer survival rates, achieving survival probabilities of 90% for at least 5 years after diagnosis in most developed countries. However, the 5-year survival rate drops to 27% in case of metastatic disease, which is considered barely curable with currently available therapies. For patients without metastatic disease, therapeutic goals are tumor eradication, by surgery

pharmaceutics

MDPI

Article

Microfluidic Formulation of DNA-Loaded Multicomponent Lipid Nanoparticles for Gene Delivery

Erica Quagliarini [1], Serena Renzi [2], Luca Digiacomo [2], Francesca Giulimondi [2], Barbara Sartori [3], Heinz Amenitsch [3], Valentina Tassinari [2], Laura Masuelli [4], Roberto Bei [5], Lishan Cui [6], Junbiao Wang [6], Augusto Amici [6], Cristina Marchini [6], Daniela Pozzi [2,*] and Giulio Caracciolo [2,*]

[1] Department of Chemistry, "Sapienza" University of Rome, 00185 Rome, Italy; erica.quagliarini@uniroma1.it
[2] Department of Molecular Medicine, "Sapienza" University of Rome, 00161 Rome, Italy; serena.renzi@uniroma1.it (S.R.); luca.digiacomo@uniroma1.it (L.D.); francesca.giulimondi@uniroma1.it (F.G.); valentina.tassinari@uniroma1.it (V.T.)
[3] Institute of inorganic Chemistry, Graz University of Technology, 8010 Graz, Austria; barbara.sartori@tugraz.at (B.S.); amenitsch@tugraz.at (H.A.)
[4] Department of Experimental Medicine, "Sapienza" University of Rome, 00185 Rome, Italy; laura.masuelli@uniroma1.it
[5] Department of Clinical Sciences and Translational Medicine, University of Rome "Tor Vergata", 00133 Rome, Italy; bei@med.uniroma2.it
[6] School of Biosciences and Veterinary Medicine, University of Camerino, 62032 Camerino, Italy; lishan.cui@unicam.it (L.C.); junbiao.wang@unicam.it (J.W.); augusto.amici@unicam.it (A.A.); cristina.marchini@unicam.it (C.M.)
* Correspondence: daniela.pozzi@uniroma1.it (D.P.); giulio.caracciolo@uniroma1.it (G.C.)

Abstract: In recent years, lipid nanoparticles (LNPs) have gained considerable attention in numerous research fields ranging from gene therapy to cancer immunotherapy and DNA vaccination. While some RNA-encapsulating LNP formulations passed clinical trials, DNA-loaded LNPs have been only marginally explored so far. To fulfil this gap, herein we investigated the effect of several factors influencing the microfluidic formulation and transfection behavior of DNA-loaded LNPs such as PEGylation, total flow rate (TFR), concentration and particle density at the cell surface. We show that PEGylation and post-synthesis sample concentration facilitated formulation of homogeneous and small size LNPs with high transfection efficiency and minor, if any, cytotoxicity on human Embryonic Kidney293 (HEK-293), spontaneously immortalized human keratinocytes (HaCaT), immortalized keratinocytes (N/TERT) generated from the transduction of human primary keratinocytes, and epidermoid cervical cancer (CaSki) cell lines. On the other side, increasing TFR had a detrimental effect both on the physicochemical properties and transfection properties of LNPs. Lastly, the effect of particle concentration at the cell surface on the transfection efficiency (TE) and cell viability was largely dependent on the cell line, suggesting that its case-by-case optimization would be necessary. Overall, we demonstrate that fine tuning formulation and microfluidic parameters is a vital step for the generation of highly efficient DNA-loaded LNPs.

Keywords: lipid nanoparticles; microfluidics; transfection efficiency; lipofectamine

Citation: Quagliarini, E.; Renzi, S.; Digiacomo, L.; Giulimondi, F.; Sartori, B.; Amenitsch, H.; Tassinari, V.; Masuelli, L.; Bei, R.; Cui, L.; et al. Microfluidic Formulation of DNA-Loaded Multicomponent Lipid Nanoparticles for Gene Delivery. *Pharmaceutics* **2021**, *13*, 1292. https://doi.org/10.3390/pharmaceutics13081292

Academic Editors: María Luisa Moyá, Manuel López-López and Xiangyang Shi

Received: 6 July 2021
Accepted: 14 August 2021
Published: 19 August 2021

1. Introduction

1.1. Lipid-Based Gene Delivery Systems

To exert their function properly, nucleic acids (NAs) such as messenger RNA (mRNA), short interfering RNA (siRNA), and plasmid DNA (pDNA) need to reach their target tissue without any alterations of their complex structures and, subsequently, interact with cytosol and/or nucleus of target cells [1]. Nevertheless, free NAs are highly susceptible to rapid degradation in biological media and clearance from the circulation. As demonstrated in a seminal paper by the Nobel Prize M.R. Capecchi, even if directly injected in the cell cytoplasm naked NAs do not work at all [2]. Such limitations can be circumvented

Pharmacological Research 161 (2020) 105123

Contents lists available at ScienceDirect

Pharmacological Research

journal homepage: www.elsevier.com/locate/yphrs

Acetylshikonin isolated from *Lithospermum erythrorhizon* roots inhibits dihydrofolate reductase and hampers autochthonous mammary carcinogenesis in Δ16HER2 transgenic mice

Junbiao Wang[a], Romilde Iannarelli[b], Stefania Pucciarelli[a], Emiliano Laudadio[c], Roberta Galeazzi[d], Mara Giangrossi[a], Maurizio Falconi[a], Lishan Cui[a], Aleix Marti Navia[b], Michela Buccioni[b], Gabriella Marucci[b], Daniele Tomassoni[a], Laura Serini[a], Stefania Sut[e], Filippo Maggi[b], Stefano Dall'Acqua[f,*], Cristina Marchini[a,**,1], Augusto Amici[a,1]

[a] School of Biosciences and Veterinary Medicine, University of Camerino, 62032, Camerino, Italy
[b] School of Pharmacy, University of Camerino, 62032, Camerino, Italy
[c] Dipartimento Scienze e Ingegneria della Materia, dell'Ambiente ed Urbanistica, Università Politecnica delle Marche, Ancona, 60128, Italy
[d] Dipartimento di Scienze della Vita e dell'Ambiente, Università Politecnica delle Marche, Ancona, 60128, Italy
[e] DAFNAE Dipartimento di Agronomia, Animali, Alimenti, Risorse naturali e Ambiente, University of Padova, 35020, Legnaro, Italy
[f] DSF Department of Pharmaceutical and Pharmacological Sciences, University of Padova, 35121, Padova, Italy

ARTICLE INFO

Keywords:
Lithospermum erythrorhizon
Acetylshikonin
Breast cancer
Dihydrofolate reductase (DHFR)
Apoptosis
Δ16HER2 mice

ABSTRACT

Breast cancer (BC) is the most common cancer in women and, among different BC subtypes, triple negative (TN) and human epidermal growth factor receptor 2 (HER2)-positive BCs have the worst prognosis. In this study, we investigated the anticancer activity of the root ethanolic and hexane extracts from *Lithospermum erythrorhizon*, a traditional Chinese herbal medicine known also as *tzu ts'ao* or *tzu-ken*, against *in vitro* and *in vivo* models of TNBC and HER2-positive BC. Treatment with *L. erythrorhizon* root extracts resulted in a dose-dependent inhibition of BC cell viability and in a significant reduction of the growth of TNBC cells transplanted in syngeneic mice. Acetylshikonin, a naphthoquinone, was identified as the main bioactive component in extracts and was responsible for the observed antitumor activity, being able to decrease BC cell viability and to interfere with autochthonous mammary carcinogenesis in Δ16HER2 transgenic mice. Acetylshikonin anticancer effect depends on its ability to act as a potent inhibitor of dihydrofolate reductase (DHFR), to down-regulate key mediators governing cancer growth and progression, such as HER2, Src and STAT3, and to induce apoptosis by caspase-3 activation. The accumulation of acetylshikonin in blood samples as well as in brain, kidney, liver and tumor tissues was also investigated by liquid chromatography coupled with tandem mass spectrometry (LC–MS/MS) highlighting that *L. erythrorhizon* treatment is effective in delivering the active compound into the target tissues. These results provide evidence that *L. erythrorhizon* extract and in particular its main component acetylshikonin are effective against aggressive BC subtypes and reveal new acetylshikonin mechanisms of action.

1. Introduction

Breast cancer (BC) is the most common cancer in women and includes different subtypes with different prognostic and therapeutic implications. On the basis of ER (estrogen receptor), PR (progesterone receptor) and HER2 (human epidermal growth factor receptor 2) expression, BC can be classified into four main molecular subtypes that comprise luminal A (ER-positive, PR-positive and HER2-negative), luminal B (ER-positive, PR-positive and HER2-positive), HER2 overexpression (ER-negative, PR-negative, HER2-positive) and basal-like (ER-negative, PR-negative, HER2-negative (triple negative)) tumors [1,2]. Among the four molecular subtypes, HER2-positive and triple negative BCs are widely recognized to cause the poorest survival in patients [3]. In particular, triple negative BC is associated with the worst prognosis and lack of targeted therapies, while HER2-positive BCs have an aggressive behavior, but they can be treated with HER2-

* Corresponding author at: School of Biosciences and Veterinary Medicine, via Gentile III da Varano, University of Camerino, Camerino, MC, 62032, Italy.
** Corresponding author.
E-mail addresses: stefano.dallacqua@unipd.it (S. Dall'Acqua), cristina.marchini@unicam.it (C. Marchini).
[1] These authors contributed equally to this work.

https://doi.org/10.1016/j.phrs.2020.105123
Received 10 June 2020; Received in revised form 16 July 2020; Accepted 28 July 2020
Available online 19 August 2020

ACKNOWLEDGMENTS

This research was supported by Regione Marche.

I would like to express my deepest appreciation to my supervisors, Prof. Cristina Marchini and Prof. Augusto Amici, and the Chair of the Committee, for their invaluable patience and feedback. I am very grateful to Prof. Cristina Marchini, an excellent mentor who gave me the opportunity, knowledge and ability to successfully complete my research. She is the most heartwarming person I have ever met. Thanks should also go to Prof. Augusto Amici, who guided my Ph.D. research with infinite enthusiasm. Whenever I encountered difficulties in the process of doing experiments, he would continue to encourage me, believe me. This endeavor would not have been possible without their support and guidance.

Many thanks to our collaborator Prof. Giulio Caracciolo, Prof. Daniela Pozzi and their research team at Sapienza University of Rome, who generated lipid nanoparticles capable of encapsulating our DNA vaccines. Special thanks to Mauro Provinciali and Fiorenza Orlando (IRCA, Ancona) for providing young and old mice for *in vivo* experiments. I'd like to acknowledge our collaborators Prof. Roberta Galeazzi and her group in Marche Polytechnic University performed *in silico* analysis of the structure of the S1-TM. Thanks also to Luca Pesce from the University of Pisa, who performed the confocal microscopy analysis, and all others for their contributions to collaborating and completing this work.

I would like to extend my sincere thanks to my colleagues, research assistants, and study participants from the university, who impacted and inspired me.

Lastly, I would be remiss in not mentioning my family, especially my parents. Wherever I am, they are always supporting me and encouraging me with their best wishes.